The Dissertation Committee for Ryan Lance Burns Certifies that this is the approved version of the following dissertation:

Investigation of Poly(pyrrolone-imide) Materials for the Olefin / Paraffin Separation

Committee:

William J. Koros, Supervisor

C. Grant Willson, Co-Supervisor

Roger T. Bonnecaze

R. Bruce Eldridge

Isaac C. Sanchez

George Huff

Investigation of Poly(pyrrolone-imide) Materials for the Olefin / Paraffin Separation

by

Ryan Lance Burns, B.S. Ch.E.

Dissertation

Presented to the Faculty of the Graduate School of

The University of Texas at Austin

in Partial Fulfillment

of the Requirements

for the Degree of

Doctor of Philosophy

The University of Texas at Austin

December, 2002

Dedication

To My Family

Acknowledgements

I would like to thank everyone who has contributed to my education and experience throughout graduate school. I am especially grateful to my advisor, Professor Koros, for his guidance, humor, and good advice. Dr. Koros works harder than anyone I have met in my life, and his work ethic and high energy level are contagious. I am very thankful for the chance to work for such a multitalented professor, and in a group where there have been multiple opportunities to expand my research horizons.

I would like to thank Dr. Willson for including me as part of his group from the first time I even visited The University of Texas. Interactions with Dr. Willson and his research group have been an extremely valuable and important part of my graduate school experience. I would also like to thank my committee members, Dr. Roger Bonnecaze, Dr. Bruce Eldridge, Dr. Isaac Sanchez, and Dr. George Huff for their advice and suggestions. Much gratitude also goes to Dr. Joel Miller at the University of Utah for supplying samples and advice regarding the work discussed in Appendix A.

I would like to thank my lab partner, John Wind, who has been with me from day one, and who has probably helped me with something every day of graduate school. John is a constant source of good ideas and suggestions, and we have had countless great discussions involving just about everything.

I would like to acknowledge all of the Koros group students who helped me during my initial years in graduate school. Two students who particularly

went above and beyond the call of duty are Rajiv Mahajan and De Vu. I have had many good discussions with Rajiv, which usually resulted in a solution to a problem. De is the most helpful person I have ever met in my life, and he continues to be extraordinarily valuable even though he is two time zones away. Thanks to Keisha Steel, David Punsalan and Seth Carruthers who all took extensive time to help teach me measurement techniques and provide good comments and suggestions regarding my work. I would like to thank Greg Pollock, an undergraduate researcher, who taught me polymer synthesis my first year of graduate school. I would also like to thank Cathy Zimmerman, who helped me from afar my first year through phone calls, email, and a really great dissertation.

I would like to thank my "family of friends", both literally and figuratively, who have been with me throughout my college years. My fiancée, Linda, has been super supportive, patient, and helpful (not to mention a good cook) throughout graduate school. My brother, Sean, Lindsay and Gerard have also helped out with just about anything and everything.

Also, thanks to all of the students in the Koros research group, especially Ted and Shilpa, who have been tremendously helpful with the move and the long distance communication. Last, but not least, I would like to thank my family and extended family for always being supportive throughout college and graduate school.

Investigation of Poly(pyrrolone-imide) Materials for the Olefin / Paraffin Separation

Publication No._____

Ryan Lance Burns, Ph. D.

The University of Texas at Austin, 2002

Supervisors: William J. Koros and C. Grant Willson

The separation of olefin and paraffin gases is one of the most important processes in the petrochemical industry. Currently, this separation is done using low temperature distillation, which is very expensive and energy intensive. In an effort to decrease cost and save energy membrane separations have been considered as an attractive alternative. The present work examines behavior of poly(pyrrolone-imide) membrane materials for the olefin / paraffin separation based on mobility selectivity. It was found that rigid materials such as carbon molecular sieves and poly(pyrrolone-imides) exhibit a surprising C_3H_6/C_3H_8 selectivity maximum as the structure of the material is varied at fixed operating conditions. The structure of the carbon materials is controlled by the magnitude of the thermal treatment. Similarly, the structure of the poly (pyrrolone-imides) is varied by changing monomer stoichiometry. This work provides a fundamental

understanding for this maximum in selectivity and continues to examine the utility of this behavior. This unexpected behavior is explained by a straightforward model, which considers a pore size distribution for the carbons, or a distribution of chain spacings for the rigid poly (pyrrolone-imides). This work has also demonstrated that swelling induced plasticization of rigid well-packed poly(pyrrolone-imides), as well as increases in temperature have resulted in a surprising *increase* in C_3H_6/C_3H_8 selectivity, as well as C_3H_6 permeability. Observation and understanding of this novel behavior provides potential uses for rigid materials that show undesirable transport properties under ambient and low pressure feed stream conditions. Furthermore, a fundamental understanding of this material behavior has been developed through modeling efforts, which take into account a distribution of selective entities within the material.

Table of Contents

List of Tables

List of Figures

CHAPTER 1: INTRODUCTION

1.1 CURRENT PROPYLENE PRODUCTION

Propylene was the first raw material used on a commercial scale in the petrochemical industry. It was initially used for the production of isopropanol over 70 years ago. Since that time the growth of ethylene production has helped expand the markets for propylene because it is largely a byproduct of ethylene formation. In 1998, the U.S. produced 28 billion pounds of propylene, 35 % more than it produced 10 years earlier. Propylene is the second largest volume organic feedstock produced in the U.S., trailing only the manufacture of ethylene [1]. Today propylene finds multiple uses depending on market conditions. The primary use for propylene is a feedstock for plastics (polypropylene) and various chemical products including acrylonitrile, oxo alcohols, propylene oxide, butanol, cumene, propylene oligomers, acrylic acid, allyl chloride, and ethylene-propylene elastomers [2]. Polypropylene is used in automotive parts, appliances, film, fiber, and filaments. Figure 1.1 shows a flow diagram illustrating the chemical use of propylene, and the dozens of consumer products that utilize propylene feedstock. Propylene is also used as a feedstock for polygasoline, which is used for octane enhancement in gasoline. Additionally, propylene has a heating value of 45.8 MJ/kg, and refinery grade propylene is added to refinery fuel when the economics for the previous uses are unfavorable, or propylene recovery systems are limited

[3]. Figure 1.2 shows a breakdown of the fraction of propylene used for various chemical products in world markets during 1992.

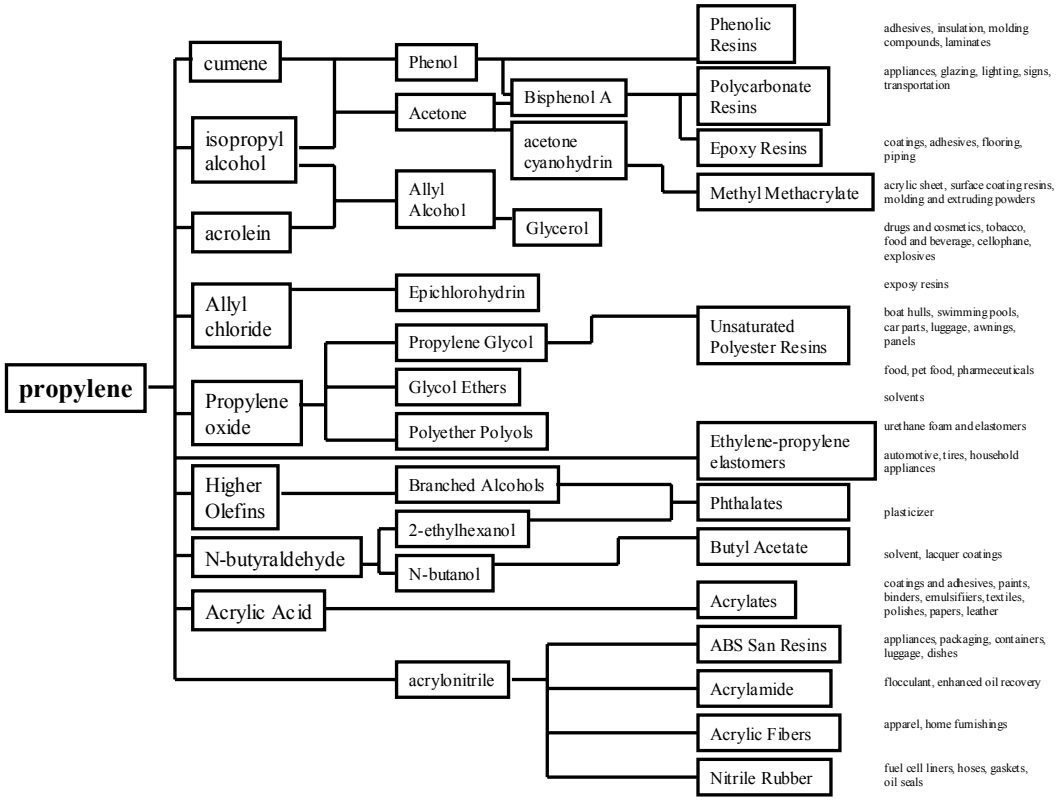

Figure 1.1. Flow diagram illustrating the use of propylene in dozens of consumer products. Adapted from work by Dr. Jos. P. Wristers, ExxonMobil.

Propylene can be manufactured in 3 ways: steam cracking, refinery production (catalytic cracking), and catalytic dehydrogenation of propane. In 1990, 77% of the world's propylene production originated as a byproduct from the steam cracking process used to produce ethylene. In the United States, 56% of the total propylene manufactured came from steam cracking. This is because the U.S. has a large motor gasoline market that increases the capacity of fluid catalytic cracking, and therefore increases the production of propylene as a byproduct.

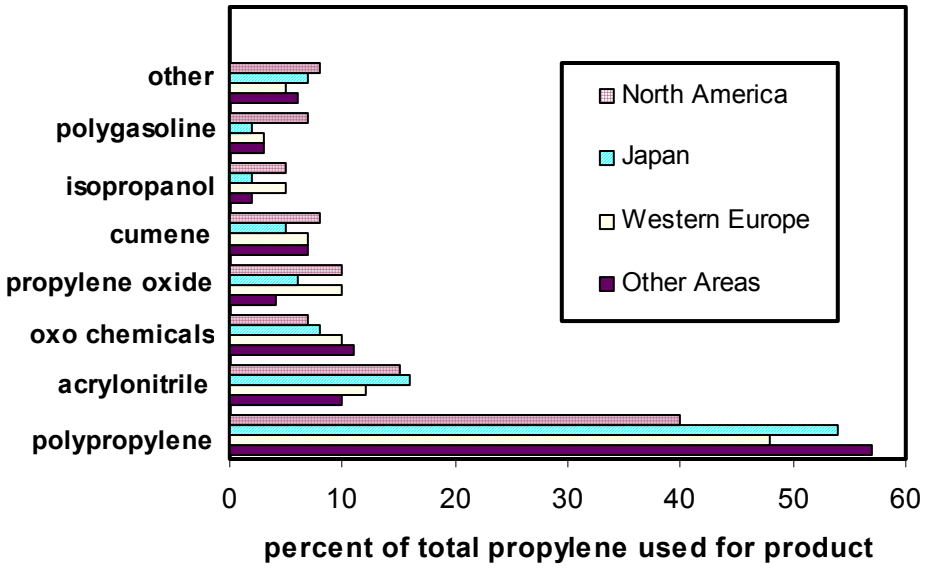

Figure 1.2. Percent of products derived from propylene feedstocks in specific world markets.

Steam cracking or pyrolysis is a process for the production of ethylene. Over 97 % of the world's production of ethylene originates from steam cracking, and other olefin byproducts are also a result of the process, such as propylene. The process involves preheating a mixture of hydrocarbons and steam to 600^{o}C before heating to the cracking temperature (750 – 900^{o}C). Saturated hydrocarbons in the feed crack into smaller olefin molecules including ethylene and propylene.

Propylene is also produced from refinery processes, such as fluid catalytic cracking or thermal cracking. A fluid catalytic cracking (FCC) may be one of the most important processes in an integrated refinery today, as this operation is a major step in converting low-value feedstocks into more valuable products. The process contacts a partially vaporized gas oil with a zeolite catalyst at a pressure of 2.5 – 4 atm and a temperature of 450 – 580^{o}C. The products from an FCC are dry gas, liquefied petroleum gas (LPG), gasoline, decanted oil, and coke. The LPG is rich in olefins such as propylene and butylenes. Typical propylene yields for an FCC process are 2 – 5% depending on the feedstock, and operating conditions [4].

As outlined above, the majority of propylene is produced from processes designed for the manufacture of other products, such as ethylene in steam cracking, and gasoline in the case of refinery conversion processes (catalytic

cracking). Therefore, the availability of propylene is determined by the market demand for these other products (ethylene and gasoline), and to some extent specific process conditions. Increased demand for propylene products in the 1980's, such as polypropylene, created the incentive to develop a process for the "intentional" manufacture of propylene, and this brought about the technology for the dehydrogenation of propane. This reaction is endothermic and is generally carried out in the presence of a catalyst such as platinum. There are multiple commercial methods for the dehydrogenation of propane including the Oleflex process developed by UOP, the Catofin process developed by Air Products, and the STAR process developed by Phillips Petroleum.

1.2 OLEFIN/PARAFFIN SEPARATION TECHNOLOGY

Since, none of the processes discussed in Section 1.1 produces pure propylene, additional separation and processing steps are necessary to provide chemical grade propylene (92 – 94 wt %) or polymer grade propylene (99.0 – 99.8 wt %). The similar boiling points of propylene (-47 ^{o}C) and propane (-42.1 ^{o}C) require complex distillation units for separation with high reflux ratios (12-20). The feed stream to the propylene/propane splitter may come from the previous methylacetylene and propadiene removal step. The bottoms product of the tower will be propane rich, and this is usually recycled for cracking.

Propylene fractionation towers may require 100 – 300 trays [2]. The capital cost for a typical propane / propylene splitter is in the range of 40 million to 60 million dollars. A U.S. Department of Energy study estimated that 1.2×10^{14} BTU / year are used for olefin / paraffin separations [5]. This large capital expense and energy cost have created incentive for extensive research in this area of separations. Consequently, membrane separations have been considered as an attractive alternative.

There are currently no commercial membrane applications for olefin / paraffin separations. Baker predicts that for vapor/vapor separations (including propylene/propane, ethylene/ethane, and n-butane/isobutane), the membrane market will reach $30 million by 2010, and $125 million by 2020. At this time, this class of separations is predicted to represent 16 % of the total membrane market [6].

At this point in time it is unlikely that membranes would completely replace distillation as a means of olefin / paraffin separation, because of the large capital investment in these plants. However, there are process locations where membrane units could be used to debottleneck existing processes. Figure 1.3 illustrates a membrane-distillation hybrid unit, in which the membrane could be used as a first cut for the separation, and the distillation column could be used to further purify the olefin providing the required product stream.

Figure 1.4 shows another possible application for polymer membranes suggested by Baker [6]. After the polymerization reaction, polypropylene product is sent to a flash tank. Here propane is flared, and consequently unreacted propylene monomer is lost. It is estimated that this wasted propylene could represent a loss of $1 million per plant per year. A membrane unit inserted into the process stream could potentially recover this propylene monomer, and recycle it to the reactor, leaving residual propane to be used as fuel or flared [6].

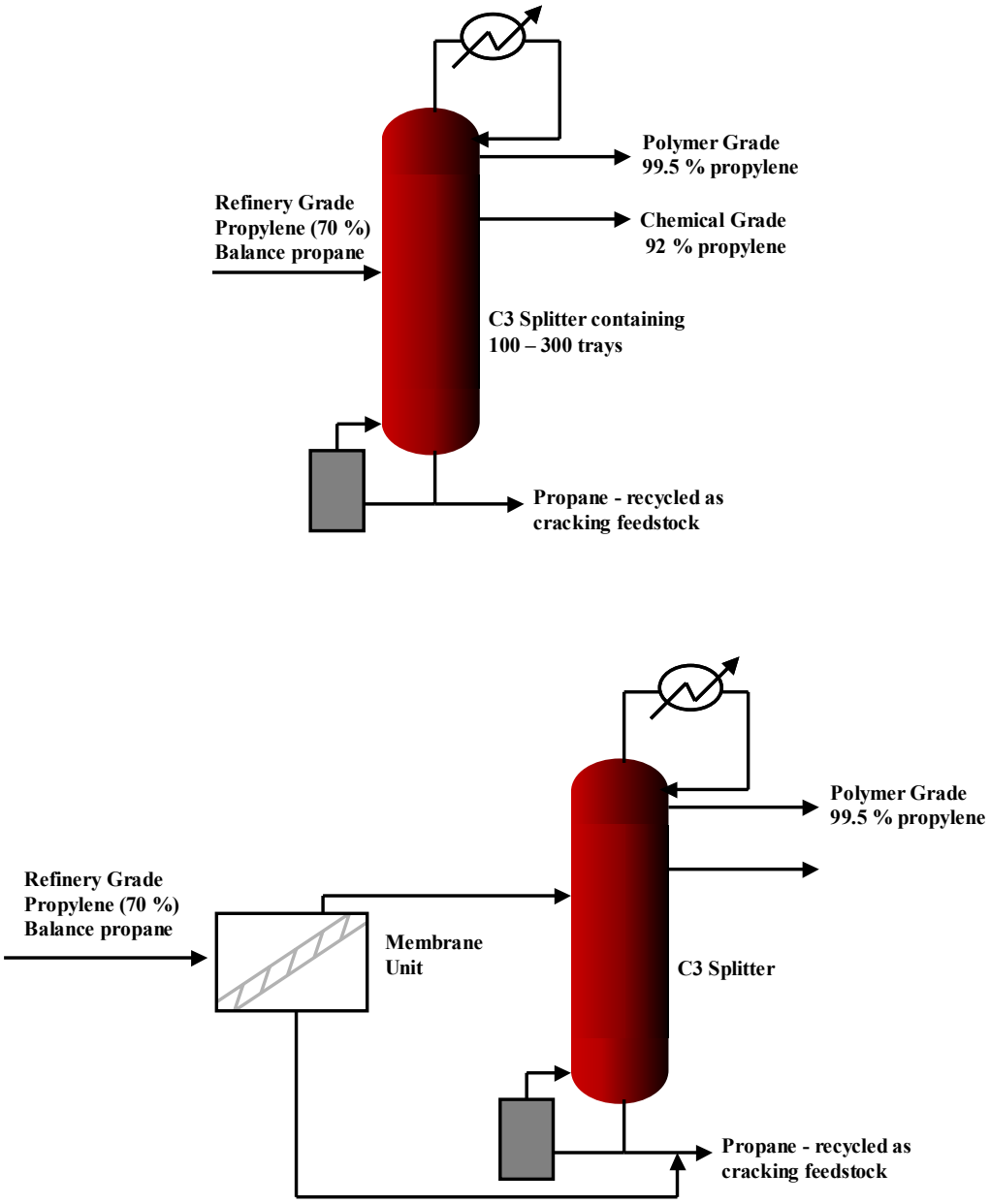

Figure 1.3. Potential membrane-distillation hybrid process for olefin/paraffin separation [7].

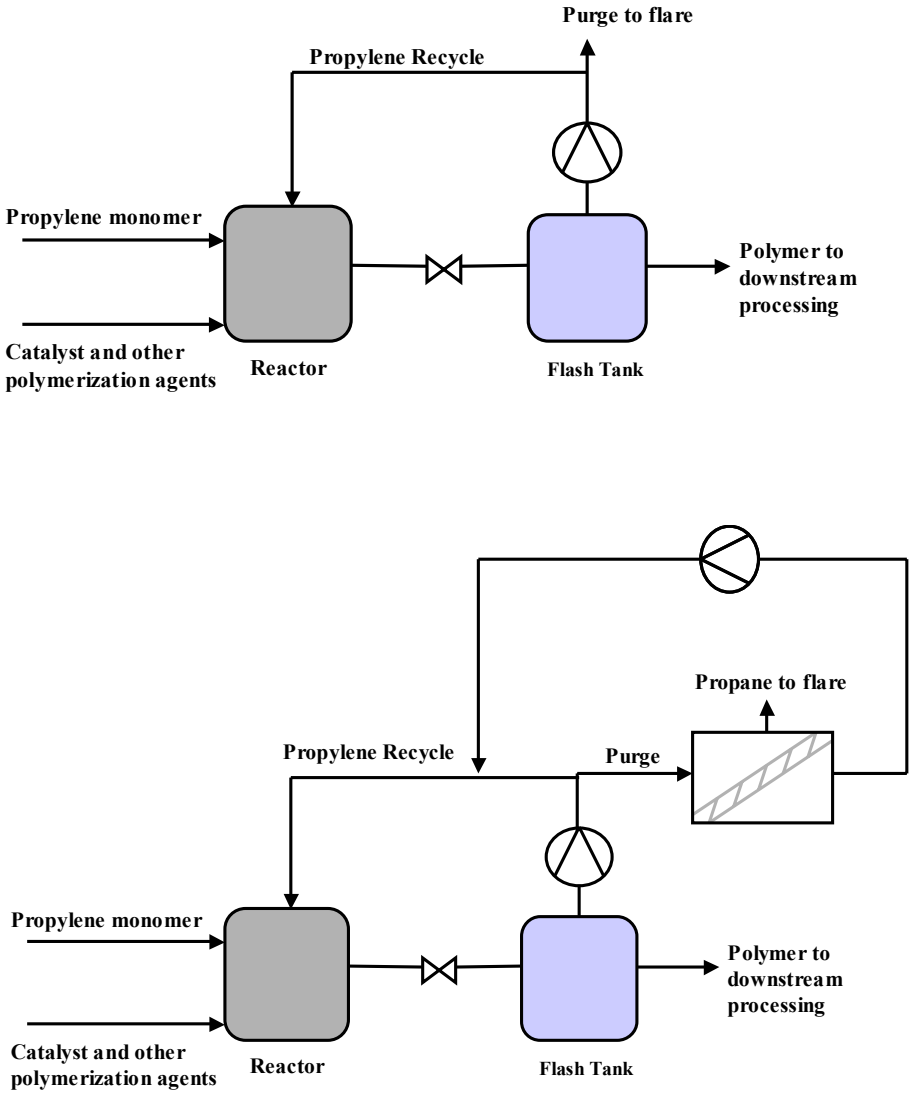

Figure 1.4. a) Source of propylene/propane vent gas in a typical polypropylene plant and b) use of a membrane system to recover and recycle the propylene to the reactor [6].

1.3 RESEARCH OBJECTIVES

1. Define the C_3H_6/C_3H_8 upper bound curve

In 1991, Robeson defined the now well-known upper bound trade-off curves for polymeric membranes for various gas pairs including O_2/N_2, H_2/CH_4, CO_2/CH_4, He/O_2, as well as other possible separations involving the same gas molecules [8]. Since this time data for permeation of heavier hydrocarbons through polymer membranes have become more available in the literature; however, no upper bound analysis has yet been established for these cases. Establishing a C_3H_6/C_3H_8 upper bound creates both a standard and a challenge for the community, in terms of what future materials research should aim to overcome. While it would appear to be straightforward to collect the C_3H_6/C_3H_8 literature results, and simply plot the data on a log / log plot of selectivity versus permeability, defining this upper limit is actually much more challenging. This is because there is a multitude of questionable C_3H_6/C_3H_8 separation data in the literature. Furthermore, there are other issues with C_3H_6/C_3H_8 separation, which are not nearly as important for lighter gas pairs, such as plasticization at low feed pressures, as well as transient effects that are very important to recognize. These topics as well as modeling work to predict the C_3H_6/C_3H_8 upper bound are presented in Chapter 4.

2. **Synthesize a family of poly(pyrrolone-imide) copolymers. Investigate the effects of subtle changes of alternating bulky and flat monomer groups on gas transport properties.**

This project seeks to utilize the concept of a rigid polymeric material with alternating open and packable regions in order to develop materials suitable for the propylene / propane separation. The first goal of this project is to synthesize a family of poly(pyrrolone-imide) copolymers, 6FDA-TAB/DAM, in order to investigate how the ratio of TAB/DAM monomers in the polymer chain affects propane / propylene transport properties. The synthesis is outlined in Chapter 3. Furthermore, it will be shown that a selectivity maximum is observed as a function of TAB/DAM ratio under "normal" feed stream conditions (2 atm and 35^{o}C), and this trend has not been reported previously for polymeric materials. A fundamental understanding of this selectivity maximum (which is also observed in carbon membranes) will be explored in Chapter 5.

3. **Perform pressure and temperature dependant gas transport experiments (both pure and mixed gas) in order to understand the behavior of C_3H_6 / C_3H_8 transport at elevated temperatures and pressures.**

The constructed upper bound limit for C_3H_6/C_3H_8 is reported at the conditions of 2 atm feed pressure and 35°C (see Chapter 4). These conditions were chosen because 2 atm feed pressure is typically a high enough pressure for which the so called "Langmuir sites" associated with glassy state packing disruptions have become saturated and the permeability has leveled off after dual mode effects for glassy polymers. This pressure (2 atm) is typically below the plasticization pressure for propane or propylene in glassy polymers. The temperature of 35°C was chosen because it is easily controllable experimentally. Many literature sources also report polymer material properties (for propane / propylene separation) at or near these conditions, which allows for ease of comparison. In a commercial process, however, it is likely desired to operate at more aggressive feed stream temperature and pressure conditions.

The objective was to perform pressure dependant permeation and sorption experiments on these materials in order to determine solubility and diffusivity coefficients, as well as the C_3H_6/C_3H_8 solubility selectivity and C_3H_6/C_3H_8 diffusivity selectivity. Based on literature data (the solubility selectivity of typical polyimides is typically 1.0 – 1.3) [7, 9] it is believed that the solubility selectivity of these materials will be close to unity, and the diffusivity selectivity should largely make up the permselectivity. Furthermore, pressure dependent studies will allow determination of the propane and propylene plasticization pressure,

which can be compared to other polyimides in the literature to indicate the effect of chain rigidity on suppressing plasticization.

Temperature dependent permeation and sorption studies allow for calculation of the activation energy for diffusion and the heat of sorption for both propane and propylene. Pressure and temperature effects on gas transport properties will be evaluated in Chapter 6. It has been shown that a selectivity maximum exists as a function of both pressure and/or temperature for certain materials, and an understanding of these surprising results will be explored as well.

4. **Determine complementary physical properties of rigid poly (pyrrolone-imide) copolymers.**

The glass transition temperature of the copolymers discussed here can be determined using differential scanning calorimetry (DSC). The glass transition temperature will indicate the rigidity of the polymer chain, and will be a good tool to measure the effect of increased amounts of the DAM monomer within the matrix. It is believed that more imide linkages will add increased flexibility to the polymer chain.

The average intersegmental distance of the polymer chains may correlate with penetrant diffusion coefficients. This d-spacing can be measured using wide

angle x-ray diffraction (WAXD). While the d-spacing in polymers is often a questionable quantitative measure of packing, it often provides a good qualitative comparison between different materials in the same polymer family. Density measurements of copolymers will also be performed using a density gradient column.

5. **Investigate the cause for significant declines (40 %) in mixed gas C_3H_6 / C_3H_8 selectivity measurements compared to pure gas measurements.**

To date, many materials reported in the literature for the C_3H_6 / C_3H_8 separation show tremendous drops in mixed gas selectivity measurements (usually close to 40 per cent) compared to pure gas permeability experiments [7, 9]. There are not many theories provided in the literature as to why this is observed, and the leading one is currently plasticization. Other possibilities worth investigating are competitive diffusion, competitive sorption, and frame of reference effects. Thus far, Tanaka et al have performed the most complete work in truly defining this problem [9]. Permeability measurements were performed on the polyimide 6FDA-DAM for both pure gas propylene and propane, as well as a 50 %/ 50 % feed gas mixture of the two. The objective of the work here is to investigate established models (such as the bulk flux model [10]) in an attempt to determine the reason for the reduction of mixed gas C_3H_6/C_3H_8 selectivity. This topic is explored in Chapter 6.

1.4 REFERENCES

[1] Facts and Figures, Chemical and Engineering News. 77 (1999) 32-39.

[2] P. Eisele and R. Killpack, in: Ullman's Encyclopedia of Industrial Chemistry, 1993, pp. 211-222.

[3] J. W. B. M.R. Schoenberg, C.G. Papadopoulos, in: Kirk-Othmer Encyclopedia, 1995, pp. 228-246.

[4] R. Sadeghbeigi, Fluid Catalytic Cracking Handbook, Gulf Publishing Company, Houston, TX, 2000.

[5] R. B. Eldridge, Olefin Paraffin Separation Technology - a Review, Ind. Eng. Chem. Res. 32 (1993) 2208-2212.

[6] R. W. Baker, Future directions of membrane gas separation technology, Ind. Eng. Chem. Res. 41 (2002) 1393-1411.

[7] C. Staudt-Bickel and W. J. Koros, Olefin/paraffin gas separations with 6FDA-based polyimide membranes, J. Membr. Sci. 170 (2000) 205-214.

[8] L. M. Robeson, Correlation of Separation Factor Versus Permeability for Polymeric Membranes, J. Membr. Sci. 62 (1991) 165-185.

[9] K. Tanaka, A. Taguchi, J. Q. Hao, H. Kita and K. Okamoto, Permeation and separation properties of polyimide membranes to olefins and paraffins, J. Membr. Sci. 121 (1996) 197-207.

[10] H. D. Kamaruddin and W. J. Koros, Some observations about the application of Fick's first law for membrane separation of multicomponent mixtures, J. Membr. Sci. 135 (1997) 147-159.

CHAPTER 2: BACKGROUND AND THEORY

2.1 SOLUTION-DIFFUSION MODEL

Transport of gases in polymers and molecular sieve materials occurs via a well-known solution-diffusion mechanism. The permeability coefficient (P_A) of a particular gas is the flux (N_A) normalized to the pressure difference across the membrane (Δp_A), as well as the membrane thickness (ℓ).

$$P_A = N_A \frac{\ell}{\Delta p_A} \tag{2.1}$$

The permeability coefficient of a particular penetrant gas is also equal to the product of the diffusion coefficient and the solubility coefficient [1].

$$P_A = D_A S_A \tag{2.2}$$

The permselectivity (α) of a membrane material (also ideal selectivity) is the ratio of the permeability coefficients of a penetrant pair for the case where the downstream pressure is negligible relative to the upstream feed pressure. Substituting equation (2), the permselectivity (also termed "ideal selectivity") can be expressed as a product of the diffusivity selectivity and solubility selectivity of the particular gas pair.

$$\alpha_{A/B} = \frac{P_A}{P_B} = \frac{D_A}{D_B} \bullet \frac{S_A}{S_B} \tag{2.3}$$

In mixed gas permeation measurements the selectivity is defined as:

$$\alpha_{A/B} = \left(\frac{y_A / y_B}{x_A / x_B} \right) \tag{2.4}$$

where y_i and x_i are the mole fractions of the components at the downstream and upstream faces, respectively.

2.2 PRESSURE DEPENDENCE OF PERMEABILITY

2.2.1 Dual Mode Model

The variation of gas permeability with pressure in glassy polymers is often represented by the dual mode and partial immobilization model [2-4]. The model accounts for the differences in gas transport properties in both the idealized Henry's law and Langmuir domains of a glassy polymer. The pressure dependence of permeability for a single component is given by:

$$P = k_D D_D + \frac{C'_H D_H b}{1 + b p} \tag{2.5}$$

where k_D is the Henry's law constant, C_H is the Langmuir capacity constant, and b is the Langmuir affinity constant. The C'_H term characterizes the amount of unrelaxed free volume in the glassy matrix, and it allows description of the non-equilibrium nature of such materials. The affinity constant, b, characterizes the tendency of a given penetrant to sorb into the excess unrelaxed volume in the non-equilibrium matrix. The Henry's law diffusion coefficient, D_D, represents the

mobility of the component in the dissolved mode. The Langmuir diffusion coefficient, D_H, represents the mobility of the material in the unrelaxed free volume region. This model can be further extended to mixed gas permeability:

$$P_A = k_{DA} D_{DA} + \frac{C'_{HA}\, b_A D_{HA}}{1 + b_A p_A + b_B p_B} \tag{2.6}$$

This model is valid for a binary gas mixture of components A and B, and it accounts for competitive sorption in the Langmuir environment.

2.2.2 Bulk Flow Model

When predicting the permeability of a gaseous component in a mixed gas experiment, the bulk flux term in equation (2.7) is often neglected. Paul and Ebra-Lima first recognized the importance of the bulk flux term [5], and Kamaruddin and Koros showed the importance of including the bulk flux term in addition to the dual mode model to accurately predict the permeability of gaseous components in mixed gas experiments [6]. The overall flux of a component can be represented by the sum of the diffusive flux and the bulk flux:

$$n_A = n_A^{\,bulk} + n_A^{\,diff} \tag{2.7}$$

Here the bulk flux is defined as:

$$n_A^{\,bulk} = (n_A + n_B)\omega_A \tag{2.8}$$

where ω_A is the concentration of the component within the medium. Kamaruddin and Koros also define a fraction of the bulk flux for components A and B, which can be represented by:

$$\prod_A{}^{\text{bulk}} = \frac{(n_A + n_B)\omega_A{}^{\text{avg}}}{n_A} = \left(1 + \frac{1}{r}\right)\omega_A{}^{\text{avg}} \tag{2.9}$$

$$\prod_B{}^{\text{bulk}} = \frac{(n_A + n_B)\omega_B{}^{\text{avg}}}{n_B} = (1 + r)\omega_B{}^{\text{avg}} \tag{2.10}$$

where r is the ratio of the respective fluxes (n_A/n_B). The corrected permeability, $\boldsymbol{P}^*$, accounting for the bulk flux term is then represented by:

$$P_A{}^* = (1 - \prod_A{}^{bulk})P_A \tag{2.11}$$

$$P_B{}^* = (1 - \prod_B{}^{bulk})P_B \tag{2.12}$$

where P_A and P_B are the permeability values predicted from the dual model model.

Kamaruddin and Koros have shown that the frame of reference model can account for depressions in the selectivity not predicted by the dual mode model in the absence of plasticization effects [6]. Figure 2.1 shows mixed gas CO_2/CH_4

permeation data for the polypyrrolone 6FDA-TADPO, and the measurements were made by David Walker [7].

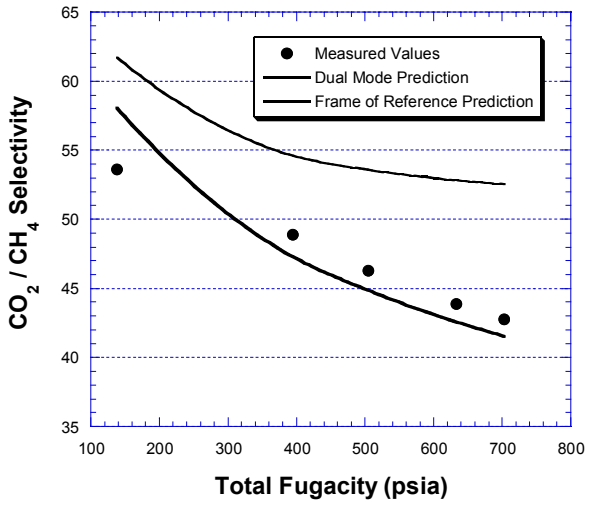

Figure 2.1. Mixed gas CO_2/CH_4 selectivity as a function of total fugacity for 6FDA-TADPO polypyrrolone. Data provided by Walker, and model predictions provided by Kamaruddin and Koros [6].

The dual mode model prediction is based on Equation 2.6, and the parameters are extracted from the pure gas data. Clearly, the dual mode model over predicts the actual measured selectivity in the mixed gas experiment even including corrections for non-ideal gas phase thermodynamics. Including the bulk flux term in the prediction allows for a close match with the experimentally

measured values without the inclusion of any additional empirical fitting parameters. In addition to correctly predicting the selectivity, the bulk flux model is able to accurately predict the *increase* in the mixed gas methane permeability, which is a phenomena most competition models are not able to describe.

2.2.3 Swelling and Plasticization of Polymeric Materials

At elevated penetrant activities highly sorbing gases such as CO_2 and hydrocarbons can begin to plasticize the glassy polymer membrane, which normally results in an increase in flux and a decrease in selectivity. Before going further it is necessary to define plasticization. Wessling writes, "In the literature, plasticization, in the context of mass transport through polymers, is often used as a term that basically covers all unexpected transport phenomena which are difficult to interpret [8]". While this definition is broad and a bit humorous, it does illustrate the difficulty that arises in fully comprehending what is meant by the term plasticization. Therefore, it is worth some effort to further elucidate the concept of plasticization. Kirk-Othmer Encyclopedia defines plasticizers as "materials which, when added to a polymer, cause an increase in the flexibility and workability, brought about by a decrease in the glass-transition temperature, T_g, of the polymer [9]". In the area of polymer membranes, the plasticization pressure has often been defined as the point of an upturn in the permeability isotherm, a definition that is actually very different than the more conventional

definition of plasticization mentioned above (involving altering the mechanical properties of a polymer and depressing the glass transition temperature). Therefore, it is reasonable to introduce a more descriptive term for plasticization in the context of polymer membranes, which can be called "permeation plasticization", and specifically refers to the upswing in the permeation isotherm. An absence or presence of permeation plasticization does not necessarily indicate whether the polymer T_g has been lowered, and this will be discussed later in this section. Figure 2.2 illustrates a general description of the pressure dependent behavior of permeation in glassy polymers, showing a decrease in permeation due to dual mode effects at low pressures, and an increase in permeability due to "plasticization." This increase in permeability with increasing pressure or fugacity is usually a result of an increased diffusion coefficient. The increase in the diffusion coefficient could be the result of the polymer chains swelling (dilating), which occurs because of the sorption of the condensable penetrant. Here dilating specifically relates to increasing the average spacing between polymer chains. This will also result in added free volume throughout the polymer matrix. Alternatively, the increase in diffusion could be a result of added flexibility within the polymer chains, which is also a result of the presence of the sorbed penetrant. In many cases permeation plasticization is probably a combination of both swelling (dilation) of the polymer matrix and added flexibility of the polymer chains. The challenge in understanding the fundamental

cause for permeation plasticization stems from the difficulty in decoupling the effects a penetrant has on the polymer (swelling and / or added flexibility), as well as the subsequent effect that change on the polymer matrix has on the diffusion coefficient of the penetrant.

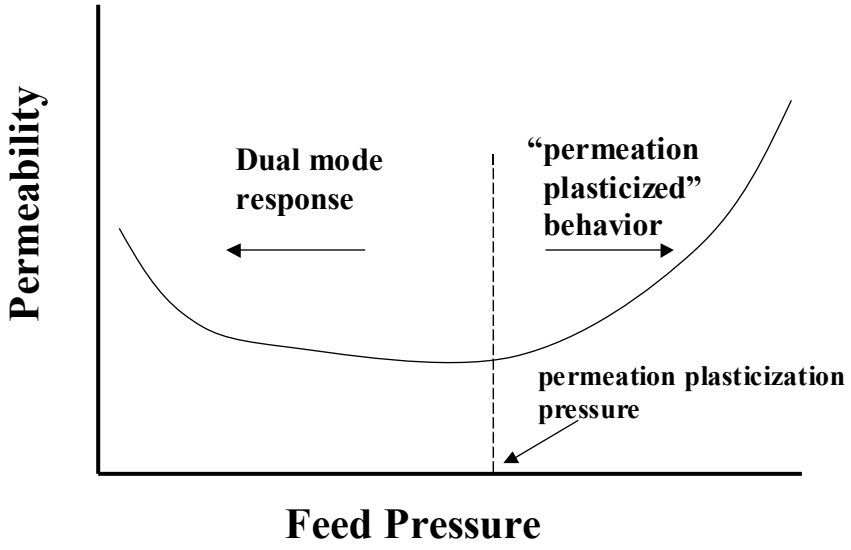

Figure 2.2. General pressure dependent permeation behavior of glassy polymers.

Many researchers have done work to characterize the effect of CO_2 on different polymer membranes. Sanders has shown that while sorbed CO_2 decreases the Tg of all polymers studied (cellulose acetate, PMMA polyethersulfone, Kapton, and PET), and alters their mechanical properties, there is no correlation between this effect and the permeability isotherm of CO_2 [10]. Some polymers studied (cellulose acetate and PMMA) exhibited an increase in

permeability with increased CO_2 pressure, while others (polyethersulfone, Kapton, PET) showed a decrease in permeability with increased CO_2 pressure up to 20 atm. This data implies that softening of polymer chains or added flexibility due to a sorbed penetrant is not the primary factor in causing an increase in the diffusion coefficient, and hence increase in permeability coefficient. Sanders further suggested that bulky side groups of the polymer chain might be the important entity in determining behavior of the diffusion coefficient.

Bos *et al.* have attempted to show that there is a correlation between CO_2 concentration in the polymer and the permeation plasticization pressure [11]. It is reported that the critical concentration of 36 ± 7 cm^3 (STP) / cm^3-polymer is the concentration where an upturn in the permeability isotherm will occur, and this is shown for 11 selected polymers ranging in Tg from 151 ^oC to 313 ^oC. Bos *et al.* also report that there is no correlation between permeation plasticization pressure and Tg or fractional free volume.

Walker has shown that for the polypyrrolone materials, 6FDA-TADPO, 6FDA-TABP, and 6FDA-6FTA there is zero or very little upturn in the permeation isotherm as high as 900 psia feed pressure [7]. However, the concentration of CO_2 in all of these materials is greater than 92 cm^3 (STP) / cm^3-polymer at only 700 psia. This data indicates that there is more involved in causing an upturn in the permeation isotherm than merely a critical concentration.

Futhermore, Wind has shown that the critical concentration for permeation plasticization does not hold true for covalently crosslinked polyimides [12]. In addition, this work has shown a qualitative correlation between dilation of the polymer matrix and permeation plasticization pressure. The argument could be made that a critical dilation would be necessary for permeation plasticization, and this may be consistent with the observations of Bos *et al.* since the dilation would likely correspond to the concentration of CO_2 if the same molar volume is assumed for CO_2 in all polymers tested. Dilation measurements under high pressure CO_2 would have to be performed for all of these polymers to test this hypothesis.

Figure 2.3 illustrates a shift in the free volume of a glassy polymer caused by a sorbing penetrant based on positron annihilation lifetime spectroscopy (PALS) measurements made *in situ* with CO_2 sorption over a range of pressures [13-15]. It is hypothesized that this shift in the free volume *distribution* is more important in facilitating an increase in the diffusion coefficient than added flexibility, and this hypothesis is supported by the above discussion regarding previous experimental studies. This concept will be discussed further in Chapters 5 and 6 with regard to the observed experimental data.

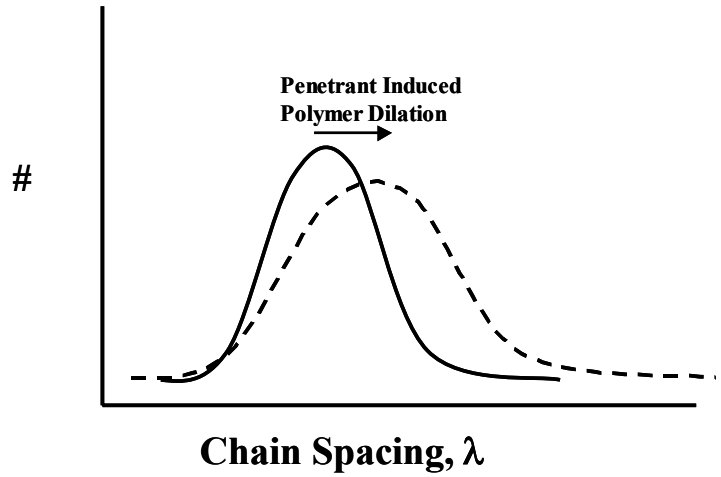

Figure 2.3. Shift of polymer chain spacing distribution upon dilation due to penetrant sorption.

2.3 TEMPERATURE DEPENDENCE OF PERMEABILITY

The temperature dependence of permeability for a given set of feed partial pressures is typically represented by an Arrhenius relationship:

$$P = P_o \, exp\left[\frac{-E_p}{RT}\right] \tag{2.13}$$

where P_o is a pre-exponential factor, E_p is the apparent activation energy for permeation, T is the temperature of permeation, and R is the universal gas constant. The permeability can further be broken up into temperature dependent diffusion and sorption coefficients. The temperature dependence of the penetrant

diffusion coefficient can also be represented by an Arrhenius relationship [16, 17].

$$D = D_o exp\left[\frac{-E_d}{RT}\right] \tag{2.14}$$

Again D_o is a pre-exponential factor, and E_d is the activation energy for diffusion. The activation energy for diffusion represents the energy required for a penetrant to diffuse or "jump" from one site within the matrix to another site. The activation energy is related to the size of the penetrant, the rigidity of the polymer chain, as well as polymeric chain packing. The temperature dependence of sorption in polymers can be described using a thermodynamic van't Hoff expression [1]:

$$S = S_o \exp\left[\frac{-H_s}{RT}\right] \tag{2.15}$$

where S_o is a pre-exponential factor, and H_s is the apparent heat of sorption as it combines the temperature dependence of sorption in both the Henry's law and Langmuir regions.

From transition state theory [18] the pre-exponential for diffusion can be represented by

$$D_o = e\lambda^2 \frac{kT}{h} \exp\left[\frac{S_d}{R}\right] \tag{2.16}$$

Here, S_d is the activation entropy, λ is the diffusive jump length, k is Boltzmann's constant, and h is Planck's constant. Substituting (2.16) into (2.14) (neglecting small differences in the jump length of similarly sized penetrants) results in the diffusive selectivity as the product of energetic and entropic terms:

$$\frac{D_A}{D_B} = \exp\left[\frac{-\Delta E_{d,A,B}}{RT}\right]\exp\left[\frac{\Delta S_{d,A,B}}{R}\right] \qquad (2.17)$$

The diffusive selectivity will be based on both the difference in activation energy for both penetrants, ΔE_d, as well as the difference in activation entropy for both penetrants, ΔS_d. These items will be discussed in the next section.

2.4 STRUCTURE-PROPERTY RELATIONSHIPS OF RIGID POLYMERIC MATERIALS

Previous researchers have examined rigid polypyrrolone materials for other gas separations, such as O_2/N_2 and CO_2/CH_4. Walker, Zimmerman, and Koros have studied structure-property relationships for polypyrrolone copolymers [7, 19]. Permeation results are shown in Figure 2.4 for O_2/N_2 separation over a variety of polypyrrolone materials. It is clear that all of the polymers reside on or above Robeson's 1991 upper bound limit [20] and exhibit separation properties superior to those of conventional polymeric materials, and that is why these ultra-rigid polymers have been termed "pseudo molecular sieves." The reason for the high-quality separation properties of these polymers is believed to be the

combination of ultra chain rigidity and increased inter-chain spacing. Figure 2.5 illustrates an idealized picture of the poly(pyrrolone-imide) materials examined in the work here. It is believed that these materials differ from conventional polymeric materials because only subtle segmental motions are involved in the activated diffusion jump. This is more similar to molecular sieving materials, such as carbons and zeolites, where the selective pores are "frozen" within the structure. Furthermore, entropic selectivity plays a major role in the ability to discriminate between similarly sized molecules, and these effects will be discussed further below.

The concept of entropic selectivity has been discussed by Koros, and this topic has been explored in a variety of membrane materials. The entropic selectivity is defined as the second term in equation (2.17), and coupled with the product of the energetic selectivity, makes up the diffusivity selectivity. Clearly, the energetic and entropic terms are equally important in determining the overall diffusivity selectivity; however, the entropic effects are often times ignored.

Singh-Ghosal and Koros have demonstrated the significance of the entropic selectivity for gas separation membranes using the O_2/N_2 separation as a case study. For seven families of polymers studied the O_2/N_2 energetic selectivity or the energetic contribution to the diffusivity selectivity varied from 4.3 to 435 [21]. The entropic selectivity varied from 0.01 to 1.11, rarely providing any enhancement to the overall separation. In the case of 4A zeolites and carbon

molecular sieves the O_2/N_2 energetic selectivity is 7.1 and 5.1, respectively, which is not greater than that of the polymers [22]. The entropic selectivity for these molecular sieves, however is 14.7 for 4A zeolite, and 4.9 – 8.8 for the carbon membrane materials. Clearly, the enhancement in entropic selectivity is a major factor in the superior transport properties of the zeolites and carbon molecular sieves.

Zimmerman and Koros have recently demonstrated that it is possible for carefully tuned polymeric materials to exhibit entropic selectivities greater than unity [23]. The polypyrrolones 6FDA-TAB and 6FDA/PMDA-TAB(50/50) show O_2/N_2 entropic selectivities of 1.4 and 2.3, respectively. The value for the (50/50) copolymer is the highest polymeric entropic selectivity reported to date (for O_2/N_2 separation), indicating that the matrix structure approaches that of a molecular sieving material.

Some debate has arisen as to whether the polymer rigidity or the "bottleneck" morphology is more important in achieving an enhancement in entropic selectivity. Rallabandi, Thompson, and Ford have conducted simulations using molecular models and transition-state theory using atactic polypropylene, and rigid dumbbells to model O_2 and N_2 molecules [24]. The results showed that while increasing polymer rigidity played a large role in larger energetic selectivities, increased rigidity alone did not improve entropic barriers to diffusion. This lends support to the hypothesis postulated by Zimmerman and

Koros that rigid polymers with carefully regulated "open" and selective "bottleneck" regions are necessary to adequately alter the degrees of freedom of a penetrant molecule in the activated state, and thereby enhance the entropic selectivity.

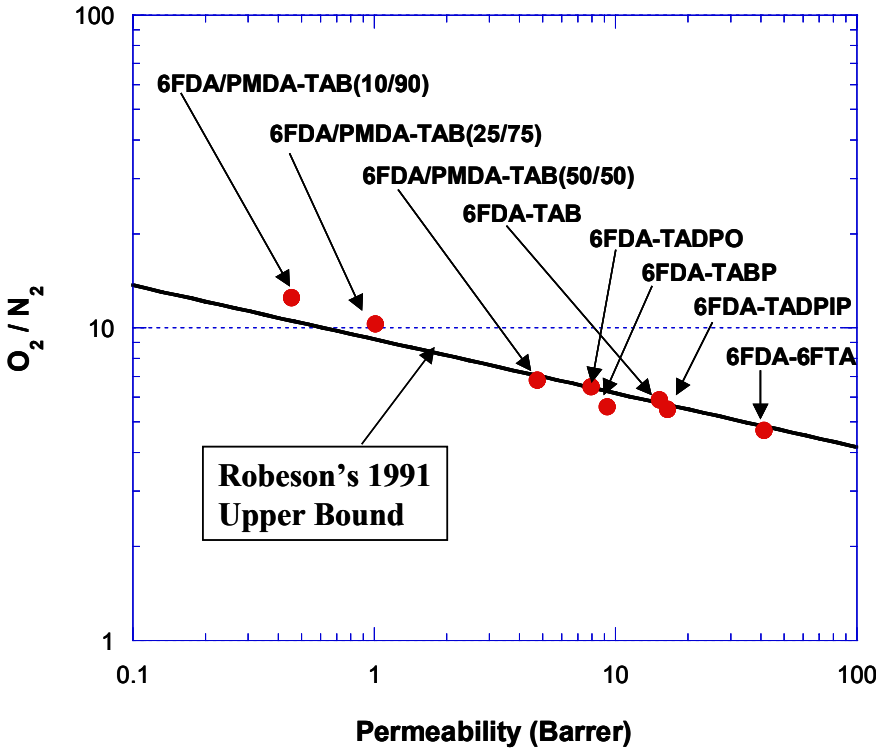

Figure 2.4. Previous polypyrrolone O_2/N_2 results plotted on Robeson's 1991 "upper bound" trade-off curve.

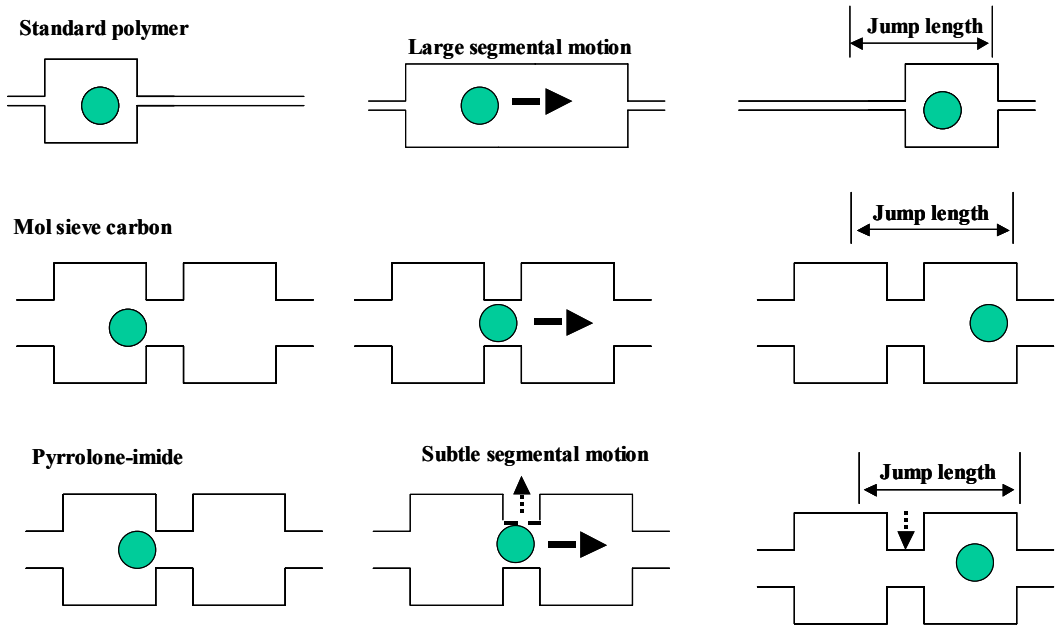

Figure 2.5. Idealized illustration of penetrant diffusive jumps in ultra-rigid poly(pyrrolone-imide) polymers.

2.5 REFERENCES

[1] J. Crank and G. S. Park, Diffusion in polymers, Academic Press, London, 1968.

[2] J. H. Petropoulos, Quantitative analysis of gaseous diffusion in glassy polymers, J. Polymer Sci. Part A-2 8 (1970) 1797-1801.

[3] W. R. Vieth and K. J. Sladek, A model for diffusion in a glassy polymer, J. Colloid Sci. 20 (1965) 1014-1033.

[4] W. J. Koros, A. H. Chan and D. R. Paul, Sorption and transport of various gases in polycarbonate, J. Membr. Sci 2 (1977) 165-190.

[5] D. R. Paul and O. M. Ebralima, Hydraulic permeation of liquids through swollen polymeric networks .3. Generalized correlation, J. Appl. Polym. Sci. 19 (1975) 2759-2771.

[6] H. D. Kamaruddin and W. J. Koros, Some observations about the application of Fick's first law for membrane separation of multicomponent mixtures, J. Membr. Sci. 135 (1997) 147-159.

[7] D. R. B. Walker, Synthesis and characterization of polypyrrolones for gas separation membranes, Ph.D. Dissertation, The University of Texas at Austin, 1993.

[8] M. Wessling, Relaxation phenomena in dense gas separation membranes, The University of Twente, 1992.

[9] D. F. Cadogan and C. J. Howick, in: Kirk-othmer encyclopedia of chemical technology, John Wiley and Sons, Inc, 1996.

[10] E. S. Sanders, Penetrant-induced plasticization and gas permeation in glassy polymers, J. Membr. Sci. 37 (1988) 63-80.

[11] A. Bos, I. G. M. Punt, M. Wessling and H. Strathmann, CO_2-induced plasticization phenomena in glassy polymers, 155 (1999) 67-78.

[12] J. D. Wind, Improving polyimide membrane resistance to CO_2 plasticization in natural gas separations, Ph D. Dissertation, The University of Texas at Austin, 2002.

[13] X. Hong, Y. C. Jean, H. J. Yang, S. S. Jordan and W. J. Koros, Free-volume hole properties of gas-exposed polycarbonate studied by positron annihilation lifetime spectroscopy, Macromolecules 29 (1996) 7859-7864.

[14] J. P. Yuan, H. Cao, E. W. Hellmuth and Y. C. Jean, Subnanometer hole properties of CO_2-exposed polysulfone studied by positron annihilation lifetime spectroscopy, J. Polym. Sci. Pt. B-Polym. Phys. 36 (1998) 3049-3056.

[15] Y. Ito, H. F. M. Mohamed, K. Tanaka, K. Okamoto and K. Lee, Sorption of CO_2 in polymers observed by positron annihilation technique, J. Radioanal. Nucl. Chem.Artic. 211 (1996) 211-218.

[16] R. Barrer, Nature of the diffusion process in rubber, Nature 140 (1937) 106.

[17] V. Stannet, in: Diffusion in polymers, Academic Press, New York, 1968.

[18] K. J. L. S. Glasstone, H. Eyring, The theory of rate processes, 1st ed, McGraw-Hill Book Co., Inc., New York, 1941.

[19] C. M. Zimmerman and W. J. Koros, Polypyrrolones for membrane gas separations. I. Structural comparison of gas transport and sorption properties, J. Polym. Sci. Part B 37 (1999) 1235-1249.

[20] L. M. Robeson, Correlation of separation factor versus permeability for polymeric membranes, J. Membr. Sci. 62 (1991) 165-185.

[21] A. Singh-Ghosal and W. J. Koros, Energetic and entropic contributions to mobility selectivity in glassy polymers for gas separation membranes, Ind. Eng. Chem. Res. 38 (1999) 3647-3654.

[22] A. Singh and W. J. Koros, Significance of entropic selectivity for advanced gas separation membranes, Ind. Eng. Chem. Res. 35 (1996) 1231-1234.

[23] C. M. Zimmerman and W. J. Koros, Entropic selectivity analysis of a series of polypyrrolones for gas separation membranes, Macromolecules 32 (1999) 3341-3346.

[24] P. S. Rallabandi, A. P. Thompson and D. M. Ford, A molecular modeling study of entropic and energetic selectivities in air separation with glassy polymers, Macromolecules 33 (2000) 3142-3152.

CHAPTER 3: MATERIALS AND EXPERIMENTAL PROCEDURE

3.1 MONOMERS INVESTIGATED

All polymers investigated incorporated a dianhydride and at least one diamine or tetraamine. In most cases the dianhydride used was 4,4'-(hexafluoroisopropylidene) diphthalic anhydride (6FDA). This monomer has been incorporated in many polyimides and polypyrrolones in the past, and it is often found to help provide excellent transport properties. The bulky CF_3 groups provide "molecular spacers", which are necessary to tune the free volume distribution of the polymer.

Trimethylphenylinediamine (TrMPD) or diaminomesitylene (DAM) is a diamine, which has also been used previously in polyimide membrane materials. In this case the methyl groups provide molecular spacers within the matrix. 1,2,4,5-tetraaminobenzine (TAB) has also been used previously in polypyrrolone materials [1-3]. This monomer is flat, packs efficiently, and also provides rigidity to the polymer matrix.

Another diamine that was studied with the intent of providing molecular spacers within the matrix was 4,4' (hexafluoro-isopropylidene) dianiline (6FpDA). Incorporating this monomer within the polymer structure is similar to the DAM monomer, and therefore an additional synthesis procedure will not be outlined for this case. The monomer 3,3'-dimethyl-4,4'diaminophenyl

(33'DMDB) was also used to form a polyimide, and this will be discussed in Chapter 4. The structures of these monomers are shown in Table 3.1.

Table 3.1. Monomers studied in this work.

6FDA	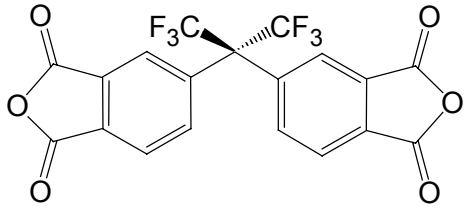
TAB	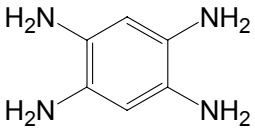
DAM(TrMPD)	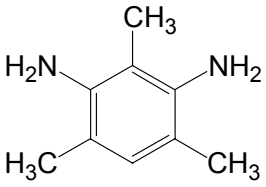
33'DMDB	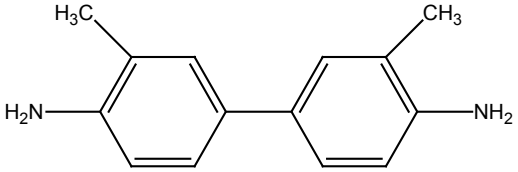
6FpDA	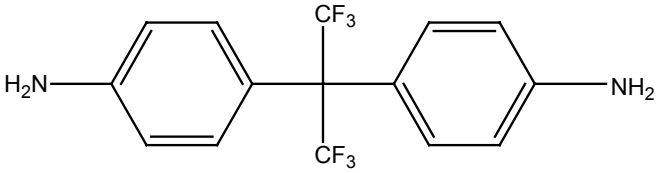

3.2 POLYMERIC MATERIALS STUDIED

3.2.1 6FDA-TAB/DAM Polymer Synthesis

The initial step of the synthesis procedure is monomer purification. The 6FDA was obtained from Hoechst Celanese and purified by sublimation under vacuum at 220 - 235^{o}C. The DAM monomer was purchased from Aldrich and purified by sublimation under vacuum at 85 - 90^{o}C. The cold finger of the sublimator was kept approximately 80 – 100^{o}C below the sublimation temperature. The TABH monomer was purchased from Aldrich and purified via recrystalization using activated carbon. The exact procedure has been provided previously [4].

The synthesis procedure for 6FDA-TAB/DAM poly(pyrrolone-imide) copolymer is outlined here. The process is slightly modified from the synthesis of a pure polypyrrolone, and many protocols have been published previously [5-10]. Zimmerman has developed a procedure for the synthesis of the pure polypyrrolone used here, 6FDA-TAB [4]. Prior to polymerization the glassware was dried under vacuum overnight at 150^{o}C in order to remove adsorbed water. Molecular sieves (4A) were activated by heating at 200^{o}C in vacuum for at least 8 hours. Anhydrous N,N-dimethylacetamide (DMAc) and pyridine were purchased from Aldrich packaged in Sure Seal® bottles. The DMAc and pyridine were dried for 12 hours prior to polymerization over the activated molecular sieves

under an inert (either argon or nitrogen) blanket. All solvents were transferred using transfer needles connected by Teflon tubing. The three purified monomers were dried under vacuum overnight at 50^{o}C.

The synthesis procedure for 6FDA-TAB/DAM(50/50) poly(pyrrolone-imide) copolymer is detailed below. In order to synthesize additional TAB/DAM copolymer compositions the monomer stoichiometry should be adjusted accordingly. All polymerization steps were done under an inert purge with continuous stirring of the reactor (through either a motorized mixer or a magnetic stir bar). The glassware (shown in Figure 3.1) was assembled and flamed with a propane torch in order to remove additional moisture. Dry TABH (3.6987 g) was added to the reaction vessel followed by approximately 100 mL DMAc. Pyridine (46 mL) was added via a syringe and the solution became orange. DAM (2.1150 g) was dissolved in approximately 50 mL DMAc, and stirred in a 100 mL round bottom flask for at least 20 minutes under an inert blanket. The mixture was then added directly to the reaction vessel through transfer needles. The empty flask was rinsed twice with 25 mL portions of DMAc and then transferred directly to the reaction vessel. 6FDA (11.5700 g) was dissolved in approximately 50 mL DMAc, and stirred in a 100 mL round bottom flask for at least 20 minutes under an inert blanket. The 6FDA mixture was transferred to the dropping funnel and added to the reaction vessel at a rate of 15 drops / minute. The 6FDA flask was rinsed twice with approximately 25 mL of DMAc, and added to the dropping

funnel. After final 6FDA addition, the reaction mixture was stirred under an inert purge for at least 36 hours. The polymer precursor was then precipitated into chloroform (which also acts as a solvent for the pyridine hydrochloride salt byproduct), and broken up in a blender. The polymer was filtered through a glass fritted funnel and washed several times with chloroform in order to remove the pyridine. The resulting polymer was dried under vacuum at no more than 50^{o}C for 2 days. The reaction mechanism for the polymer synthesis is shown in Figure 3.2.

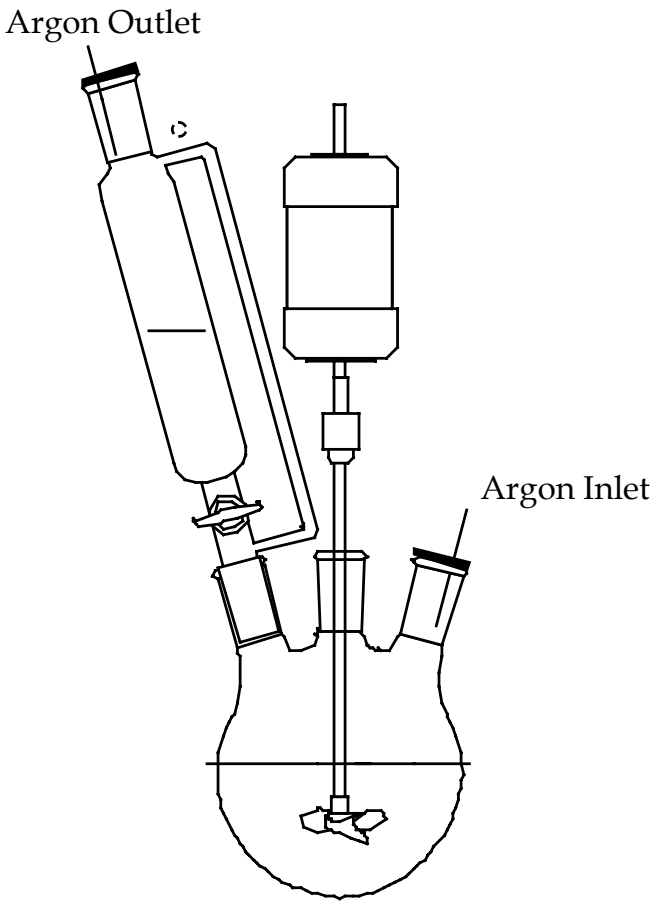

Figure 3.1. Synthesis Apparatus used for polycondensation reactions.

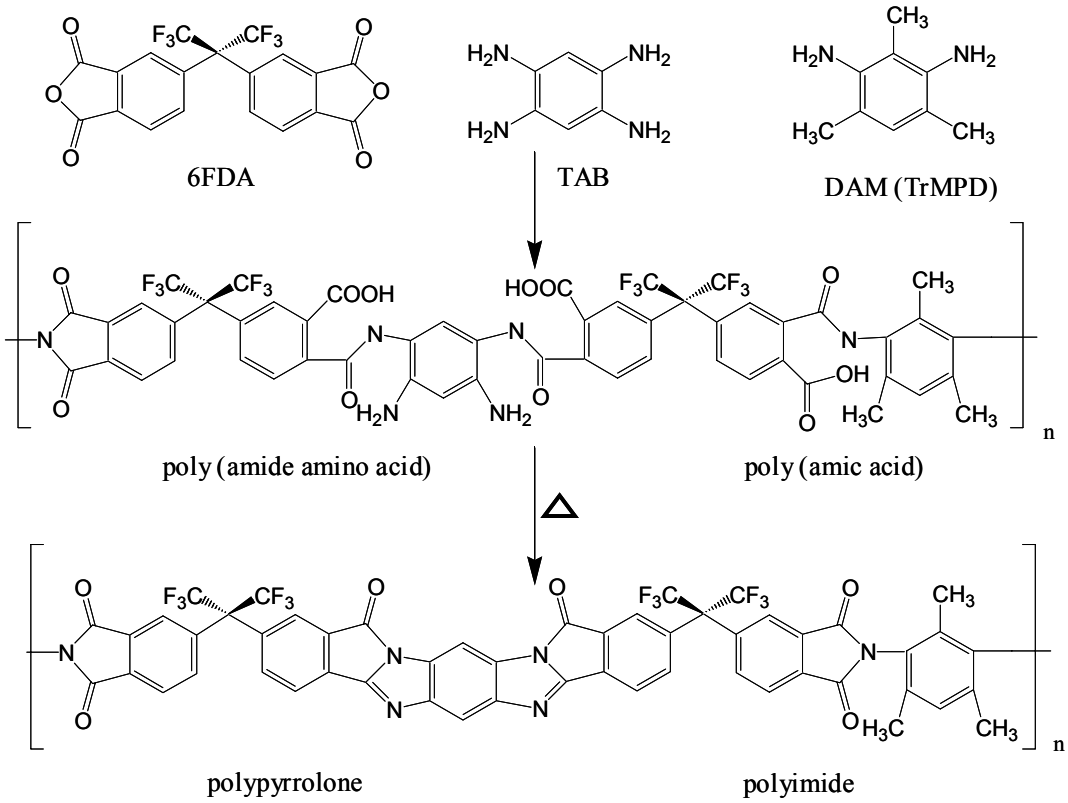

Figure 3.2. Poly(pyrrolone-imide) synthesis reaction.

3.2.2 Polyimides Studied

In addition to the poly(pyrrolone-imides) detailed in the previous section, a few select polyimides were also examined in this study. Matrimid® was provided by MEDAL, L.P. (Newport, DE) in powder form and cast into a membrane film with dicloromethane as the casting solvent using the procedure outlined in section 3.3. The chemical structure is shown in Table 3.2.

Table 3.2. Additional polyimides studied in this work.

Matrimid®	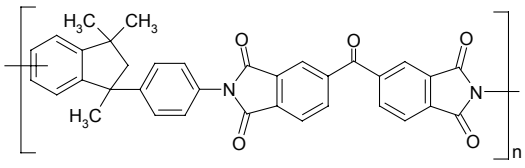
6FDA-33'DMDB	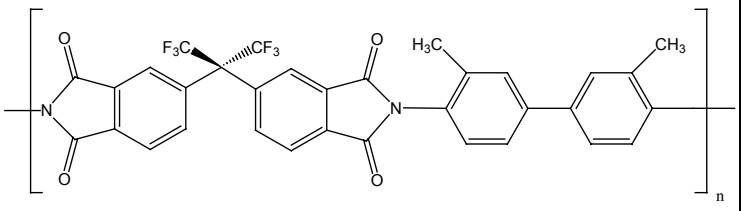

The polyimide 6FDA-33'DMDB was also studied for the C_3H_6/C_3H_8 separation, and the structure of this material is shown in Table 3.2. This polymer was synthesized and dense films were cast using the exact procedure reported previously [11, 12]. Motivation for studying this polymer and specific results will be discussed in Chapter 4.

3.3 FILM CASTING TECHNIQUES

Films of the precursor poly(pyrrolone-imide) copolymer were cast in a conventional manner and the entire procedure was done in the fume hood. The appropriate amount of polymer was dissolved in dry dimethylacetamide to form a 1 – 2 wt % solution. This solution was stirred for at least 20 minutes before filtering the solution with a 0.2 micron Teflon® syringe filter or alternatively

filter paper from Fisher Scientific of medium porosity. The filtered solution was dispensed on a clean, level Teflon® dish set on a hot plate. The dish was quickly covered with a casting funnel to control the rate of solvent removal. The hot plate was then set to 80°C surface temperature, and film formation generally occurred in under 8 hours. The films were then removed and placed in the vacuum oven at 100°C for at least 12 hours to ensure complete solvent removal. The films were then placed between two Teflon® plates to prevent curling during the ring closure heat treatment. The film "sandwich" was placed in the vacuum oven and slowly heated to 300°C over a period of 10 - 12 hours. The film was maintained at 300°C for 24 hours, and then slowly cooled to room temperature over a period of 12 – 24 hours.

3.4 PERMEATION

For all permeation experiments conducted the constant volume method was employed, which utilizes a high pressure upstream and a vacuum downstream, and this method has been described previously [15]. A diagram of the permeation system is provided in Figure 3.3 and a photograph is shown in Figure 3.4. The downstream rise in pressure is monitored over the fixed downstream volume to determine the overall gas throughput. Combining this with the membrane thickness, exposed area, and pressure driving force allows for calculation of the permeability coefficient. The permeability (P_A) was calculated from

$$P_A = \frac{\left(2.942x10^4\right)\left(\frac{dP}{dt} - leak\ rate\right) V\ \ell}{T\ A\ \Delta p_A} \qquad (3.1)$$

where (dP/dt) is the permeation rate through the membrane (torr/min), V is the calibrated downstream permeate volume (cm^3), ℓ is the membrane thickness (mils), T is the temperature (K), A is the permeation area of the film (cm^2), and Δp_A is the pressure or fugacity driving force (psi), which is simply the upstream feed condition since the downstream is under vacuum. Film thickness measurements were made using a micrometer. The permeation area of the films was determined using Scion Image® software. Gases measured include O_2, N_2, CO_2, CH_4, C_3H_6 and C_3H_8. Ultra-high purity (99.99 %) O_2, N_2, and CO_2 were used, and CP grade CH_4, C_3H_6 and C_3H_8 were used. A discussion of acceptable leak rates and time lags for the experiments is provided in Appendix B.

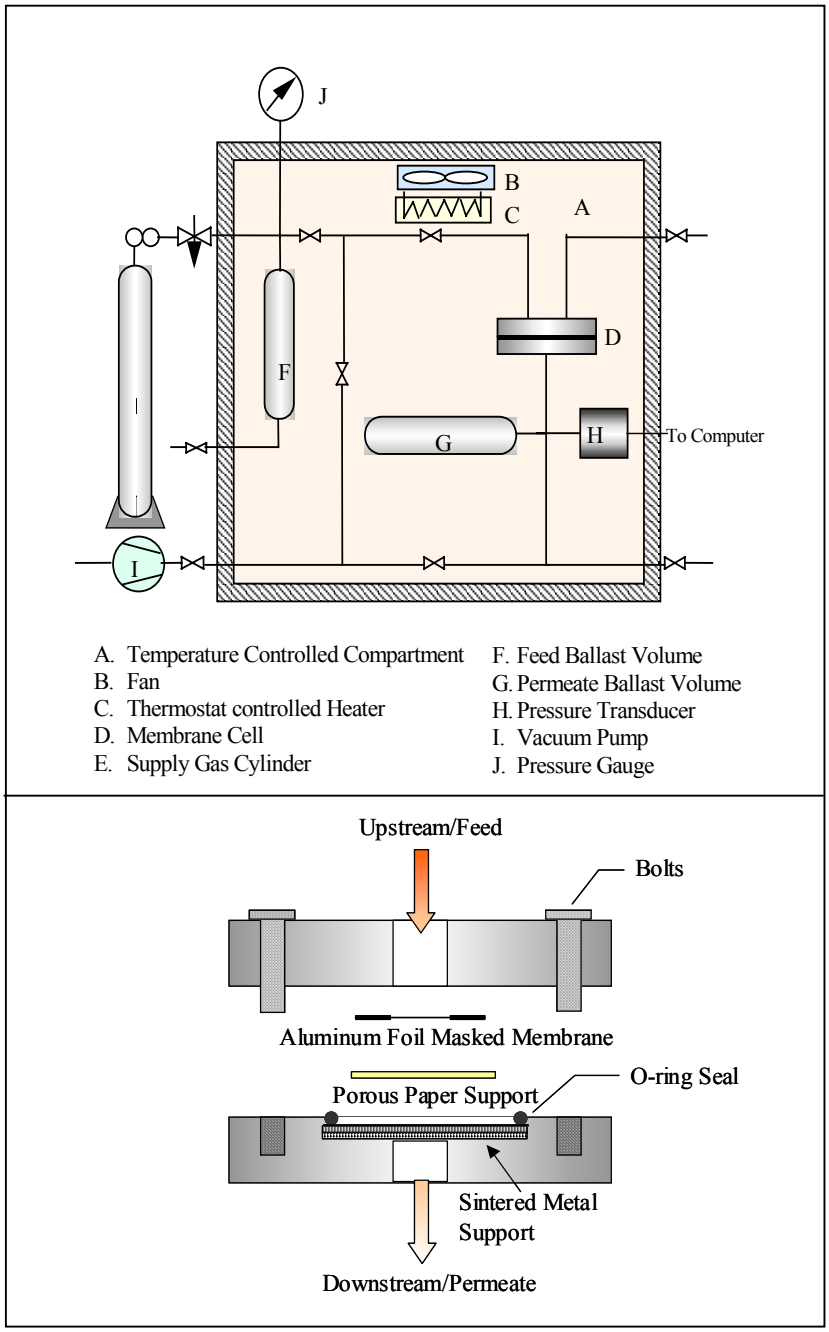

Figure 3.3. Diagram of constant volume permeation apparatus and permeation cell.

Figure 3.4. Photograph of the high temperature permeation apparatus.

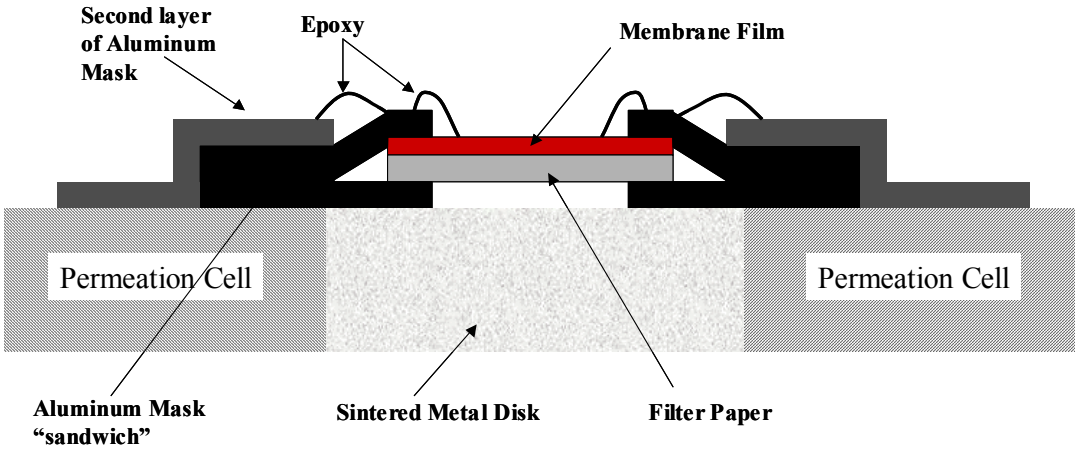

Figure 3.5. Alternative polymeric membrane masking technique for rigid polymers.

Mixed gas permeation measurements are conducted in the same manner as pure gas measurements with a few minor differences. The gas mixtures used were 50% propylene / 50% propane obtained from either Praxair or Air Liquide. The feed gas is swept over the membrane using less than a 1% stagecut (ratio of permeate flow / feed flow) to ensure a constant composition on the upstream side. This is verified using a bubble flow meter at the outlet of the feed line. Once a steady-state has been achieved, the sample is collected in the downstream volume, and the permeation rate is measured. After a sufficient pressure is achieved in the downstream volume, the sample is sent to the GC (HP 5880) loop, and automatically injected. The GC is equipped with a TCD detector, and an HP-Plot / Al_2O_3 (30m) column.

A new membrane masking technique was employed that can be used for the measurement of rigid materials, which are able to fracture if not handled properly. This technique is shown in Figure 3.5. The technique was developed by Cathy Zimmerman and Zen Mogri. The membrane film was masked using the conventional aluminum masking technique with filter paper for support. Then this was sealed in a single o-ring cell using an additional solitary piece of aluminum tape. Five-minute epoxy obtained from Devcon was applied to the membrane-mask interface and the aluminum/aluminum interface. The lower flange of the permeation cell was then attached to a permeation system, and vacuum was pulled to ensure a good membrane seal. Defects in the membrane or the mask were detected by placing a layer of laytex over the area of interest. If defects exist the laytex will be pulled into the defect sealing it to vacuum, and this

area will appear darker. Additional epoxy can then be applied to this area permanently sealing the defect. This procedure is outlined in more detail in Appendix D.

3.5 SORPTION

Gas sorption measurements were conducted on polymeric materials using a dual-volume sorption apparatus previously described in detail [16] and similar to those described previously in the literature [17]. Gases measured included O_2, N_2, CO_2, CH_4, C_3H_6 and C_3H_8, and ultra-high purity (99.99 %) gases were used in all cases. The dual-volume system is depicted in Figure 3.6 and consists of a reservoir and a cell (where the polymer sample is placed), which rest in a controlled temperature bath. A photograph is shown in Figure 3.7. The entire system is evacuated before the reservoir is charged with feed gas. The reservoir is allowed to reach equilibrium with the bath temperature before expanding into the cell. Monitoring the pressures, allowing the cell to reach equilibrium, and performing a mole balance allows for the calculation of the concentration of gas within the polymer sample. Sorption isotherms were created by continually stepping up the pressure throughout the experiment.

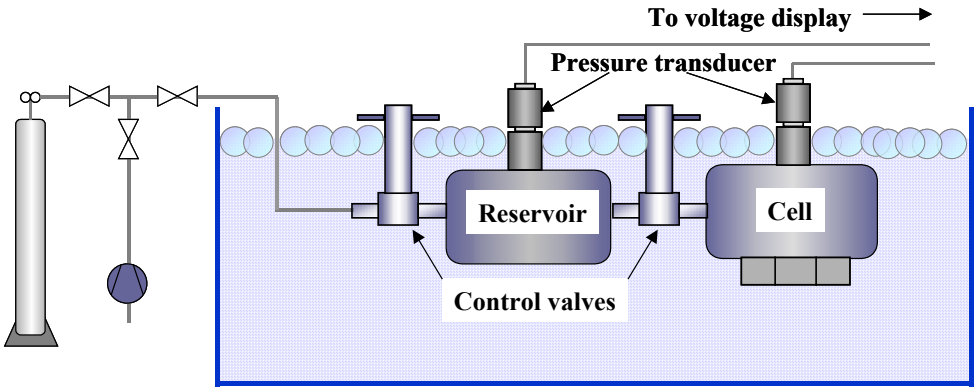

Figure 3.6. Diagram of pressure-decay sorption system.

Figure 3.7. Photograph of pressure-decay sorption bath and voltage display.

3.6 CHARACTERIZATION

3.6.1 Ellipsometry

Ellipsometry has the capability of determining the thickness and optical constants of thin films. This capability is advantageous for dynamic measurements in which both the thickness and index of refraction do not remain constant. In this case, the thickness of a thin polymer film was monitored as a function of temperature in order to determine the thermal expansion coefficient. A brief description of ellipsometry follows.

Ellipsometry is a technique that measures the change in the polarization state of light. The measurement is sensitive to the changes linearly polarized light undergoes after reflecting off a planar sample. Figure 3.8 illustrates this concept with a simplified schematic. The p plane represents the plane of the reflection, and the s plane represents the plane perpendicular to the reflection. Ellipsometry essentially measures two parameters, known as psi (Ψ) and delta (Δ). Delta is the difference in phase between the p and s planes of the reflected light and the incident light:

$$\Delta = (d^{r}{}_{p} - d^{r}{}_{s}) - (d^{i}{}_{p} - d^{i}{}_{s}) \tag{3.2}$$

The angle, Ψ, is defined by the amplitude ratios before and after reflection from a sample:

$$\tan\psi = \frac{A_p^r / A_s^r}{A_p^i / A_s^i} \tag{3.3}$$

The ellipticity, ρ, is the ratio of the Fresnel reflection coefficients, R_p and R_s, and is a function of Ψ and Δ according to the following equation:

$$\rho = \frac{R_p}{R_s} = \tan(\psi)e^{i\Delta} \tag{3.4}$$

The ellipticity is also a function of the wavelength of light, λ, the angle of incidence, Φ, the refractive index of the ambient, n_o, the refractive index of each layer, n_i, the thickness of each layer, h_i, and the complex refractive index of the substrate, N_k. Assuming all other parameters are known, the two unknown parameters of the sample (the refractive index and the thickness) can be determined through the measurement of Ψ and Δ. Multiple references exist which can provide a similar introduction to ellipsometry and significantly more detail, however, the references listed here provide an overview of what is available in the literature [18-20].

Experiments in this study were carried out with a J.A. Woollam M-2000 Variable Angle Spectroscopic Ellipsometer (Figure 3.9) equipped with a programmable hotplate. The incident angle was 70^o, and the wavelength range was 500 - 1000 nm. All of the measurements were conducted with the help and guidance of Sean Burns. Ellipsometry was used to measure the thermal expansion coefficient of poly(pyrrolone-imide) films coated on a silicon wafer. The linear coefficient of thermal expansion is defined as:

$$\beta = \frac{1}{L}\left(\frac{\partial L}{\partial T}\right) \tag{3.5}$$

For the experiments conducted here, it is assumed that the expansion is isotropic in the vertical direction.

All polymer samples were spun coat onto a silicon wafer. The wafers were soaked in a solvent bath of dimethylacetamide, rinsed with deionized water and acetone, blown dry with a nitrogen or air purge, baked on a hot plate at ~ 110^{o}C, and subsequently cooled before spin coating. With the exception of the polyimide, 6FDA-DAM, the polymer *precursors* were spun coat onto the Si wafer. All polymers were filtered through a 0.45 μm Teflon filter. The specific spinning conditions varied slightly from polymer to polymer, and are given in Table 3.3. The spinning parameters used were determined on a trial and error basis, established by those conditions that provided suitable films for testing. Film suitability was determined by visual inspection of uniformity and roughness, inspection under a profilometer, and a thickness measurement using a spectroscopic scan under the ellipsometer. Once a polymer film was determined to be suitable for further measurement, the coated film was cured using a vacuum heat treatment up to 300^{o}C. The films were heated for 12 – 24 hours and subsequently cooled for 12 – 24 hours. The exception to this procedure was the 6FDA-DAM polyimide, which was spun in the final imidized state. This film

was then dried at ~ 170°C under vacuum for 12 – 24 hours in order to remove any residual solvent.

Table 3.3. Conditions for spin coating polymeric precursor films onto Si wafers for ellipsometry measurements. *Note: 6FDA-DAM was coated as a fully imidized polymer.

Polymer precursor	Solvent	Concentration (wt %)	Spin Speed (rpm)	Time (s)
6FDA-TAB	DMAc	5	2500	30
6FDA-TAB/DAM(75/25)	DMAc	6	2500	40
6FDA-TAB/DAM(50/50)	DMAc	5	2500	40
6FDA-DAM*	DMAc	7	2500	30

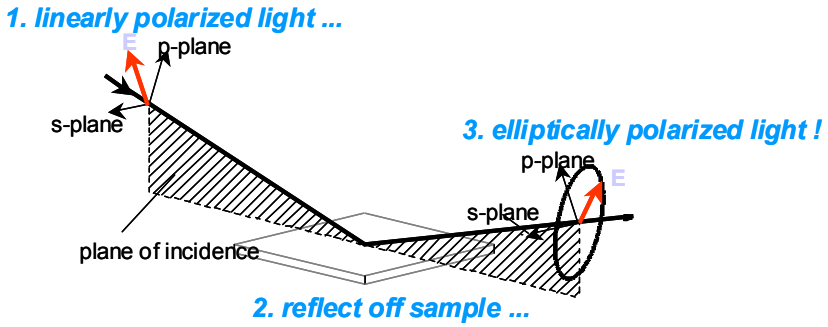

Figure 3.8. Simplified diagram of change in polarization state of light after reflecting off a polymer sample.

Figure 3.9. Photograph of Variable Angle Spectroscopic Ellipsometer (VASE), J.A. Woolam M-2000.

3.6.2 Density

The density of the polymers was measured by means of a Techne™ density gradient column, Model DC-1. The column was prepared with calcium nitrate solution. Calibrated glass beads of known density were immersed in the column and equilibrated over a 12 – 24 hour time period. The position of the beads was then used to generate a linear calibration curve over the density range

of the column. Polymer samples were then submerged and allowed to equilibrate for 24 – 48 hours. All measurements were made at 30°C.

3.6.3 X-ray diffraction

Wide angle x-ray diffraction has been commonly used to provide characterization of the polymeric chain spacing. Measurements were conducted using a Phillips PW 1710 diffractometer with Cu Kα radiation of wavelength 1.54Å. The average intersegmental distance between polymer chains or "d-spacing" is determined through Bragg's law:

$$n\lambda = 2d\sin\theta \qquad (3.6)$$

where n is the order of reflection, λ the x-ray wavelength, and θ is the angle of incidence. Amorphous materials such as polymers examined here show broad peaks due to a lack of long range order. In the past this technique has shown a good qualitative correlation between degree of packing and gas diffusion coefficients for copolymer materials.

3.6.2 DSC Measurements

Glass transition temperatures were measured using dynamic scanning calorimetry with a Perkin-Elmer DSC 7. Glass transition temperatures were determined using the onset method. Heating runs were typically done at 20°C/min up to 560°C.

3.5 REFERENCES

[1] C. M. Zimmerman and W. J. Koros, Polypyrrolones for membrane gas separations. I. Structural comparison of gas transport and sorption properties, J. Polym. Sci. Pt. B-Polym. Phys. 37 (1999) 1235-1249.

[2] C. M. Zimmerman and W. J. Koros, Polypyrrolones for membrane gas separations. II. Activation energies and heats of sorption, J. Polym. Sci. Pt. B-Polym. Phys. 37 (1999) 1251-1265.

[3] C. M. Zimmerman and W. J. Koros, Entropic selectivity analysis of a series of polypyrrolones for gas separation membranes, Macromolecules 32 (1999) 3341-3346.

[4] C. M. Zimmerman, Advanced Gas Separation Membrane Materials: Hyper Rigid Polymers and Molecular Sieve-Polymer Mixed Matrices, Ph.D. Dissertation, The University of Texas at Austin, 1998.

[5] D. R. B. Walker, Synthesis and Characterization of Polypyrrolones For Gas Separation Membranes, Ph.D. Dissertation, The University of Texas at Austin, 1993.

[6] V. L. Bell and R. A. Jewell, Synthesis and properties of polyimidazopyrrolones, J. Polym. Sci., Polym. Chem. Ed. 5 (1967) 3043-60.

[7] F. Dawans and C. S. Marvel, Polymers from ortho Aromatic Tetraamines and Aromatic Dianhydrides, J. Polymer Sci, Part A 3 (1965) 3549-3571.

[8] A. A. Berlin, B. I. Liogon'kii and G. M. Shamraev, Thermostable Polymers from Dianhydrides of Aromatic Tetracarboxylic Acids and Tetra-amines, Russian Chemical Reviews 40 (1971) 284-300.

[9] D. Sek, E. Schab-Balcerzak, E. Grabiec, A. Volozhin and T. Chamenko, New semiladder polymers: III. Synthesis and properties of new poly(etherimidazopyrrolone)s, Polymer. 41 (2000) 49-56.

[10] W. Zhou, X. Gao and F. Lu, Silicon-Containing Polypyrrolone for Gas-Separation Application, J. Applied Polymer Sci. 51 (1994) 855-861.

[11] A. Shimazu, T. Miyazaki, M. Maeda and K. Ikeda, Relationships between the chemical structures and the solubility, diffusivity, and permselectivity of propylene and propane in 6FDA-based polyimides, J. Polym. Sci. Pt. B-Polym. Phys. 38 (2000) 2525-2536.

[12] A. Shimazu, T. Miyazaki, T. Matsushita, M. Maeda and K. Ikeda, Relationships between chemical structures and solubility, diffusivity, and permselectivity of 1,3-butadiene and n-butane in 6FDA-based polyimides, J. Polym. Sci. Pt. B-Polym. Phys. 37 (1999) 2941-2949.

[13] K. Tanaka, M. Okano, H. Toshino, H. Kita and K. I. Okamoto, Effect of Methyl Substituents on Permeability and Permselectivity of Gases in Polyimides Prepared from Methyl- Substituted Phenylenediamines, J. Polym. Sci. Pt. B-Polym. Phys. 30 (1992) 907-914.

[14] K. Tanaka, Y. Osada, H. Kita and K. I. Okamoto, Gas-Permeability and Permselectivity of Polyimides with Large Aromatic Rings, J. Polym. Sci. Pt. B-Polym. Phys. 33 (1995) 1907-1915.

[15] K. C. Obrien, W. J. Koros, T. A. Barbari and E. S. Sanders, A New Technique for the Measurement of Multicomponent Gas Transport through Polymeric Films, J. Membr. Sci. 29 (1986) 229-238.

[16] L. M. Costello and W. J. Koros, Temperature dependence of gas sorption and transport properties in polymers: measurement and applications, Ind. Eng. Chem. Res. 31 (1996) 2708-2714.

[17] W. J. Koros and D. R. Paul, Design considerations for measurement of gas sorption in polymers by pressure decay, J. Polym. Sci., Polym. Phys. Ed. 14 (1976) 1903.

[18] H. G. Tompkins and W. A. McGahan, Spectroscopic Ellipsometry and Reflectometry, John Wiley & Sons, Inc, New York, 1999.

[19] D. Styrkas, S. J. Doran, V. Gilchrist, J. L. Keddie, J. R. Lu, E. Murphy, R. Sackin, T.-J. Su and A. Tzitzinou, Polymer Surfaces and Interfaces III, John Wiley and Sons, New York, 1999.

[20] S. M. Sirard, P. F. Green and K. P. Johnston, Spectroscopic ellipsometry investigation of the swelling of poly(dimethylsiloxane) thin films with high pressure carbon dioxide, J. Phys. Chem. B 105 (2001) 766-772.

CHAPTER 4. DEVELOPING THE C_3H_6/C_3H_8 UPPER BOUND

4.1 MOTIVATION FOR DEVELOPING THE C_3H_6/C_3H_8 UPPER BOUND

In 1991, Robeson published and defined the now well-known upper bound trade-off curves for polymer membranes in various applications, which consist of a log-log plot of ideal selectivity versus permeability for a particular gas pair [1]. Robeson observed that for the gas separations considered there was a linear trade-off on this plot, above which no (or exceptionally few) polymeric materials resided. At that time enough data existed to define these boundaries for a variety of light gas pair separations including O_2/N_2, H_2/CH_4, CO_2/CH_4, He/O_2, as well as other combinations of the same gas molecules. Although permeation data for heavier hydrocarbons through polymer membranes have become more available over the past ten years, no upper bound analysis has yet been established for these cases.

Additionally, for the C_3H_6/C_3H_8 separation, data exists in the literature, which are somewhat questionable, and these data will be discussed further in Section 4.3. Establishing a C_3H_6/C_3H_8 upper bound curve creates both a standard and a challenge for the community in terms of what future material research should aim to overcome. The overall goal of this chapter is to present and define the upper bound relationship for the C_3H_6/C_3H_8 separation by considering a

comprehensive review of the literature in addition to measurements reported herein.

4.2 EXPERIMENTAL C_3H_6/C_3H_8 UPPER BOUND

An upper bound plot for the C_3H_6/C_3H_8 separation was constructed using available data in the literature and measurements reported herein from 26 – 100^oC, and from 2 – 4 atm feed pressure [2-7]. This data is compiled in Table 4.1 and plotted in Figure 4.1. Table 4.2 includes a key of chemical names corresponding to abbreviations found in Table 4.1, and elsewhere throughout the chapter. Unless otherwise noted, all of the data presented in Figure 4.1 are based on pure gas measurements at steady-state using dense films under low pressure feed stream conditions and a vacuum on the downstream side, where permeation plasticization effects can be assumed to be minimal or non-existent. Two of the data points presented in Table 4.1 and Figure 4.1 are based on measurements reported herein on the polyimides Matrimid® and 6FDA-33'DMDB. The C_3H_6/C_3H_8 selectivity for Matrimid® differs slightly from that reported by Bos *et al.*, however the measurements are at two different temperatures and it is understandable that the C_3H_6/C_3H_8 selectivity is higher at the lower temperature. This temperature difference coupled with any experimental error provides a reasonable explanation for the difference between these measurements.

Table 4.1. C_3H_6/C_3H_8 permeation data used for development of the upper bound curve.

Ref #	Author	Polymer	Temp (^oC)	Feed Pressure	P_{C3H6} (Barrer)	C_3H_6/C_3H_8 Selectivity
[4]	Krol *et al.*	Matrimid®	26 ± 2	2 – 3 bar [8]	0.10	16
[4]	Krol *et al.*	Matrimid®-Thermid 85/15	26 ± 2	2 – 3 bar [8]	0.03	4
[4]	Krol *et al.*	Pyralin 2566	26 ± 2	2 – 3 bar [8]	0.09	21
[4]	Krol *et al.*	Torlon AI-10	26 ± 2	2 – 3 bar [8]	< 0.02	-
[6]	Bai *et al.*	PPO	30 ± 2	2 - 4 bar	9	4.25
[5]	Sridhar and Khan	EC	30 ± 2	3 – 3.9 atm	52 [a]	3.25 [a]
[5]	Sridhar and Khan	CA	30 ± 2	3 – 3.9 atm	15.2 [a]	2.6 [a]
[5]	Sridhar and Khan	PSF	30 ± 2	3 – 3.9 atm	25 [a]	1.4 [a]
[3]	Staudt-Bickel and Koros	6FDA-mPD	35	3.8 atm	0.13	10
[3]	Staudt-Bickel and Koros	6FDA-IpDA	35	3.8 atm	0.58	15
[3]	Staudt-Bickel and Koros	6FDA-6FpDA	35	3.8 atm	0.89	16
	This Study	Matrimid®	35	2 atm	0.10	10
	This Study	6FDA-33'DMDB	35	1.1 atm	0.15	13.2
[2]	Tanaka *et al.*	6FDA-TeMPD	50	2 atm	37	8.6
[2]	Tanaka *et al.*	6FDA-TrMPD	50	2 atm	30	11
[7]	Okamoto *et al.*	6FDA-DDBT	50	2 atm	1.8	20
[2]	Tanaka *et al.*	6FDA-DDBT	50	2 atm	0.76	27
[2]	Tanaka *et al.*	BPDA-TeMPD	50	2 atm	3.2	13
[2]	Tanaka *et al.*	PPO	50	2 atm	2.3	9.1
[2]	Tanaka *et al.*	P4MP	50	2 atm	54	2
[2]	Tanaka *et al.*	1.2PB	50	2 atm	260	1.7
[2]	Tanaka *et al.*	PDMS	50	2 atm	6600	1.1
[2]	Tanaka *et al.*	6FDA-ODA	100	2 atm	0.48	11

[a] mixed gas results: 55 % propylene / 45 % propane feed

Table 4.2. List of abbreviations and chemical names.

Abbreviation	Chemical Name
6FDA	4,4'-(hexafluoroisopropylidene) diphthalic anhydride
6FpDA (BAAF)	4,4' (hexafluoro-isopropylidene) dianiline
TrMPD (DAM)	trimethylphenylinediamine
DDBT	dimethyl-3,7-diaminodiphenylthiophene-5,5-dioxide
33'DMDB	3,3'-dimethyl-4,4'diaminophenyl
Matrimid® (BTDA-DAPI)	3,3',4,4'-benzophenone tetracarboxylic dianhydride and 5(6)-amino-1-(4'aminophenyl)-1,3-trimethylindane
BPDA	3,3',4,4'-biphenyltetracarboxylic dianhydride
mPD	1,3-phenylenediamine
IPDA	4,4'-(isopropylidene) dianiline
ODA	4,4'-oxydianiline
TeMPD	2,3,5,6-Tetramethyl-1,4-phenylenediamine
1.2PB	1,2-polybutadiene
PDMS	polydimethylsiloxane
EC	ethylcellulose
CA	cellulose acetate
PSF	polysulfone
P4MP	poly(4-methylpentene-1-co-α-olefin)
Thermid®	6FDA based oligomer
Torlon® AI-10	poly(amide-imide) precursor as supplied (subsequently imidized)
Pyralin 2566	polyimide precursor based on 6FDA-ODA (subsequently imidized)

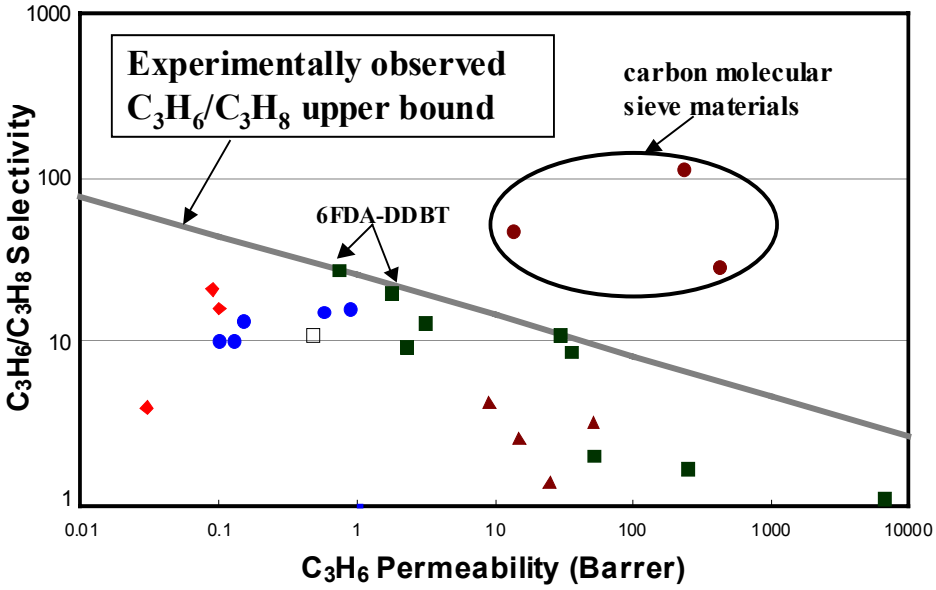

Figure 4.1. C_3H_6/C_3H_8 experimental upper bound based on pure gas permeation data over the range 1 – 4 atm feed pressure. □ = 100°C, ■ = 50°C, ● = 35°C, ▲= 30°C, ◆ = 26°C.

The data for 6FDA-33'DMDB polyimide will be discussed in section 4.3.

The assertion that permeation plasticization effects are minimal for the measurements reported here is based on the dense film data available in the literature, which are discussed below. Tanaka *et al.* report an upturn in the C_3H_6 permeability curve for the material 6FDA-TrmPD at just over 4 atm [2]. Staudt-Bickel and Koros report an upturn in the C_3H_6 permeability curve for 6FDA-6FpDA at 4 atm feed pressure as well [3]. Ilinitch *et al.* report an upturn in the

C_3H_6 permeability curve between 3 – 4 atm for a PPO copolymer and a poly(amide-imide) copolymer [9]. Permeability data was also reported for poly(vinyl-trimethylsilane); however, it is difficult to determine a plasticization pressure from the data provided because of the large interval between experimental measurements. These reported data for the pressure dependence of C_3H_6 permeability provide adequate evidence to claim that permeation plasticization effects are minimal at the feed pressures considered for the C_3H_6/C_3H_8 upper bound analysis presented here below 4 atm.

It should be noted that the polymers currently defining the upper bound are 6FDA-DDBT and 6FDA-TrMPD, and the structures of these materials are shown in Table 3.2 and Figure 3.2. Permeation measurements for the polymer 6FDA-DDBT are different in two references by the same authors, as indicated in Figure 4.1 [2, 7]. Personal communication with the authors verified that these measurements were done on two different films of the same material, 6FDA-DDBT, and both sets of data were reported accurately [10]. It is also worth mentioning that while only two polymeric materials strictly define the C_3H_6/C_3H_8 upper bound, this is not exceedingly different from what Robeson observed in many other circumstances, where only a few polymers defined the upper bound. For example, in the CO_2/CH_4 case only 2-3 polymers actually lie directly on the upper bound, as it was published in 1991 [1].

The temperature of each particular measurement is also indicated in Figure 4.1. While the temperature range under consideration is relatively moderate, it is still important to consider this distinction. Robeson did not account for temperature differences for different permeation measurements in the initial development of the upper bound trade off curves [1], however for lighter gases this differentiation may be less critical, because the activation energy for permeation is relatively small, on average. However, as the penetrant diameter increases the activation energy for permeation is expected to increase based on previously observed trends [2, 11, 12]. Therefore, it is important to clearly define the temperature conditions of the measurement if one is to compare the C_3H_6/C_3H_8 separation performance of two or more materials. At this point the experimental C_3H_6/C_3H_8 upper bound is defined by measurements made at 50°C. Since this is the highest temperature considered, it is reasonable to make the assumption the materials measured at lower temperatures would not be able to "out perform" these polyimides (in terms of C_3H_6 permeability / C_3H_6/C_3H_8 selectivity trade-off) at 50°C. Therefore, this is the most adequate experimental representation of the C_3H_6/C_3H_8 upper bound.

A few selected pure gas C_3H_6/C_3H_8 permeation measurements are shown in Figure 4.1 for carbon molecular sieve materials [13]. The carbon membranes shown here have been pyrolyzed from the polyimide precursor Matrimid® and the polyimide 6FDA/BPDA-DAM at various processing conditions reported

elsewhere [13]. For other gas separations (O_2/N_2, for example) carbon membrane materials have been shown to be superior to polymeric materials in terms of their transport properties [14], and this is also true for the C_3H_6/C_3H_8 case described here as the carbon materials lie above and beyond the polymeric upper bound.

4.3 ADDITIONAL C_3H_6/C_3H_8 LITERATURE DATA

There is a considerable amount of additional literature data that was not included in the development of the C_3H_6/C_3H_8 upper bound for multiple reasons, which are discussed below. Lee and Hwang report C_3H_6/C_3H_8 separation results for a polyimide hollow fiber [15]. The ideal selectivity is reported to be 15, however the permeability is unknown because of the uncertainty in the thickness of the dense layer of the asymmetric membrane. Therefore, these results were not included in the upper bound analysis.

Ito and Hwang report C_3H_6/C_3H_8 permeation results for ethyl cellulose and cellulose acetate polymers and derivatives for dense films and hollow fibers, however the temperature of the permeation experiments is not clear [16]. The highest performing result for the dense film measurements was ethyl cellulose with a high temperature treatment. This showed a C_3H_6/C_3H_8 selectivity of 7, with a C_3H_6 permeability of ~ 20 Barrers, which is below the currently defined upper bound. These results were not included in the present analysis for consistency because they were measured with a pressure of 1 atm on the

downstream side, and not under vacuum. Similarly, Henley and Santos report C_3H_6/C_3H_8 permeation results for polyethylene [17]. In this case the material actually shows preferential permeation to propane over propylene, and this was also done with 1 atm pressure on the downstream side, so again these results were not included to maintain consistency.

A 1992 publication by Ilinitch *et al.* reports C_3H_6/C_3H_8 permeation data for polyphenyleneoxide (PPO) and two PPO-based copolymers [18]. The data reported lie above the C_3H_6/C_3H_8 upper bound developed here. Through personal communication the authors have expressed that the C_3H_8 permeation results are most likely in a transient state [19]. The authors have explained that the permeation experiments were conducted for several hours; however, the films tested were relatively thick (70 μm) and the diffusion coefficient of C_3H_8 was relatively small. Therefore the time lag for C_3H_8 permeation would have been on the order of many, many hours, which would have resulted in a measurement of the transient C_3H_8 permeation coefficient instead of a steady-state measurement. A separate publication by the same authors gives a more detailed explanation of these transient effects for the case of ethylene/ethane separation [20].

An additional reference exists, which reports C_3H_6/C_3H_8 permeation data for a variety of polyimides [21]. These data are not included in the development of the C_3H_6/C_3H_8 upper bound because the data are believed to be questionable. First, there are large differences between data reported in this publication and data

reported previously for the same polyimide materials. For example, the polyimide 6FDA-BAAF (known elsewhere as 6FDA-6FpDA), is reported to have a C_3H_6/C_3H_8 pure gas selectivity of 19.8, while a separate publication by the same authors reports the pure gas C_3H_6/C_3H_8 selectivity of this polyimide to be 77 [22]. There is no explanation provided for this inconsistency. It should also be noted that Staudt-Bickel and Koros have reported the pure gas C_3H_6/C_3H_8 selectivity for this material to be 16 at 35°C [3].

Another example is the polyimide 6FDA-mPD. Shimazu *et al.* report this material to have a C_3H_6/C_3H_8 selectivity of ~ 140 in the mixed gas experiment at 25°C and 2 atm total feed pressure. Staudt-Bickel and Koros have previously reported the same polyimide, 6FDA-mPD, to have a pure gas C_3H_6/C_3H_8 selectivity equal to 10 at 35°C and 3.8 atm feed pressure [3]. This order of magnitude difference in selectivity has not previously been addressed. Conventionally, it would be expected that the C_3H_6/C_3H_8 selectivity in the mixed gas experiment would be lower than in the pure gas experiment based on previous observations [2, 3]. It is unlikely that slight changes in experimental protocol (such as slightly lower feed pressures or small changes in film formation) could result in such a drastic improvement in separation performance.

However, to be sure that slight changes in experimental protocol could not be the reason for improvements in C_3H_6/C_3H_8 separation, experimental efforts were focused on one of the higher performing polyimides, 6FDA-33'DMDB,

reported previously [21]. The structure of this material is shown in Table 3.2. This polyimide was synthesized, and dense films were cast using the exact procedure reported previously [21, 23]. Permeation measurements were conducted at the same feed pressures as those reported by Shimazu (1.1 atm). All permeation and sorption measurements in the work reported here were done at 35^{o}C. The results obtained in this study are shown in Table 4.3, and compared to the measurements reported by Shimazu *et al.* The pure gas C_3H_6/C_3H_8 selectivity reported here (α = 13.2) is lower by a factor of 3. The mixed gas C_3H_6/C_3H_8 selectivity (α = 10) is lower by a factor of ~ 4.5, and the C_3H_6/C_3H_8 pure gas solubility selectivity is lower by a factor of 5.2. The reason for these large discrepancies is currently unclear, but it reflects the same discrepancies noted above with regard to the other polyimide samples (6FDA-6FpDA and 6FDA-mPD).

Measurements for the solubility isotherms conducted in the present study for C_3H_6 and C_3H_8 in 6FDA-33'DMDB are shown in Figure 4.2. The measurement for C_3H_6 solubility is similar to that measured by Shimazu *et al.*, so it appears to be the depression of the C_3H_8 solubility, which is responsible for the elevated C_3H_6/C_3H_8 solubility selectivity, reported previously [21]. In fact, the same trend is prevalent throughout that publication [21], where it is clear the materials reported to have enhanced C_3H_6/C_3H_8 solubility selectivity do so because of a lower propane solubility coefficient in comparison to other

Table 4.3. Comparison of the C_3H_6/C_3H_8 transport data for 6FDA-33'DMDB.

Ref#	P_{C3H6} [b] (pure gas)	α_{ideal} C_3H_6/C_3H_8	P_{C3H6} [b] (mixed gas)	α_{mix} C_3H_6/C_3H_8	S [c] C_3H_6	S_{C3H6} / S_{C3H8}
[21]	0.263	39.4	~ 0.6 [d]	~ 45 [d]	0.255	4.90
This Study	0.15	13.2	0.32	10.4	0.22	0.94

[b] = Barrer = 10^{-10} $\frac{cc(STP)cm}{cm^2\ s\ cmHg}$ [c] = $\frac{cc(STP)}{cc\ polymer - cmHg}$

[d] These values are estimated from the chart provided in Figure 6 of reference [21].

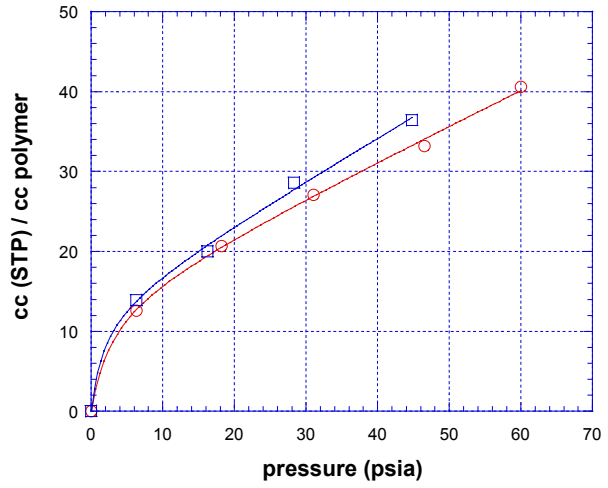

Figure 4.2. C_3H_6/C_3H_8 pure gas sorption isotherms for 6FDA-33'DMDB at 35°C, ○ = C_3H_6, □ = C_3H_8.

polyimides reported to date [2, 3]. The unconventional depression in propane solubility reported by Shimazu *et al.* has not previously been addressed [21].

4.4 PREDICTION OF THE C_3H_6/C_3H_8 UPPER BOUND

At this point the C_3H_6/C_3H_8 upper bound is essentially only defined by measurements on two materials. Therefore, it is useful to consider modeling work in an effort to predict where the C_3H_6/C_3H_8 upper bound should lie, which would also provide validation for the experimentally defined boundary.

A previous analysis by Freeman provides a general quantitative description of the upper bound performance of polymeric membranes [24], which can be represented by the following equation describing the trade-off relationship between the permeability of the "fast" gas and the selectivity of the gas pair:

$$\alpha_{A/B} = \frac{\beta_{A/B}}{P_A^{\lambda_{A/B}}} \qquad \textbf{(4.1)}$$

The parameter $\lambda_{A/B}$ has been shown to be proportional to the size difference of the gas molecules,

$$\lambda_{A/B} = \left(\frac{d_B}{d_A}\right)^2 - 1 \qquad \textbf{(4.2)}$$

where **d** is the penetrant diameter. The parameter β can be represented by the following equation [24]:

$$\beta_{A/B} = \frac{S_A}{S_B} S_A^{\lambda_{A/B}} \exp\left\{-\lambda_{A/B}\left[b - f\left(\frac{1-a}{RT}\right)\right]\right\} \qquad \textbf{(4.3)}$$

where S is the equilibrium solubility of a gaseous species within a polymer, **a** and **b** are coefficients of the "linear free energy" relation, and f is a parameter relating to interchain spacing.

In order to apply this analysis to the case of the C_3H_6/C_3H_8 upper bound a few extensions are necessary. First, it is important to represent the size of the molecules using the Lennard-Jones diameter instead of the kinetic diameter. While the kinetic diameter provides an accurate representation of the size of inorganic molecules and CH_4, it becomes increasingly poor for hydrocarbons with increasing number of carbon atoms. Similar conclusions have been reached by Steel with regard to correlation of propylene and propane diffusion coefficients in molecular sieving carbon materials [13]. Furthermore, Tanaka *et al.* have shown a linear correlation with log of diffusion coefficient vs. the Lennard-Jones diameter with gas molecules ranging in size from O_2 to n-C_4H_{10} for the polymers PPO and 6FDA-TrMPD [2]. Therefore, it is reasonable that the Lennard-Jones diameter provides the best representation of the size of C_3H_6 and C_3H_8 for this analysis. For consistency, the values for the Lennard-Jones parameters were used as reported by Tanaka et al [2] (4.68 Å for C_3H_6 and 5.06 Å for C_3H_8), and these values can be found elsewhere [25, 26].

It is also necessary to assume that the parameter, **f**, of the highest performing polymers, which is a fitted parameter in the previous analysis [24], can be extended to the C_3H_6/C_3H_8 prediction. To do this it must also be assumed

that there is a linear relationship between activation energy and the square of the penetrant diameter:

$$E_{D_A} = cd_A^2 - f \qquad \textbf{(4.4)}$$

where **c** is an additional constant, which is dependant on the polymer in question. In some cases, for hydrocarbon penetrants, it has been shown that the activation energy vs. penetrant squared relationship deviates from this linear relationship. However, for the rigid polyimides that largely define the upper bound relationship the data necessary to adequately evaluate the validity of Equation 4.4 is limited. Therefore, for lack of information supporting the contrary, the assumption has been made that the value of the fitted parameter, **f**, in the previous analysis (12,600 cal/mol) [24] can be extended to the prediction of the C_3H_6/C_3H_8 upper bound, and it will later be possible to qualitatively evaluate this assumption based on the agreement between the upper bound prediction and the experimental definition of this boundary.

The next step to generate a prediction of the C_3H_6/C_3H_8 upper bound is to define an average C_3H_6 solubility and C_3H_6/C_3H_8 solubility selectivity. Since the experimental upper bound is defined at 50°C, it is also necessary to create a prediction at this temperature, and therefore it is essential to choose C_3H_6/C_3H_8 solubility measurements conducted at 50°C. Tanaka *et al.* have performed C_3H_6/C_3H_8 solubility measurements at 50°C using five glassy polyimides ranging in Tg from 205°C to >490°C [2], and these data are shown in Table 4.4.

Furthermore, it is appropriate to choose these polyimides to represent average C_3H_6/C_3H_8 solubility measurements because these polymers are largely representative of high performing polymers for the C_3H_6/C_3H_8 separation reported to date.

The prediction of the C_3H_6/C_3H_8 upper bound is shown in Figure 4.3. It agrees quite nicely with the experimentally observed upper bound. Almost all of the experimental data lies below the prediction, with the exception of the polymer 6FDA-DDBT. A more quantitative analysis is shown in Table 4.5. The calculated values of λ and β are compared with the values fit to the experimental data. The measurements used for the fit are from the two polymers that define the C_3H_6/C_3H_8 experimental upper bound, 6FDA-DDBT and 6FDA-TrMPD. As discussed earlier, the results for the polymer 6FDA-DDBT are slightly different depending on the reference. Therefore, two experimental fits were done using the two different data for 6FDA-DDBT, and the singular measurement for 6FDA-TrMPD in each case. Clearly, using reference [7] for 6FDA-DDBT provides a better correlation with the prediction of the upper bound. In fact, using this reference for the data the argument could be made that the prediction is within experimental error of the permeation measurements.

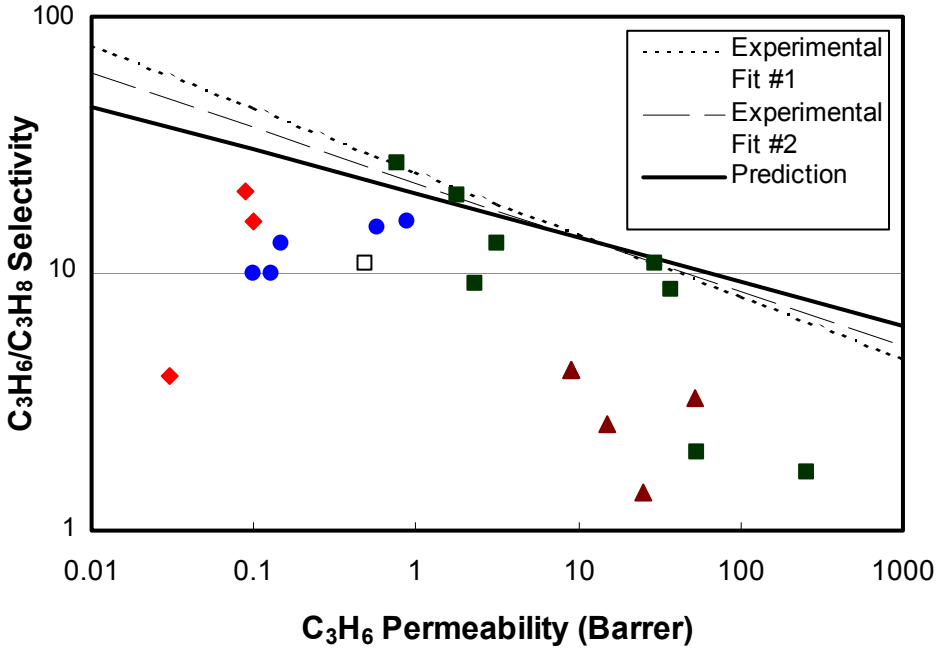

Figure 4.3. Comparison of the C_3H_6/C_3H_8 upper bound prediction to the experimental data. Fit #1 is done using 6FDA-DDBT from reference [2]. Fit # 2 is done using 6FDA-DDBT from reference [7].

Table 4.4. Determination of average C_3H_6 solubility and average C_3H_6/C_3H_8 solubility selectivity for the upper bound prediction. Data obtained from reference [2].

Material	Tg (K)	Tg (^oC)	S [c] C_3H_6	S_{C3H6} / S_{C3H8}
6FDA-TeMPD	693	420	0.20	1.3
6FDA-TrMPD	650	377	0.23	1.2
6FDA-DDBT	> 763	> 490	0.18	1.0
BPDA-TeMPD	> 763	> 490	0.15	1.2
PPO	478	205	0.13	1.2
Average			**0.178**	**1.16**

[c] $= \frac{\text{cc(STP)}}{\text{cc polymer} - \text{cmHg}}$

Table 4.5. Comparison between the calculated parameters, λ and β, with the experimentally fitted values. β is determined using permeability values expressed in units of Barrer.

	$\lambda_{C3H6/C3H8}$	$\beta_{C3H6/C3H8}$
Calculated using Equations (2) and (3)	0.170	20.4
Experimental Fit #2 using reference [7] for 6FDA-DDBT	0.212	22.6
Experimental Fit #1 using reference [2] for 6FDA-DDBT	0.244	25.2

4.5 IMPLICATIONS OF THE UPPER BOUND MODELING

A prediction of the C_3H_6/C_3H_8 upper bound was presented using an extension of the analysis by Freeman, which correlates remarkably well with the experimental upper bound defined here. It should be noted that the prediction is based on an average C_3H_6/C_3H_8 solubility selectivity, an average value of the parameter, **f** (for high permeability, high selectivity polymers) and a temperature of 50^{o}C. The theory would predict that there are essentially two methods to "move" or "beat" the currently existing upper bound.

The first approach would be to increase the polymer chain rigidity, while simultaneously increasing inter-chain spacing. This could be accomplished by using an ultra-rigid polymeric material such as a polypyrrolone, and this is the strategy that will be pursued in the work here. Experimental evidence provided

by Zimmerman (see section 2.4) has shown that these ultra-rigid polymers can surpass the upper bound for the O_2/N_2 separation [27], which is consistent with the quantitative analysis. The second method would be to increase the C_3H_6 solubility (and consequently the C_3H_6/C_3H_8 solubility selectivity), while maintaining the diffusivity selectivity. This approach has been attempted with varying degrees of success using facilitated transport membranes of different varieties [28-36]. Typically, these membranes are composed of metal ion salts, where the metal cation is able to undergo pi bonding with the olefin, and in some cases this has been shown to enhance the overall permselectivity. The remaining challenge for this class of membrane materials appears to be the fact that the olefin-metal ion complex is poisoned by even small amounts of hydrogen gas, carbon monoxide, acetylene, or hydrogen sulfide in the feed stream. It seems alternate materials, which interact with olefins without being poisoned by the aforementioned components, would be necessary in order to attain commercially feasible membranes with enhanced C_3H_6/C_3H_8 solubility selectivity. Experimental efforts were focused on this particular strategy, and these will be discussed in Appendix A.

4.6 REFERENCES

[1] L. M. Robeson, Correlation of separation factor versus permeability for polymeric membranes, J. Membr. Sci. 62 (1991) 165-185.

[2] K. Tanaka, A. Taguchi, J. Q. Hao, H. Kita and K. Okamoto, Permeation and separation properties of polyimide membranes to olefins and paraffins, J. Membr. Sci. 121 (1996) 197-207.

[3] C. Staudt-Bickel and W. J. Koros, Olefin/paraffin gas separations with 6FDA-based polyimide membranes, J. Membr. Sci. 170 (2000) 205-214.

[4] J. J. Krol, M. Boerrigter and G. H. Koops, Polyimide hollow fiber gas separation membranes: Preparation and the suppression of plasticization in propane/propylene environments, J. Membr. Sci. 184 (2001) 275-286.

[5] S. Sridhar and A. A. Khan, Simulation studies for the separation of propylene and propane by ethylcellulose membrane, J. Membr. Sci. 159 (1999) 209-219.

[6] S. Bai, S. Sridhar and A. A. Khan, Metal-ion mediated separation of propylene from propane using PPO membranes, J. Membr. Sci. 147 (1998) 131-139.

[7] K. Okamoto, K. Noborio, J. Hao, K. Tanaka and H. Kita, Permeation and separation properties of polyimide membranes to 1,3-butadiene and n-butane, J. Membr. Sci. 134 (1997) 171-179.

[8] G. H. Koops, private communication, 2002.

[9] O. M. Ilinitch, A. A. Lapkin and K. I. Zamaraev, Propylene in polyphenylene oxides membranes - unusual permeability vs pressure behavior, J. Membr. Sci. 98 (1995) 287-290.

[10] K. Okamoto, private communication, 2001.

[11] C. M. Zimmerman and W. J. Koros, Polypyrrolones for membrane gas separations. II. Activation energies and heats of sorption, J. Polym. Sci. Part B 37 (1999) 1251-1265.

[12] L. M. Costello and W. J. Koros, Temperature dependence of gas sorption and transport properties in polymers: Measurement and applications, Ind. Eng. Chem. Res. 31 (1996) 2708-2714.

[13] K. Steel, Carbon membranes for challenging gas separations, Ph. D. Dissertation, The University of Texas at Austin, 2000.

[14] A. Singh-Ghosal and W. J. Koros, Air separation properties of flat sheet homogeneous pyrolytic carbon membranes, J. Membr. Sci. 174 (2000) 177-188.

[15] K. R. Lee and S. T. Hwang, Separation of propylene and propane by polyimide hollow-fiber membrane module, J. Membr. Sci. 73 (1992) 37-45.

[16] A. Ito and S. T. Hwang, Permeation of propane and propylene through cellulosic polymer membranes, J. Appl. Polym. Sci. 38 (1989) 483-490.

[17] E. J. Henley and M. L. D. Santos, Permeation of vapors through polymers at low temperature and elevated pressures, 13 (1967) 1117-1119.

[18] O. M. Ilinitch, G. L. Semin, M. V. Chertova and K. I. Zamaraev, Novel polymeric membranes for separation of hydrocarbons, J. Membr. Sci. 66 (1992) 1-8.

[19] O. M. Ilinitch, private communication, 2002.

[20] O. M. Ilinich and K. I. Zamaraev, Separation of ethylene and ethane over polyphenyleneoxides membranes - transient increase of selectivity, J. Membr. Sci. 82 (1993) 149-155.

[21] A. Shimazu, T. Miyazaki, M. Maeda and K. Ikeda, Relationships between the chemical structures and the solubility, diffusivity, and permselectivity of propylene and propane in 6FDA-based polyimides, J. Polym. Sci. Pt. B-Polym. Phys. 38 (2000) 2525-2536.

[22] A. Shimazu, Method of selectively separating unsaturated hydrocarbon, U.S. Patent 5,749,943, Petroleum Energy Center, Tokyo, Japan, 1998.

[23] A. Shimazu, T. Miyazaki, T. Matsushita, M. Maeda and K. Ikeda, Relationships between chemical structures and solubility, diffusivity, and permselectivity of 1,3-butadiene and n-butane in 6FDA-based polyimides, J. Polym. Sci. Pt. B-Polym. Phys. 37 (1999) 2941-2949.

[24] B. D. Freeman, Basis of permeability/selectivity tradeoff relations in polymeric gas separation membranes, Macromolecules 32 (1999) 375-380.

[25] A. L. Hines and R. N. Maddox, Mass transfer fundamentals and applications, Prentice Hall PTR, Englewood Cliffs, 1985.

[26] J. H. Hirchfelder, C. F. Curtiss and R. B. Bird, Molecular theory of gases and liquids, Wiley, New York, 1964.

[27] C. M. Zimmerman and W. J. Koros, Polypyrrolones for membrane gas separations. I. Structural comparison of gas transport and sorption properties, J. Polym. Sci. Pt. B-Polym. Phys. 37 (1999) 1235-1249.

[28] S. Bai, S. Sridhar and A. A. Khan, Recovery of propylene from refinery off-gas using metal incorporated ethylcellulose membranes, J. Membr. Sci. 174 (2000) 67-79.

[29] S. U. Hong, J. H. Jin, J. Won and Y. S. Kang, Polymer-salt complexes containing silver ions and their application to facilitated olefin transport membranes, Adv. Mater. 12 (2000) 968.

[30] Y. H. Kim, J. H. Ryu, J. Y. Bae, Y. S. Kang and H. S. Kim, Reactive polymer membranes containing cuprous complexes in olefin/paraffin separation, Chem. Commun. (2000) 195-196.

[31] Y. S. Park, J. Won and Y. S. Kang, Facilitated transport of olefin through solid paam and paam- graft composite membranes with silver ions, J. Membr. Sci. 183 (2001) 163-170.

[32] S. Sunderrajan, B. D. Freeman, C. K. Hall and I. Pinnau, Propane and propylene sorption in solid polymer electrolytes based on poly(ethylene oxide) and silver salts, J. Membr. Sci. 182 (2001) 1-12.

[33] I. Pinnau and L. G. Toy, Solid polymer electrolyte composite membranes for olefin/paraffin separation, J. Membr. Sci. 184 (2001) 39-48.

[34] J. C. Davis, R. J. Valus, R. Eshraghi and A. E. Velikoff, Facilitated transport membrane hybrid systems for olefin purification, Sep. Sci. Technol. 28 (1993) 463-476.

[35] W. S. Ho and D. C. Dalrymple, Facilitated transport of olefins in Ag+-containing polymer membranes, J. Membr. Sci. 91 (1994) 13-25.

[36] G. H. Hsiue and J. S. Yang, Novel methods in separation of olefin/paraffin mixtures by functional polymeric membranes, J. Membr. Sci. 82 (1993) 117-128.

CHAPTER 5: STRUCTURE-PROPERTY RELATIONSHIPS OF POLY(PYRROLONE-IMIDE) COPOLYMERS

5.1 STRUCTURE-PROPERTY DISCUSSION AND SPACE-FILLING MODEL REPRESENTATION

As discussed in Chapters 2 and 3 the strategy and motivation for using polypyrrolones and poly(pyrrolone-imide) copolymers lies in the fact that these ultra-rigid polymers can mimic molecular sieves [1, 2]. In addition to rigidity it is necessary to attempt to alternate "open" regions and "bottleneck" selective regions by tuning the polymeric matrix through the use of different monomer stoichiometry. The copolymer chosen was 6FDA-TAB/DAM, and in this case the matrix properties can be carefully adjusted by varying the tetraamine to diamine ratio. Figure 5.1 shows the structure of the 6FDA-TAB/DAM copolymer, as well as 3-dimensional drawings created by HyperChem® software. The first noticeable element of the 3-dimensional structures is that the 6FDA monomer (because of the CF_3 groups) must "fold" upon itself, creating disruptions along the polymer chain. Clearly, this monomer creates packing disruptions, and adds to the free volume throughout the matrix. As observed in the lower drawing in Figure 5.1, the tetraamine monomer is planar, very flat, and therefore able to pack closely to other polymer chains. Additionally, the tetraamine provides a ladder structure, and hence rigidity to the material. Conversely, the methyl groups of the diamine (DAM), provide spacers within the matrix. It is also hypothesized that

since the lowest energy conformation of the diamine monomer is perpendicular to the dianhydride counterpart (determined by Hyperchem® software), this steric hindrance provides an additional mode in order to create space between the polymer chains. Due to the stoichiometry in the polymerization reaction it is necessary to have alternating dianhydrides and amines. Therefore, it is a reasonable choice to allow 6FDA to comprise the dianhydride monomer, and to vary the ratio of the TAB and DAM within the stoichiometry because these monomers function differently in terms of their effect on transport properties. The remainder of this chapter will examine structure-property relationships varying the TAB/DAM ratio within the copolymer.

The density of each copolymer is shown in Figure 5.2 as a function of mol % TAB / amine unit within the copolymer. There is a considerable density difference between 6FDA-DAM and 6FDA-TAB, and this is one reason these particular polymers were chosen to comprise this copolymer family. Altering the TAB/DAM ratio provides a considerable amount of tunability with respect to the density of the copolymer.

X-ray diffraction data is shown in Figure 5.3, and d-spacings are provided in Table 5.1. In many cases two peaks are observed in the spectra, as noted previously for these types of materials [3]. From the 50/50 TAB/DAM copolymer to the 100/0 TAB/DAM copolymer the smallest spacing is reduced significantly from 4.5 to 3.5 Å, however the larger d-spacings remain virtually

unchanged. The observation of two d-spacings, also indicates the likelihood of a bi-modal distribution of free volume. Other researchers have also noted bi-modal free volume distributions of glassy polymers characterized using positron annihilation lifetime spectroscopy (PALS) [4, 5]. A more comprehensive discussion on free volume distributions in these rigid copolymers will be presented in Section 5.5.

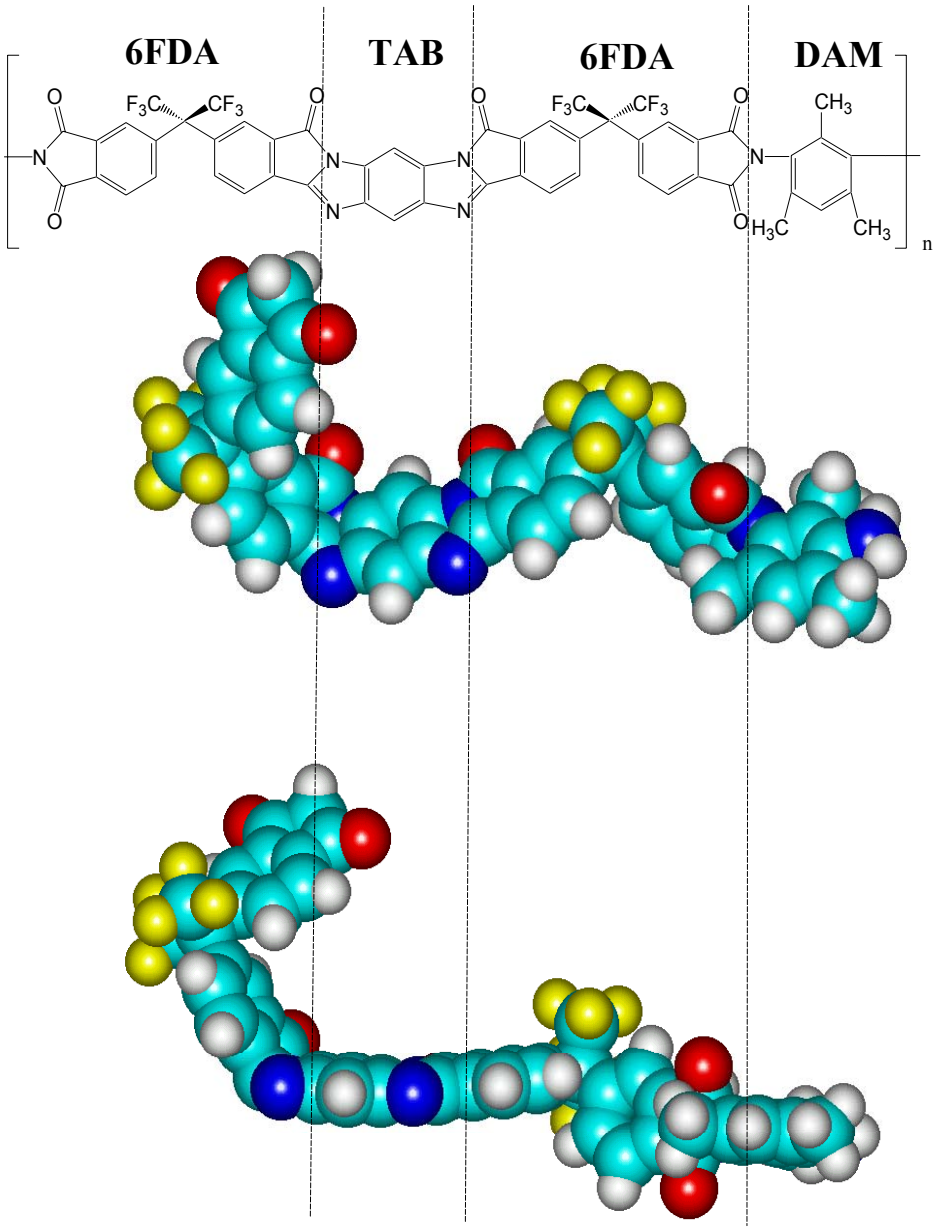

Figure 5.1. One unit of the 6FDA-TAB/DAM(50/50) copolymer. 3-dimensional drawings were created using HyperChem® software.

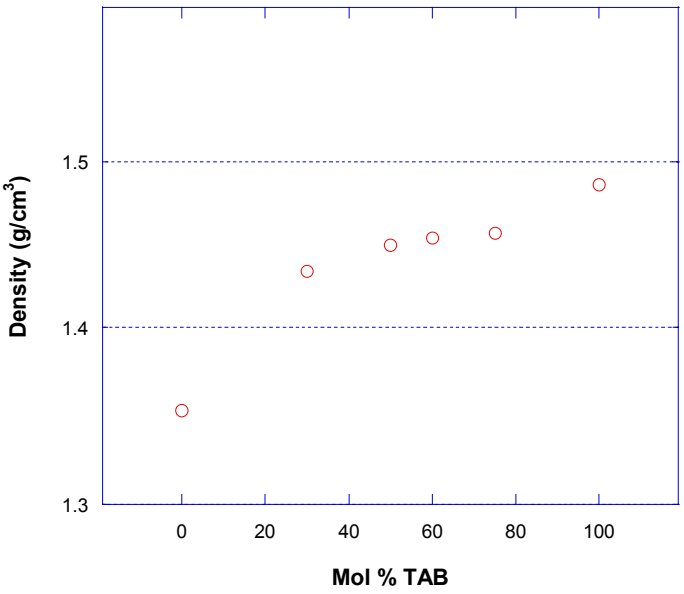

Figure 5.2. Density of the 6FDA-TAB/DAM copolymer as a function of the TAB/DAM ratio.

Table 5.1. Physical properties of 6FDA-TAB/DAM copolymers.

Polymer	**Density** (g/cm^3)	**Tg** (^oC)	**d-spacing** (Å)
6FDA-DAM	1.352	375	3.7, 6.2
6FDA-TAB/DAM(30/70)	1.433	> 560	-
6FDA-TAB/DAM(50/50)	1.449	> 560	4.2, 5.6
6FDA-TAB/DAM(75/25)	1.456	> 560	4.1, 5.7
6FDA-TAB	1.486	> 560	3.5, 5.7

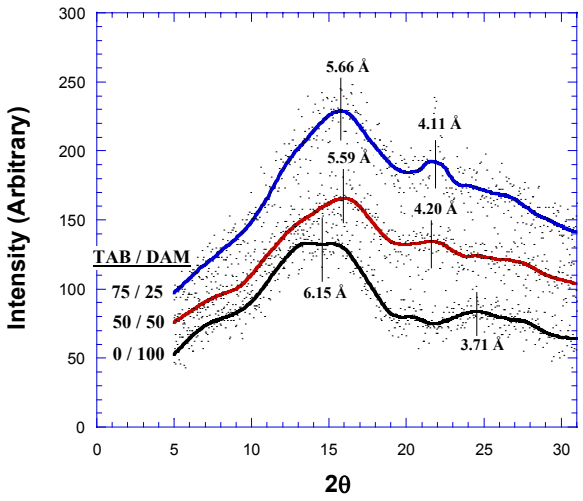

Figure 5.3. Wide angle x-ray diffraction results for 6FDA-TAB/DAM copolymers.

5.2 PERMEABILITY COEFFICIENTS AND PERMSELECTIVITIES

5.2.1 Permeability Results for the 6FDA-TAB/DAM Copolymer Family

Pure gas permeation results for the penetrants O_2/N_2, CO_2/CH_4, and C_3H_6/C_3H_8 are provided in Table 5.2. These results are also shown in Figures 5.4 – 5.6 plotted on the upper bound graphs for each particular separation [6]. For O_2/N_2 separation the copolymers tested lie on or slightly below the 1991 upper bound limit, shown in Figure 5.4. The CO_2/CH_4 permeation results lie on or above the 1991 upper bound limit, shown in Figure 5.5. The pure polypyrrolone,

6FDA-TAB, exhibits the best exchange of CO_2 permeability and CO_2/CH_4 selectivity, and this result has been published previously [3]. It is believed the ultra-rigid structure of these copolymers coupled with the correctly tuned average chain spacing allows them to behave as psuedo molecular sieves, resulting in the high-quality separation properties. The trend in the results is very similar for both the O_2/N_2 and the CO_2/CH_4 case. Upon increasing the TAB/DAM ratio in the copolymer, the matrix becomes more tightly packed, and the fractional free volume decreases. As expected, this results in a reduction in permeability and an increase in permselectivity with increasing TAB/DAM ratio.

Table 5.2. Permeability coefficients and permselectivities for poly(pyrrolone-imide) copolymers at 35°C and 2 atm unless otherwise noted.

Polymer	P_{O2}[a]	P_{CO2}[a]	P_{C3H6}[a]	P_{O2} / P_{N2}	P_{CO2} / P_{CH4}	P_{C3H6} / P_{C3H8}
6FDA-TAB	15.2	54	0.09	5.9	60	2.6
6FDA-TAB/DAM(75/25)	15.9	73.7	0.38	5.2	44	8.0
6FDA-TAB/DAM(50/50)	30.3	155	2.3	4.6	34	23
6FDA-DAM	109	370	28.7	3.7	21	10.1

[a] = Barrer = 10^{-10} $\frac{cc(STP)cm}{cm^2\ s\ \ cmHg}$

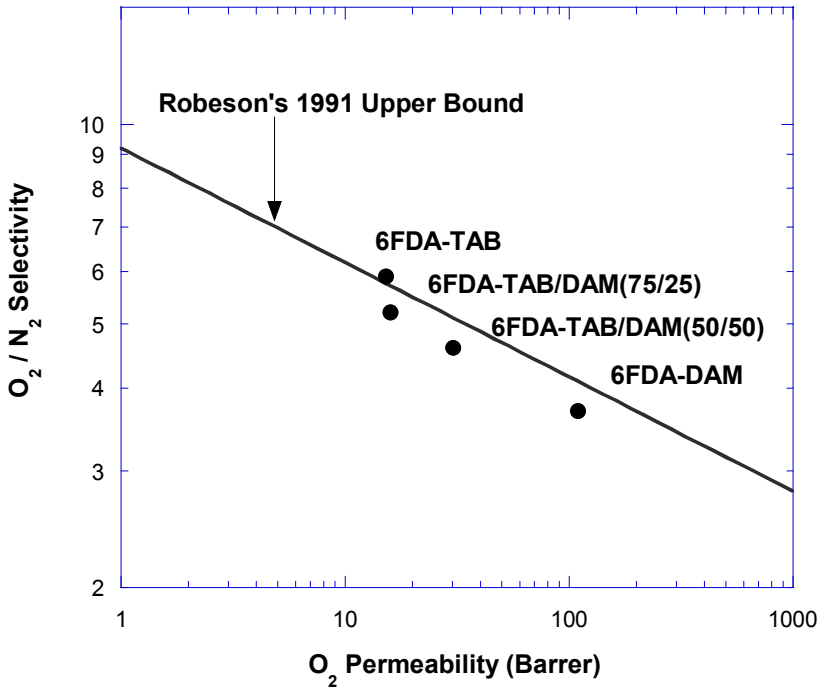

Figure 5.4. O_2/N_2 transport properties of 6FDA-TAB/DAM copolymers at 35°C.

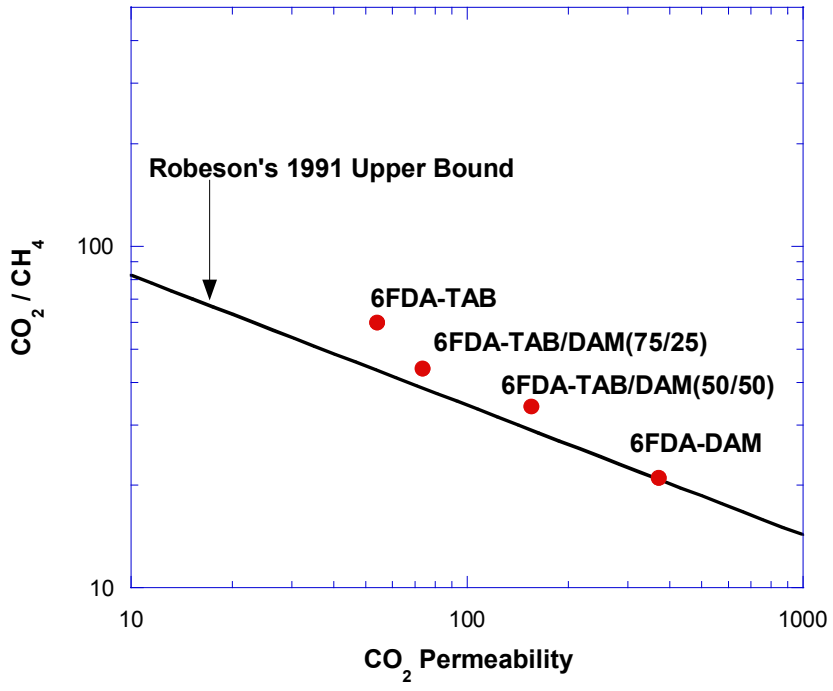

Figure 5.5. CO_2/CH_4 transport properties of 6FDA-TAB/DAM copolymers at 35°C.

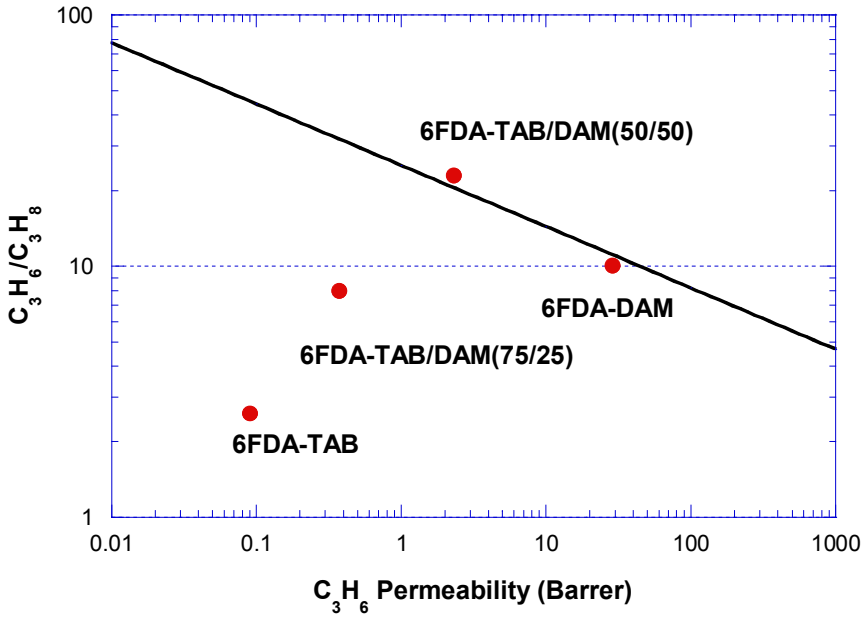

Figure 5.6. C_3H_6/C_3H_8 transport properties of 6FDA-TAB/DAM copolymers at 35°C.

The C_3H_6/C_3H_8 case is quite different than for O_2/N_2 and CO_2/CH_4. In this case the copolymers 6FDA-DAM and 6FDA-TAB/DAM(50/50) lie on or near the upper bound trade off curve defined in Chapter 4. Surprisingly, with a further increase in TAB/DAM ratio a reduction in both permeability and selectivity is observed. The resulting low C_3H_6 flux and low C_3H_6/C_3H_8 selectivity for both 6FDA-TAB and 6FDA-TAB/DAM(75/25) would be commercially undesirable

under the operating conditions tested, which is surprising considering the high performance of these materials for O_2/N_2 and CO_2/CH_4 separation. For the C_3H_6/C_3H_8 case there is a selectivity maximum observed as a function of TAB/DAM ratio. For the cases considered here the TAB/DAM(50/50) copolymer lies at the height of the maximum.

It has been proposed previously that the permeability of a copolymer can be predicted from the permeability of the pure homopolymers by the following equation [7]:

$$\ln P = \phi_1 \ln P_1 + \phi_2 \ln P_2 \qquad (5.1)$$

where ϕ is the volume fraction, and the subscripts 1 and 2 refer to the homopolymers, 6FDA-DAM and 6FDA-TAB in this case. In Figure 5.7 the permeability results for 6 gas penetrants are plotted on a log scale versus mol % TAB in the copolymer. The permeability measurements for 6FDA-DAM and 6FDA-TAB/DAM(50/50) were used along with Equation (5.1) to predict the permeability results for the pure polypyrrolone, 6FDA-TAB, and the copolymer 6FDA-TAB/DAM(75/25). The prediction using Equation (5.1) is represented by the solid line for each gas penetrant shown in Figure 5.7. For the smaller gas penetrants (O_2, N_2, CO_2, CH_4), the prediction matches the data nicely. However, for C_3H_6 and C_3H_8, deviations from the experimental data are observed. Propane permeability, in particular, is an order of magnitude larger than the predicted value for 6FDA-TAB. This illustrates that Equation (5.1) may not always be

strictly obeyed, and although it fits nicely for certain systems, it is not able to describe the trends shown here with larger molecules.

In the carbon molecular sieve literature this surprising trend of a maximum in selectivity as a function of material structure has been observed for a variety of gas pairs. Steel has observed this trend for C_3H_6/C_3H_8 separation as a function of pyrolysis temperature, shown in Figure 5.8 [8]. In this case the carbon materials were formed from the polyimide precursor, 6FDA/BPDA-DAM, via a vacuum pyrolysis. Varying the temperature of the heat treatment changes the material structure, similar to changing the monomer stoichiometry for the poly(pyrrolone-imide) copolymers. It would be expected that an increased heat treatment would provide a smaller average pore size, resulting in a decrease in permeability and an increase in selectivity based on previous observations [9-11]. Clearly, this is not the observed trend for the C_3H_6/C_3H_8 case, where a decrease in both permeability and selectivity from a 550^{o}C heat treatment to an 800^{o}C heat treatment is observed (Figure 5.8). Interestingly, O_2/N_2 and CO_2/CH_4 show the expected trend of a decrease in permeability and an increase in selectivity (not shown here) [8], which corresponds to the poly(pyrrolone-imide) case outlined earlier. These two examples show a selectivity maximum for only C_3H_6 and C_3H_8 (the largest molecules tested); however, an extensive search of the carbon literature has found evidence of the phenomena for many different gas pair separations.

Okamoto *et al.* have observed a selectivity maximum for C_3H_6/C_3H_8 as a function of pyrolysis temperature using a polyimide precursor [12]. Ogawa and Nakano have observed a selectivity maximum for CO_2/CH_4 as a function of gelation temperature [13]. Kusuki *et al.* have observed a maximum in selectivity for H_2/CH_4 as a function of heat treatment [14]. Kane *et al.* have observed an O_2/N_2 selectivity maximum as a function of synthesis temperature for carbon molecular sieve materials [15]. Hayashi *et al.* have observed a maximum in selectivity for both O_2/N_2 and CO_2/N_2 as a function of CVD time (which qualitatively controls the pore size distribution) [16]. In a separate publication Hayashi *et al.* observe a He/N_2 selectivity maximum as a function of carbonization temperature [17]. It is possible that other examples of this trend exist in the carbon literature, but the examples cited here are intended to show that the observation of a maximum in selectivity is not uncommon in carbon materials for many different gas separations. However, this observed trend remains largely unidentified and under discussed within the literature. Potential causes of this observed maximum in selectivity are discussed in section 5.5.

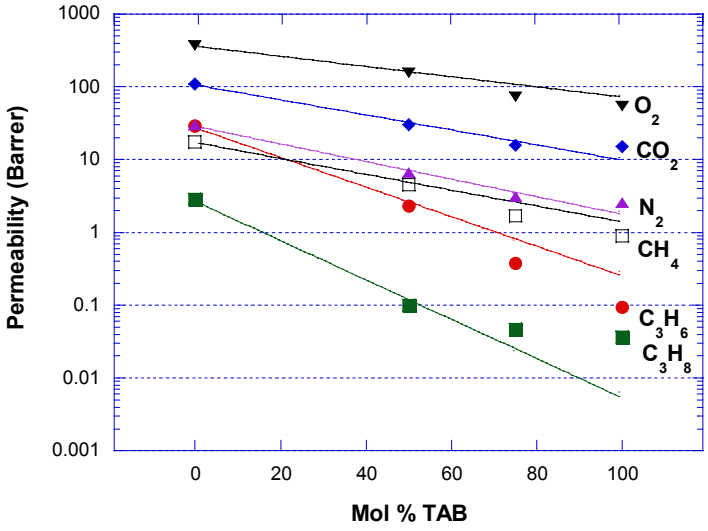

Figure 5.7. Gas permeability as a function of TAB/DAM ratio in the copolymer.

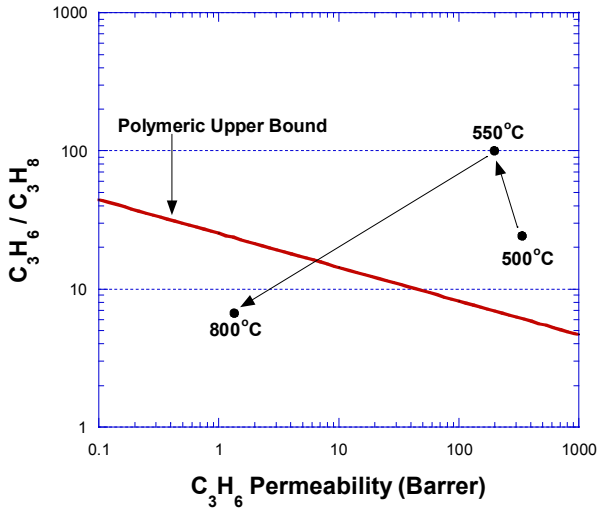

Figure 5.8. Carbon molecular sieve materials pyrolized from 6FDA/BPDA-DAM precursor. Transport results, as a function of heat treatment in the material formation, show a selectivity maximum [8].

5.2.2 Pemeability Results for 6FDA-TAB/6FpDA(50/50)

The motivation for studying this alternate copolymer was to examine the effect of an alternate diamine monomer on transport properties. Based on the 3–dimensional pictures shown in Figure 5.1, it would be expected that the 6FpDA monomer should mirror the effects of 6FDA (due to the bulky CF_3 groups) creating a larger average distance between polymer chains in the matrix and hence, an increased permeability. Pure gas permeation results for the penetrants O_2/N_2, CO_2/CH_4, and C_3H_6/C_3H_8 are provided in Table 5.3 at 35^oC and 2 atm. The results did not follow the hypothesis, since a relatively low permeability was observed in all cases. Essentially, the trends follow those from the 6FDA-TAB/DAM copolymer family, since the O_2/N_2 and CO_2/CH_4 separations show reasonable selectivity results, and the C_3H_6/C_3H_8 separation shows a low permeability and low selectivity. It would be expected that if the 6FpDA content was increased, it could be shown to have a selectivity maximum with respect to C_3H_6/C_3H_8. However, this trend has been well characterized in the other copolymer system, and adding additional 6FpDA would make the copolymer largely a polyimide, which strays somewhat from the original concept of an ultra-rigid ladder polymer. It remains unknown why including the 6FpDA monomer within the matrix provides a significantly lower permeability compared to the DAM monomer. One possible reason is that DAM is significantly smaller, which causes more 6FDA units per unit length of the polymer, in turn causing more disruption within the polymer chains, and additional free volume.

Table 5.3. Permeability coefficients and permselectivities for 6FDA-TAB/6FpDA(50/50) copolymer at 35 °C and 2 atm.

Polymer	P_{O2}[a]	P_{CO2}[a]	P_{C3H6}[a]	P_{O2} / P_{N2}	P_{CO2} / P_{CH4}	P_{C3H6} / P_{C3H8}
6FDA-TAB/6FpDA (50/50)	7.9	48.9	0.41	3.5	44	2.5

[a] = Barrer

5.3 COPOLYMER SORPTION ISOTHERMS

5.3.1 Sorption Coefficients

Solubility measurements were made for the range of copolymers for the gases O_2, N_2, CO_2, CH_4, C_3H_6, and C_3H_8 using the constant volume pressure decay method described in Chapter 3, and the solubility coefficients are shown in Table 5.4.

Table 5.4. Sorption coefficients and solubility selectivities of 6FDA-TAB/DAM copolymers at 35°C and 2 atm unless otherwise noted.

Polymer	S_{O2}[b]	S_{CO2}[b]	S_{C3H6}[b]	S_{O2}/ S_{N2}	S_{CO2}/ S_{CH4}	S_{C3H6}/ S_{C3H8}
6FDA-TAB	0.109	0.456	0.982	1.49	2.90	1.23
6FDA-TAB/DAM (75/25)	0.063	-	0.820	1.54	-	1.03
6FDA-TAB/DAM (50/50)	0.075	0.600	0.863	1.29	2.50	1.11
6FDA-DAM	0.086	0.413	1.152	1.23	2.99	1.26

[b] = $\frac{cc(STP)}{cc\ polymer - psia}$

There is no significant difference between the sorption coefficients for any particular penetrant molecule over the range of the copolymers studied. This finding is consistent with what Zimmerman found for another polypyrrolone copolymer family, 6FDA/PMDA-TAB, with gas molecules including He, O_2, N_2, CO_2, and CH_4 [18]. Since these materials contain a large amount of unrelaxed free volume, there is not a considerable distinction in the overall sorption level over the range of copolymers, and this will be evaluated more extensively in the next section.

Figure 5.9 depicts the natural log of the sorption coefficient plotted against the Lennard-Jones energy parameter of each penetrant (which is a measure of the condensability of the molecule) for the polypyrrolone, 6FDA-TAB. There is a linear correlation, which is also consistent with previously reported trends for 6FDA-DAM [19].

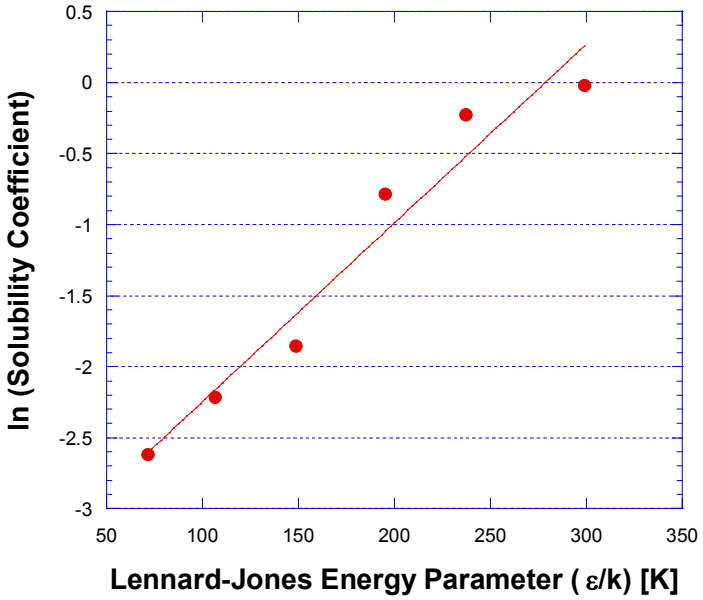

Figure 5.9. Log plot of solubility coefficient vs Lennard-Jones energy parameter for 6FDA-TAB.

5.3.2 Dual Mode Analysis

As discussed in Chapter 2, the dual mode model has been able to describe sorption into glassy polymers using the assumption that two regimes are acting in tandem to enable penetrant sorption. One regime is the unrelaxed free volume of the glassy polymer, and sorption into these sites can be described by the Langmuir model. At higher pressures this free volume becomes saturated, and the Henry's law region dominates. In this case sorption occurs between densified polymer chains, and the sorption level is linearly proportional to the pressure or fugacity driving force. The dual mode model combines these two regimes into one model

with three parameters fitted using a non-linear least squares regression of the sorption data. The Henry's law constant, k_D, is a measure of the penetrant's affinity for the dissolved mode of the dense polymer. Often times the Henry's law constant can be correlated with the condensability of the penetrant. The Langmuir capacity constant, $C'_{H,}$ measures the sorption capacity of the unrelaxed free volume. The Langmuir affinity constant, b, is a measure of the penetrant's ability to sorb into the free volume Langmuir sites.

Table 5.5 lists dual mode parameters of C_3H_6 for the copolymer family, 6FDA-TAB/DAM, and the sorption isotherms are shown in Figure 5.10. Generally speaking there is not a strong deviation in any parameter across the range of copolymers. The Henry's law coefficient exhibits an increase with a decreasing TAB/DAM ratio (shown in Figure 5.11), and this is expected. As the copolymer moves toward the pure polyimide the matrix becomes more flexible (albeit still a very rigid polymer) than the polypyrrolone. This additional chain flexibility provides less of an entropic penalty to C_3H_6 sorption, and thus the Henry's law coefficient is increased. It is also consistent that 6FDA-TAB is insoluble in typical organic solvents, whereas 6FDA-DAM is readily soluble. Previous studies have demonstrated that similar rigid-chain ladder polymers are insoluble in common organic solvents due to both intramolecular rigidity and intermolecular interchain attractions [20]. These interchain attractions provide more of the entropic penalty discussed above. However, compared to the permeability coefficients of C_3H_6, which span greater than *2 orders of magnitude* over the range of copolymers, the increase in Henry's law coefficient is a

relatively small effect. Clearly the diffusion coefficient is the dominant factor in affecting changes in permeability, and this will be demonstrated in the next section.

The Langmuir capacity constant, C'_H, shows no trend or extensive change over the range of copolymers in Table 5.5, meaning the amount of unrelaxed free volume does not appreciably change over the range of copolymers. Essentially, this is the reason the C_3H_6 sorption coefficients show no apparent trend in the previous section.

The Langmuir affinity constant, b, shows an increasing trend with decreasing TAB/DAM ratio. It should be noted that there is more error in the fit for this parameter (5 – 31 %), and the error could be minimized with additional data at low pressures. Again, the trends in the affinity constant are relatively small compared to the order of magnitude differences in the permeability coefficients.

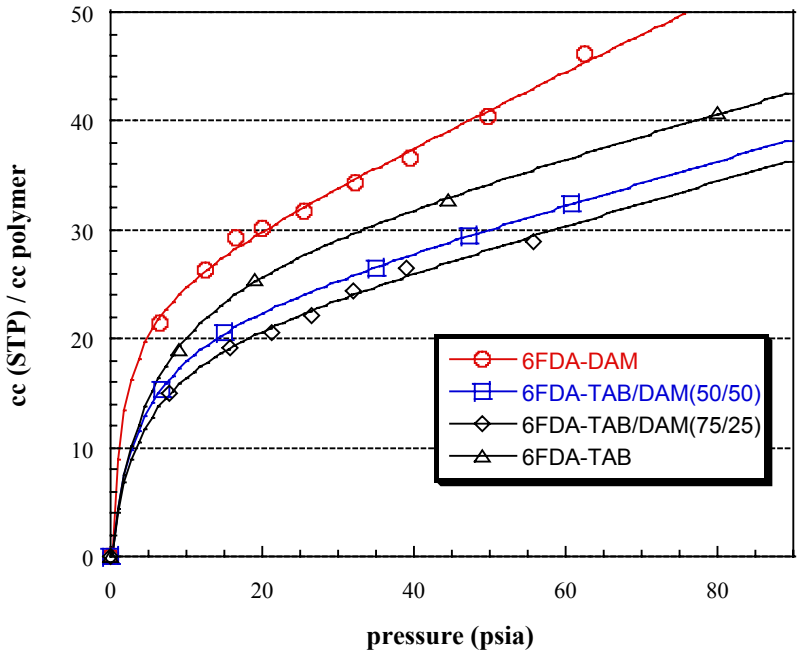

Figure 5.10. Sorption isotherms of C_3H_6 for the 6FDA-TAB/DAM copolymer family at 35°C.

Table 5.5. Dual mode parameters for C_3H_6 in various 6FDA-TAB/DAM copolymers at 35°C.

Parameter	6FDA-TAB	6FDA-TAB/DAM (75/25)	6FDA-TAB/DAM (50/50)	6FDA-DAM
k_D	0.184 ± 0.012	0.191 ± 0.032	0.191 ± 0.006	0.335 ± 0.023
C'_H	27.6 ± 1.0	20.1 ± 1.9	22.0 ± 0.4	25.1 ± 1.3
b	0.194 ± 0.021	0.259 ± 0.080	0.263 ± 0.014	0.572 ± 0.179

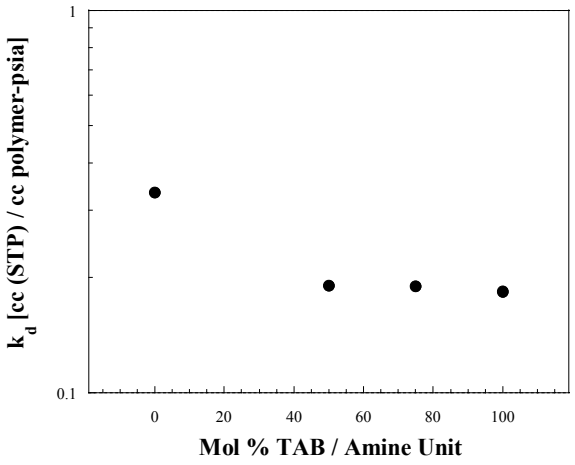

Figure 5.11. C_3H_6 Henry's law coefficient, k_D, as a function of the TAB/DAM ratio.

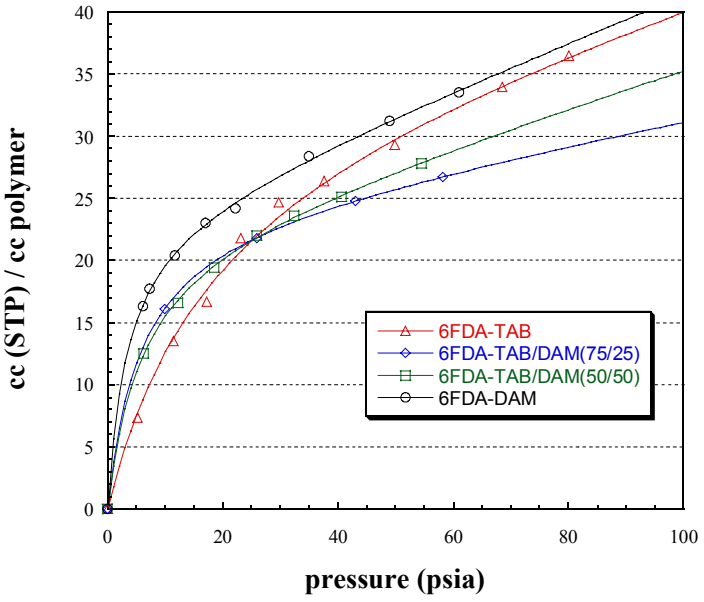

Figure 5.12. Sorption isotherms of C_3H_8 for the 6FDA-TAB/DAM copolymer family at 35°C.

Table 5.6. Dual mode parameters for C_3H_8 in various 6FDA-TAB/DAM copolymers at 35°C.

Parameter	6FDA-TAB	6FDA-TAB/DAM (75/25)	6FDA-TAB/DAM (50/50)	6FDA-DAM
k_D	0.135 ± 0.047	0.085 ± 0.003	0.143 ± 0.012	0.184 ± 0.012
C'_H	31.1 ± 5.6	23.8 ± 0.2	22.1 ± 0.7	23.7 ± 0.7
b	0.056 ± 0.015	0.180 ± 0.004	0.174 ± 0.014	0.296 ± 0.030

Sorption results for C_3H_8 are shown in Figure 5.12, and dual mode parameters are shown in Table 5.6. The trends for the C_3H_8 dual mode parameters generally follow those for C_3H_6. Consistent with the C_3H_6 results, there is no observed trend in the Langmuir capacity constant. Similarly, there is an increase in the affinity constant with decreasing TAB/DAM ratio. The Henry's law constant shows a slight increasing trend. The aforementioned arguments for C_3H_6 can be applied to this case as well.

5.4 DIFFUSION COEFFICIENTS

Diffusion coefficients are calculated from the permeation and sorption data in Tables 5.2 and 5.4 using the solution diffusion model. The diffusion coefficients for various gas molecules are plotted versus the TAB/DAM ratio in Figure 5.13. As the effective diameter of the gas molecule increases the diffusion coefficient decreases as expected. Another noticeable trend is that with increasing TAB/DAM ratio, the diffusion coefficient decreases in an exponential fashion.

This is expected since TAB packs more efficiently than DAM. The combination of these trends leads to the observation that with increasing molecular size the diffusion coefficient experiences greater depression over the range of copolymers. This is true with the exception of C_3H_8, the largest molecule tested. The C_3H_8 curve breaks off sharply at the 6FDA-TAB/DAM(50/50) copolymer resulting in only a moderate decrease in diffusivity from the 6FDA-TAB/DAM(50/50) copolymer to the 6FDA-TAB homopolymer. Clearly, this phenomena leads to the permselectivity maximum demonstrated in Section 5.2. Potential causes of this surprising trend will be discussed in the next section.

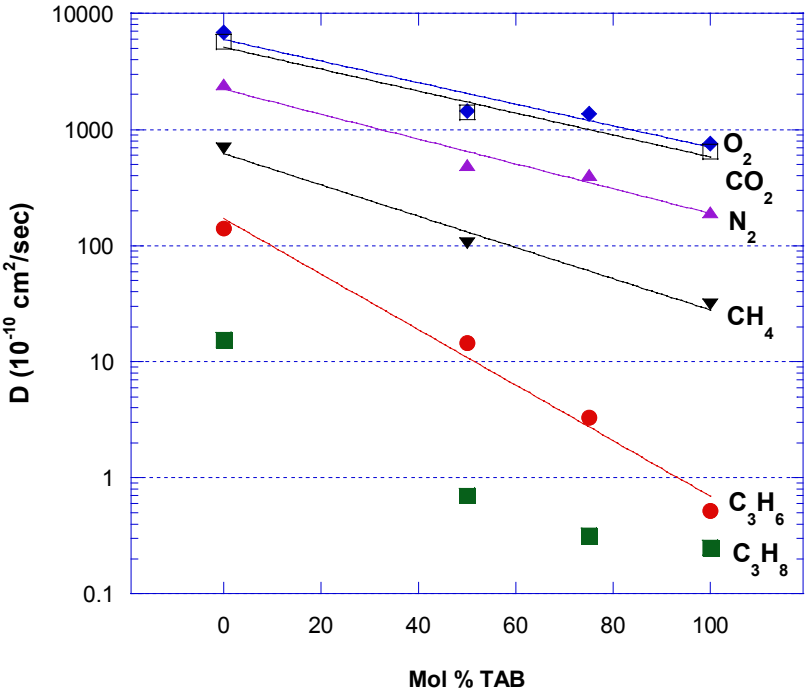

Figure 5.13. Diffusion coefficients as a function of the 6FDA-TAB/DAM copolymer ratio for gas molecules considered in this study.

5.5 UNDERSTANDING THE SELECTIVITY MAXIMUM PHENOMENA

5.5.1 Introduction

The observation of a selectivity maximum with changes in material structure has been discussed in section 5.2 and 5.4. The work presented here appears to be the first indication of the phenomena with regard to copolymers. However, the trend has been observed in the literature for carbon molecular sieve

membranes for a variety of gas separations. It is possible that other examples of this trend exist in the literature, which are not noted here, however, it is believed that the most prominent cases have been found and these cases will be discussed below. Although the trend has been noticed in the past with carbon materials, reasons for the unexpected behavior have not been hypothesized and discussed within the literature. The purpose of this section is to provide some theoretical explanations for this surprising trend. Understanding of this phenomena could lead to improvement in materials engineering for gas separation membranes.

The conventional belief in the literature is that as the average size of the selective regions within a material (whether it is a pore of a carbon material or the chain spacing of a rigid polymer) decrease, the diffusion coefficient of a particular probe molecule decreases as well. The following analysis will attempt to demonstrate why this trend does not necessarily hold true. It is believed the overlooked assumption in the preceding notion is the fact that the average size of the selective regions is the most important variable. More rigorously, it is very valuable to account for the *distribution* of size selective entities, either the distribution of pore sizes in a carbon material, or the distribution of chain spacings within a rigid polymeric material (alternatively the distribution of free volume).

5.5.2 Modeling distributions of selective entities

For simplicity, it is useful to first consider a porous carbon material. Later it will be possible to connect these notions with the rigid polymeric materials. Various researchers have characterized the micropore distribution of carbon materials. Ogawa and Nakano have characterized the micropore distribution of

carbonized membranes prepared by gel modification from 3.3 Å to greater than 5.0 Å [13]. Steel has characterized the micropore distribution of carbon materials using density functional theory for pores ranging in size of 4 - 11 Å [8]. Hayashi *et al.* have characterized pore distributions using sorption isotherms, and the Dubinin-Astakhov equation [16]. These studies represent the fact that carbon molecular sieve materials are comprised of discrete micropore distributions. Therefore, it is useful to consider modeling work in an effort to correctly describe the effect of these pore distributions on the resulting transport properties, and attempt to explain possible causes of the selectivity maximum phenomena.

To begin, the assumption is made that a bulk carbon molecular sieving membrane can be considered as a *composite* material made up of an assembly of multiple discrete pore sizes. Each characteristic domain is envisioned as possessing an intrinsic permeability for an individual gas molecule, which would be the effective permeability if the membrane were composed of only that particular pore size. Ideally, these different local domains with distinct characteristic permeability properties can be combined by some "mixing rule" to yield the effective properties of the bulk medium. Initially, a parallel model for gas permeability is chosen to represent the effective permeability through a material of n characteristic domains:

$$\mathrm{P}_{Eff} = \sum_{1}^{n} P_i \bullet \phi_i \qquad (5.2)$$

This equation can also be viewed in terms of probabilities, where the number fraction of pore i, ϕ_i, represents the probability of the penetrant molecule finding

that pore, and the permeability, P_i, represents the probability of going through that pore. It can further be assumed that the equilibrium solubility within the material is the same throughout because the solubility is related to the size of the larger cavities and the condensability of the penetrant, but not necessarily the size of the selective micropores. The solubility coefficient can then be factored out of the previous equation to provide a parallel model for the effective diffusivity,

$$D_{Eff} = \sum_{1}^{n} D_i \bullet \phi_i \qquad (5.3)$$

which can be used to demonstrate why the selectivity maximum phenomena is observed for some gas separations, yet not for others over the same range of material structures.

A hypothetical distribution comprising domains characterized by one of 3 idealized pore sizes is considered, labeled pore1, pore2, and pore3. These domains are assigned permeability values that might be observed in a medium comprised only of such pores for two penetrants A and B, shown in Table 5.7. Membrane materials can then be created hypothetically with different distributions of pore1, pore2, and pore3. For simplicity, these materials can be labeled membrane A, membrane B, and membrane C. Membrane A will be composed of 99 % pore1, and the balance an equal amount of pore2 and pore3. Membrane B will be 99 % pore2, and so on. The results are shown in Figure 5.14, using Equation 5.2 to calculate the permeability of penetrant A, and the selectivity (P_A/P_B), for each membrane.

Table 5.7. Assigned permeability values of penetrants A and B for pore1, pore2, and pore3.

Pore	Permeability A (Barrer)	Selectivity A/B
Pore1	400	5
Pore2	40	50
Pore3	4	500

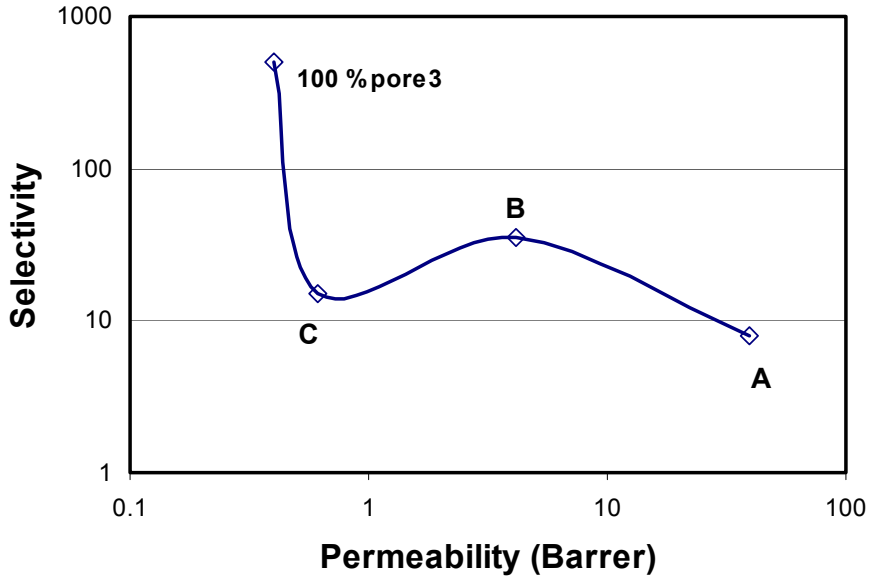

Figure 5.14. Illustration of selectivity maximum based on a hypothetical pore size distribution, and a parallel permeability model.

The properties of membranes A and B are as expected, very near to those of 100 % pore1 and very near to those of 100 % pore2, respectively. On the other hand, membrane C (which is 99 % pore3) does not fall anywhere near the data point for 100 % pore3. In fact, membrane C shows a selectivity of only16, in spite of the

fact that 99 % of the material has an overall selectivity of 500. This hypothetical situation is simply intended to illustrate how the selectivity maximum phenomena could arise. It is useful, however, to understand the drawbacks of this hypothetical, and attempt to extend these ideas in a more critical fashion.

The first obvious shortcoming of the previous hypothetical is the designation of permeability values. While the values were assigned based on expected trends, this designation is still somewhat arbitrary, and there is value in making it more rigorous. Furthermore, the experimental data has shown that this phenomena can exist for certain separations, yet not others, over the same range of material structures (this has been shown for the poly(pyrrolone-imide) copolymers and the carbon materials). It is important to be able to explain these results over multiple data sets.

Teplyakov and Meares have demonstrated an empirical relationship between diffusion coefficient and molecular size of the gas molecule:

$$D = K_1 \exp^{-K_2(\sigma_{eff})^2} \qquad (5.4)$$

where σ_{eff} is the effective size of a molecule, and K_1 and K_2 are empirically fit coefficients. This expression can be used as a method to assign diffusion coefficients to specific selective entities (or pores). Choosing this particular expression is not necessarily better or worse than choosing other expressions, which might be proposed in the literature for the diffusion dependence of a

penetrant based on size of the penetrant. It is only designed to provide structure to the assignment of the diffusion coefficient for each pore. Table 5.8 lists the K_1 and K_2 coefficient values for the given pores. Table 5.9 lists the effective diameter of six gas molecules of interest, and the subsequent diffusion coefficient (arbitrary units) in hypothetical pores 1-3, based on Equation 5.4. These values are then used, along with the parallel model (Equation 5.2) to calculate results for membranes A, B, and C, which are defined just as they were in the last discussion. The results of this exercise are shown in Figure 5.15. It can be seen that in all cases membranes A and B closely match the results of pure pore1 and pure pore2. Membrane C begins to show deviations from the pure pore3 in all cases, and this is because pore3 does not necessarily dominate transport even though it is by far in the largest percentage. The term in Equation (5.2) that determines which pore or entity dominates transport is ($\boldsymbol{P}_i \bullet \phi_i$), meaning that a pore can completely dominate transport even if it is the pore in the lowest percentage of the membrane. From the results in Figure 5.15 it can be seen that for O_2/N_2, and CO_2/CH_4, pore1 begins to have some influence on the overall transport, which causes membrane C to deviate considerably from the results of pure pore3. However, there is still a linear relationship between membranes A, B, and C on a log / log plot of diffusivity and diffusivity selectivity for O_2/N_2, and CO_2/CH_4, which would be exactly what is expected from the view of the experimentalist. The C_3H_6/C_3H_8 case is quite different because now pore1

completely dominates transport, and this results in membrane C having both a low diffusivity and low diffusivity selectivity, providing the selectivity maximum phenomena. Since the diffusion coefficient becomes a stronger function of size, this phenomena results for the larger molecules in this case. Figure 5.16 shows the diffusivity for each membrane and all 6 gas penetrants. Clearly, as the size of the pentrant increases the trend deviates from the exponential decline in diffusion coefficient.

This hypothetical discussion is simply intended to show how the phenomena can occur for one separation and not another. In practice, the constants K_1 and K_2 could vary depending on the particular pore or selective entity, and this would describe why the selectivity maximum phenomena has been seen for a variety of gas pair separations (observed experimentally in the literature for carbon molecular sieve membranes). The final point of this exercise is that membrane C appears to be very poor for the C_3H_6/C_3H_8 separation, yet the reason is not because it does not possess selective entities, but that these entities are not being utilized (not dominating transport). This realization is important, because other engineering variables, such as temperature and pressure, could possibly be used to change this fact.

Table 5.8. K_1 and K_2 values for pore1, pore2, and pore3.

	K_1	K_2
Pore1	1×10^6	-0.5
Pore2	1×10^6	-0.7
Pore3	1×10^6	-0.9

Table 5.9. Diffusivity of pores based on the effective diameter and Equation 5.4.

Penetrant	Effective Diameter (Å)	Diffusivity (pore1)	Diffusivity (pore2)	Diffusivity (pore3)
CO_2	3.30	4318	489	55.4
O_2	3.44	2694	253	23.7
N_2	3.66	1234	84.7	5.81
CH_4	3.81	704	38.6	2.12
C_3H_6	4.68	17.5	0.219	0.00275
C_3H_8	5.06	2.76	0.0165	0.00010

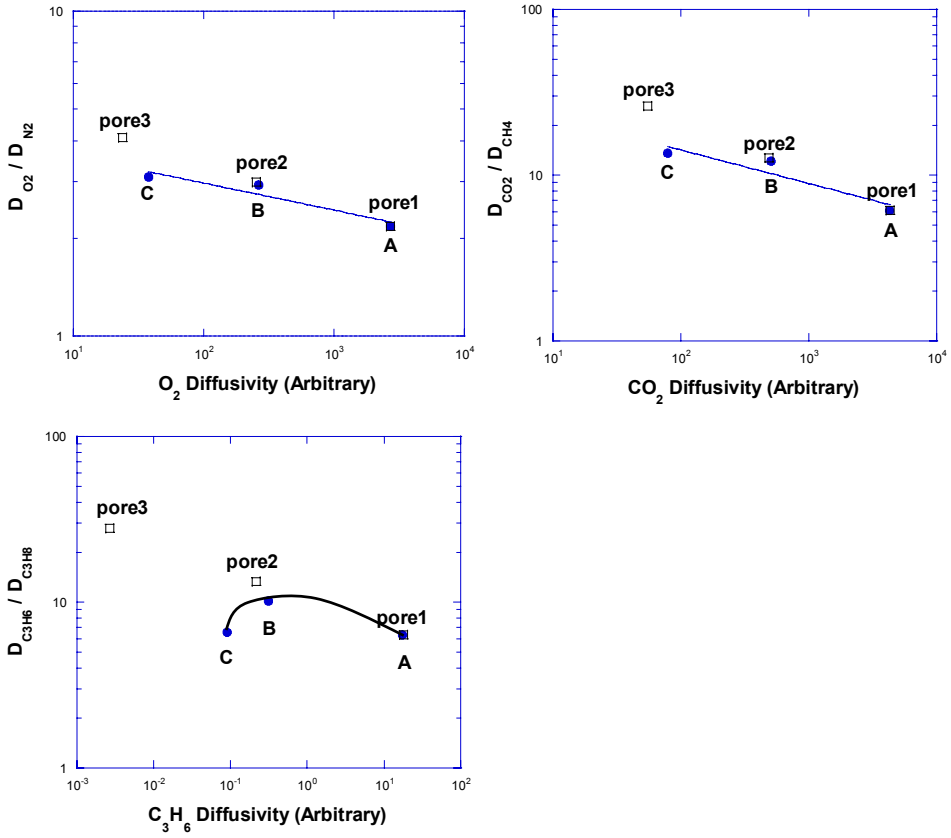

Figure 5.15. Diffusivity selectivity versus diffusivity for 3 hypothetical separations of O_2/N_2, CO_2/CH_4, and C_3H_6/C_3H_8. □ represents the pure pore. ● represents membrane A, B, or C. The solid lines are trends for the membranes A, B, and C.

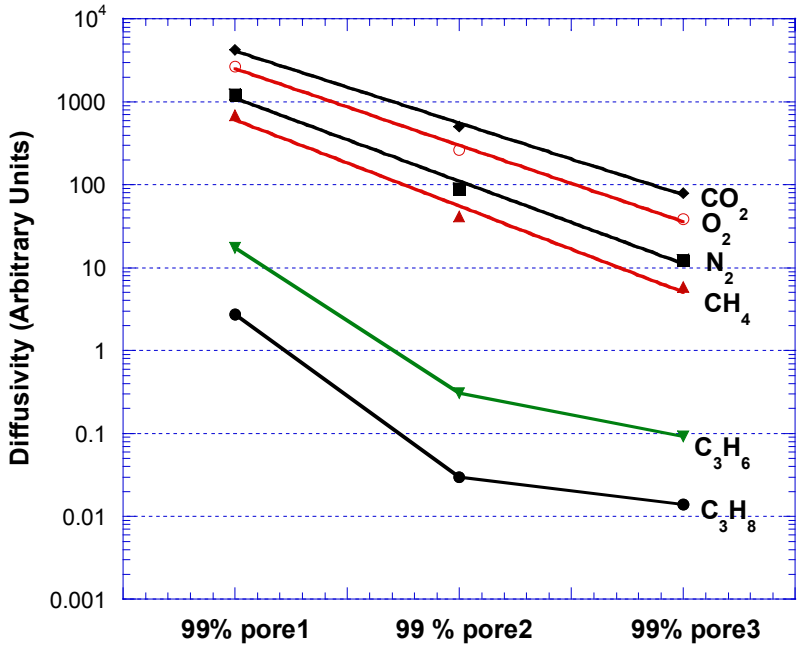

Figure 5.16. Diffusivity for membranes A, B, and C over the range of penetrants, created using the Meares Equation and the parallel model.

The parallel model for gas permeability (or diffusion) is only one model that can describe transport behavior in composite materials. It is useful to consider additional models to understand any limitations of the parallel model. Additional models include the series model:

$$P_{Eff} = \frac{1}{\sum_{1}^{n} \frac{\phi_i}{P_i}} \qquad (5.5)$$

and the Maxwell model:

$$P_{Eff} = P_c \left[\frac{P_d + 2P_c - 2\Phi_d (P_c - P_d)}{P_d + 2P_c + \Phi_d (P_c - P_d)} \right] \tag{5.6}$$

where the subscript, c, denotes the continuous phase, and the subscript, d, denotes the dispersed phase. Figure 5.17 shows these different models for a composite of 2 pore sizes, pore1 have a permeability of 400 Barrer, and pore2 having a permeability of 4 Barrer. In this case the Maxwell model is plotted assuming pore1 is the continuous phase. Clearly, the parallel and series models differ strongly in their prediction of the overall transport permeability. The Maxwell model closely follows the parallel model, and it can be shown that if pore2 was taken as the continuous phase the Maxwell model would closely match the series model prediction. However, experimental reality must lie somewhere in between the parallel and series models. At low fractions of pore1 it follows that pore2 would be the continuous phase, and the series model would be more accurate. The converse it also true, and at higher percentages the parallel model would be more accurate. A weighted combination model can be introduced that incorporates this concept:

$$P_{eff} = \left(\frac{1}{\frac{\phi_1}{P_1} + \frac{\phi_2}{P_2}} \right) \phi_2 + (\phi_1 P_1 + \phi_2 P_2) \phi_1 \tag{5.7}$$

This model is plotted in Figure 5.17, illustrating a fairly appropriate combination of both the parallel and series models. While this model captures the correct effects, it is currently limited because it cannot be extended to multiple pore sizes.

Effective Medium Theory (EMT) was created to describe conduction effects in a nonhomogeneous mixture. This theory assumes that the material is a homogeneous effective medium with local fluctuations in conductivity. Davis extended this theory to apply to transport in composite materials, which can be represented by [21, 22]:

$$\sum_{1}^{n} \Phi_i \frac{\alpha_m - \alpha_i}{\alpha_i + 2\alpha_m} = 0 \qquad (5.8)$$

where α represents the conductivity, which is simply a proportionality constant relating a flux, J, and a driving force, $\nabla\mu$:

$$J = -\alpha \nabla\mu \qquad (5.9)$$

The analogy can be made to Fick's law in order to extend the theory to the diffusion coefficient of a medium:

$$\sum_{1}^{n} \Phi_i \frac{D_m - D_i}{D_i + 2D_m} = 0 \qquad (5.10)$$

Assuming that the equilibrium sorption of the pore cavities is constant throughout the medium, this can also be applied to the effective permeability:

$$\sum_{1}^{n} \Phi_i \frac{P_{Eff} - P_i}{P_i + 2P_{Eff}} = 0 \qquad (5.11)$$

For the circumstances described here, EMT is the most useful model because it appropriately weights the percentage of a pore within the material (similar to the weighted combination model shown in Figure 5.17), and it can be applied to an infinite number of selective entities.

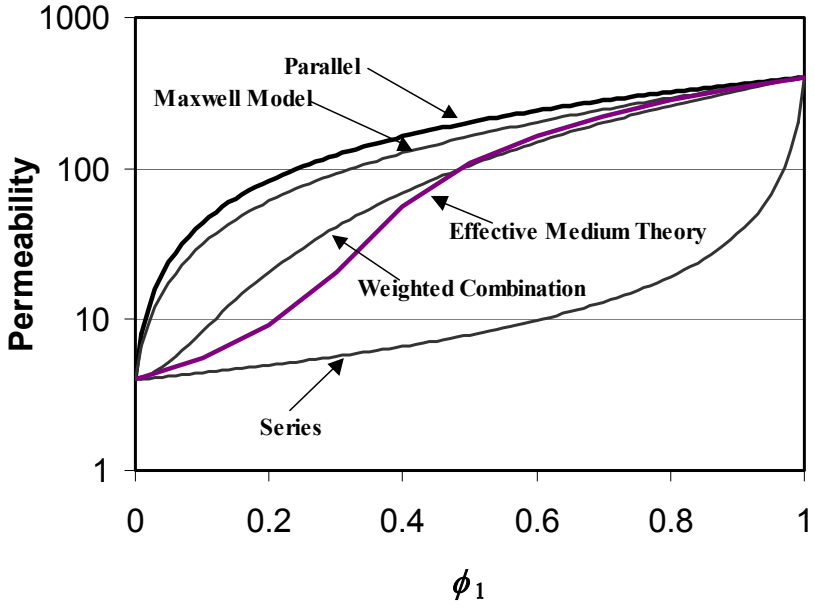

Figure 5.17. Comparison of the effective permeability as a function of pore size distribution using the Parallel, Series, Maxwell, Weighted Combination, and EMT models for a hypothetical binary composite material.

Since the effective permeability for EMT cannot be solved for explicitly, a FORTRAN program was created with the help of Sean Burns in order to generate a selectivity "map" for a material of 3 pores over the range of possible distributions. The entire program is provided in Appendix C. The program solves for the effective diffusivity using the series model as an initial guess, and converges using Newton's method. The inputs to the program are the diffusivity (or alternatively permeability) of both gases for all 3 pores, and in this case the diffusivity values generated in Table 5.9 for CO_2, O_2, N_2, CH_4, C_3H_6, and C_3H_8

were used. The results are shown in Figure 5.18 with diffusivity selectivity as a function of the number fraction pore1. The solid lines represent constant pore3 curves. In this manner the entire distribution of 3 pores can be represented on a 2-dimensional plot. The first noticeable trend is that the selectivity decreases in all cases with increasing pore1 up to ~ 60 % pore3, which is somewhat intuitive since pore1 is slowly replacing pore2, a more selective entity. Surprisingly, the slopes of the curves change at ~ 70 – 80% pore3, which indicates an increasing selectivity upon addition of a less selective pore (exchanging pore1 for pore2). Physically, the reason for this is the difference in diffusivity between pore1 and pore3. Essentially, gas molecules are able to pass easily through pore1 relative to pore3, and this allows pore3 to dominate transport. Another way of viewing the situation is that pore1 provides less competition with pore3 than does pore2. Essentially for O_2/N_2 and CO_2/CH_4 this is a subtle effect occurring at 80% pore3, with only a slight increase in selectivity. In the C_3H_6/C_3H_8 case the effect occurs earlier (between 60 – 70% pore3), and more intensely, as evidenced by the large gap in selectivity between the 60% and 70% curves. This means that a subtle altering of the material composition in this range could have a much larger effect on the C_3H_6/C_3H_8 separation relative to O_2/N_2 and CO_2/CH_4. Figure 5.19 illustrates this concept. Upon shifting the pore size distribution to an *average* larger pore size (left to right), the O_2/N_2 and CO_2/CH_4 selectivities decrease as expected, while the C_3H_6/C_3H_8 extends through a maximum. It should also be noted that the x-axis spacing between distributions in Figure 5.19 is somewhat arbitrary, and therefore the concavity of the curves is also subjective. However,

the objective is only to illustrate that larger molecules may show more dramatic responses to subtle shifts in the distribution of selective entities.

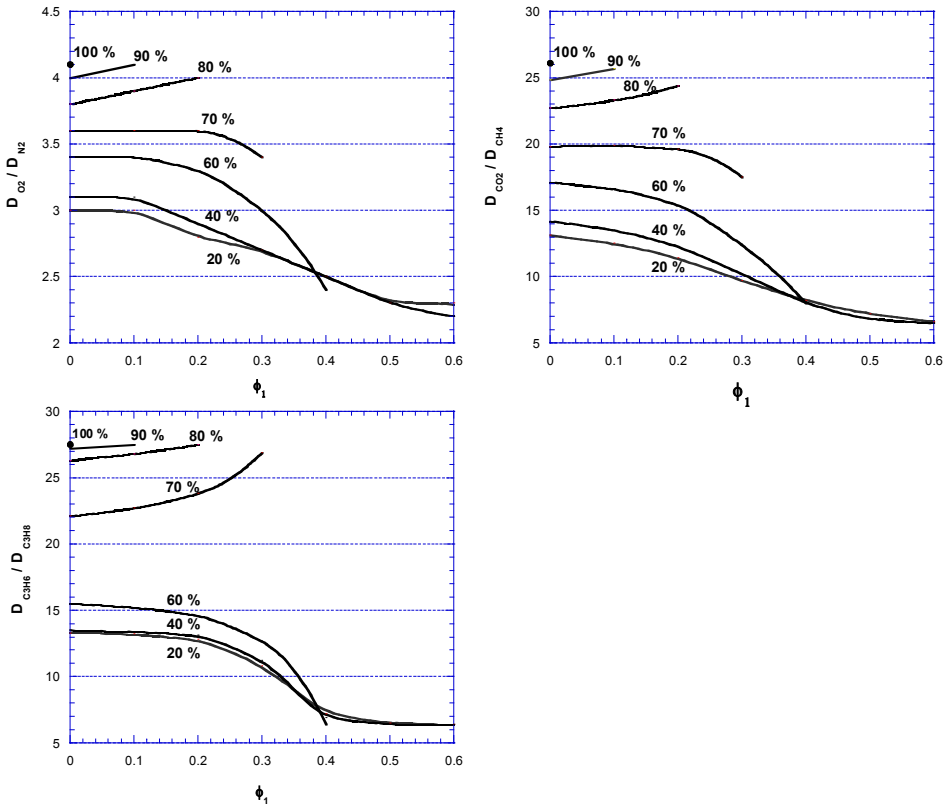

Figure 5.18. EMT predictions of diffusivity selectivity over the range of pore distributions. Values for the diffusivity of pore1, pore2 and pore3 were obtained from Table 5.9. Solid lines represent constant pore3 compositions. The overall pore distribution is determined from the relationship $\sum \phi_i = 1$.

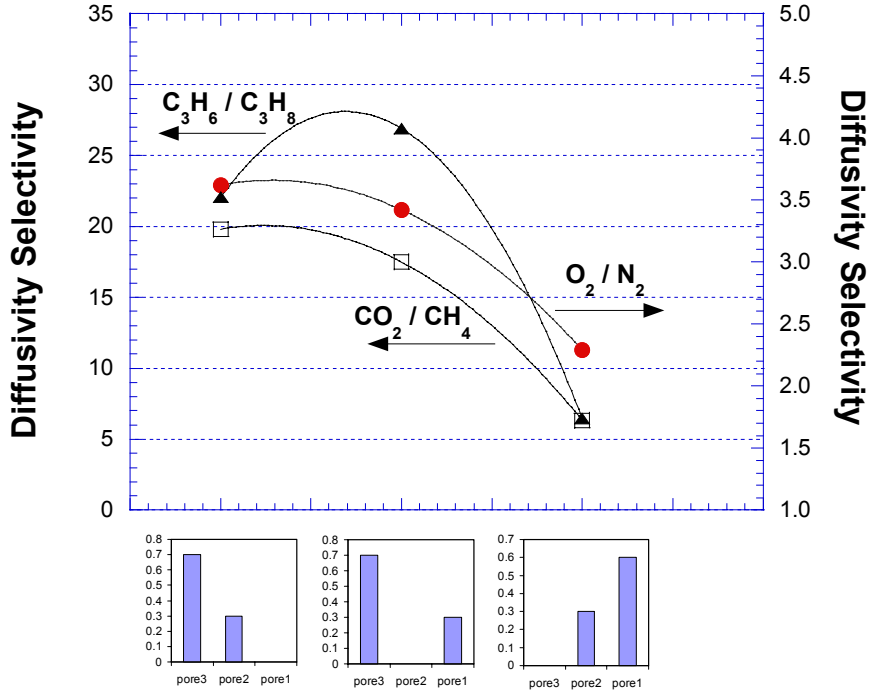

Figure 5.19. Diffusivity selectivity as a function of pore size distribution, predicted using EMT.

5.5.3 Free Volume Distributions in Polymeric Materials

The concepts involving the distribution of pore sizes in carbon materials can also be analogous to the distribution of chain spacings within a polymeric material or alternatively the free volume distribution. Similar to the carbon materials, as the average segmental spacing becomes smaller, it would be expected that the overall free volume distribution would also be shifted toward smaller distances. Clearly, this would be the expected trend as the TAB/DAM

ratio is increased for the copolymer family discussed in this work. Therefore the trends in the diffusion coefficients shown in Figure 5.13 can be understood through analogy to the above modeling arguments for the microporous carbon membranes. The only known way to measure the free volume distribution in polymeric materials is by positron annihilation lifetime spectroscopy (PALS). Many literature articles are available describing this technique for polymer membranes, and a few are provided here for reference [4, 23-25]. Zimmerman attempted this technique for polypyrrolone membranes, with somewhat ambiguous results [18]. In analyzing positron annihilation results it is the third lifetime, the ortho-positronium, which is understood to correlate with free volume 'holes' in polymeric materials. For the polypyrrolone, 6FDA-TAB (as well as other polypyrrolones) the third lifetime, τ_3, as well as the intensity, I_3, were unusually depressed. Evidence has shown that these aromatic ultra-rigid polymer segments act as Lewis bases, and are strong electron donors [20]. This is consistent with the fact that the polymers are insoluble in typical organic solvents, because they have strong intermolecular interactions. It is believed that the ortho-positronium is annihilated more rapidly in these "electron rich" free volume areas of the polypyrrolone, and therefore provides ambiguous results as to the interpretation of the accessible free volume of the matrix. For these reasons further study with PALS was not attempted on the poly(pyrrolone-imide) materials in this work.

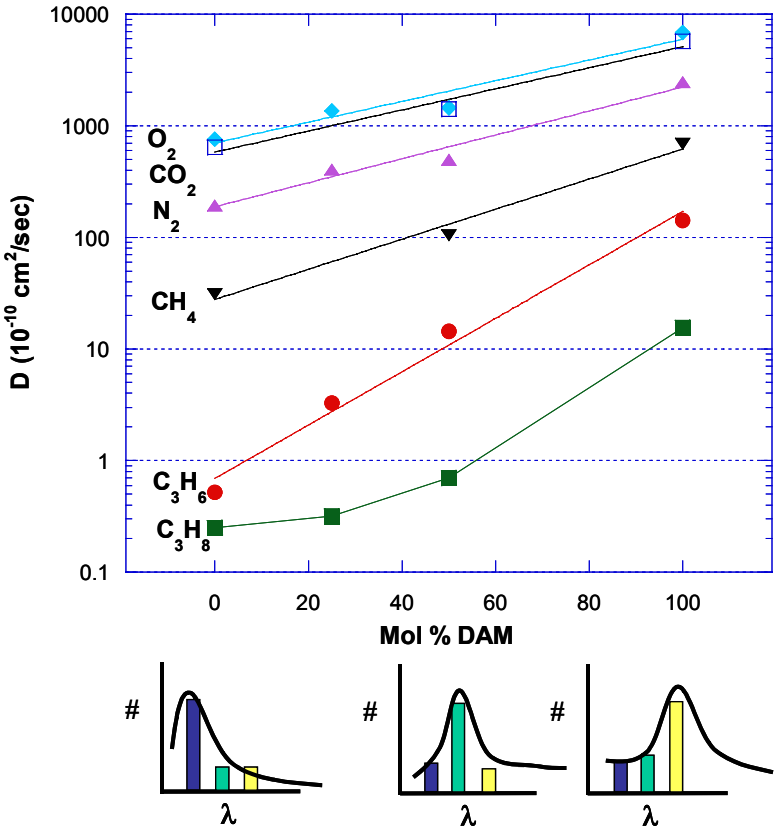

Figure 5.20. Expected shift in chain spacing distributions with altering TAB/DAM ratio. Size and shape of distributions are unknown, however a 'shift' is expected based on x-ray diffraction data, and diffusion coefficient data shown here.

Although free volume distributions could not be directly measured using PALS, a shift in the distribution is still expected with altering TAB/DAM stoichiometry. A visual example of this expected shift is shown in Figure 5.20. This anticipated change is based on the x-ray diffraction data noted earlier, the 3-

dimensional Hyperchem® drawings shown earlier, and the diffusion coefficient data shown here. It should be noted that the size and shape of the segmental distributions in Figure 5.20 are currently unknown, and are only drawn to provide an example of the expected shift in free volume distribution with material structure. Again, the analogy to the modeling of the carbon materials can be used to understand the reason for the unexpected trend in the diffusion coefficient for the larger C_3H_8 molecule (shown in Figure 5.20).

Assuming a shift in the free volume distribution to smaller chain spacings leads to high selectivity materials for O_2/N_2 and CO_2/CH_4, but not C_3H_6/C_3H_8, it is interesting to examine how this may be useful for the C_3H_6/C_3H_8 separation. For polymeric materials (unlike carbon materials) the distribution of free volume can be altered via a number of different avenues (other than monomer stoichiometry), most of which are usually unintentional. For example, physical aging of polymeric materials is believed to be caused by a shift in the free volume distribution to lower average chain spacings. Physical aging almost always results in depressed permeability and increased selectivity. Another example is penetrant induced swelling or plasticization. In this case, it has been well documented (for polycarbonate and polysulfone) using PALS *in situ* with CO_2 sorption that a broadening and shift of the accessible free volume distribution occurs upon increasing CO_2 pressure [23, 25]. Ito *et al.* have observed similar trends for polyimide materials [24]. This evidence also suggests that penetrant induced swelling of poly(pyrrolone-imides) with C_3H_6 (or C_3H_8) would lead to a broadening or shift of the free volume distribution to larger average chain

spacings. Normally, this would be expected to result in an increase in the diffusion coefficient and a decrease in the diffusive selectivity, typically seen for the CO_2/CH_4 case, for example. However, based on Figure 5.20 one could foresee shifting the free volume distribution of 6FDA-TAB (based on penetrant induced swelling) resulting in a significantly increased C_3H_6 diffusion coefficient and only a moderately increased C_3H_8 diffusion coefficient. Overall, it is hypothesized that this would result in an increase in C_3H_6 permeability and an *increase* in C_3H_6/C_3H_8 selectivity. Furthermore, increasing temperature is a method to create a shift in the free volume distribution towards average larger segmental spacings through thermal expansion. Researchers have also demonstrated this effect on the free volume for other glassy polymers using PALS [26]. Based on the same arguments as those given for penetrant induced dilation, it would be hypothesized that increasing temperature in permeation experiments for 6FDA-TAB would result in decreases in selectivity for O_2/N_2 and CO_2/CH_4, but alternatively increases in both C_3H_6 permeability and C_3H_6/C_3H_8 selectivity. These hypotheses regarding pressure and temperature effects are examined in more detail in Chapter 6.

5.6 REFERENCES

[1] C. M. Zimmerman and W. J. Koros, Entropic Selectivity Analysis of a Series of Polypyrrolones for Gas Separation Membranes, 32 (1999) 3341-3346.

[2] D. R. B. Walker, Synthesis and Characterization of Polypyrrolones For Gas Separation Membranes, Ph.D. Dissertation, The University of Texas at Austin, 1993.

[3] C. M. Zimmerman and W. J. Koros, Polypyrrolones for Membrane Gas Separations. I. Structural Comparison of Gas Transport and Sorption Properties, J. Polym. Sci. Part B 37 (1999) 1235-1249.

[4] V. P. Shantarovich, I. B. Kevdina, Y. P. Yampolskii and A. Y. Alentiev, Positron annihilation lifetime study of high and low free volume glassy polymers: Effects of free volume sizes on the permeability and permselectivity, Macromolecules 33 (2000) 7453-7466.

[5] Y. P. Yampolskii, A. P. Korikov, V. P. Shantarovich, K. Nagai, B. D. Freeman, T. Masuda, M. Teraguchi and G. Kwak, Gas permeability and free volume of highly branched substituted acetylene polymers, Macromolecules 34 (2001) 1788-1796.

[6] L. M. Robeson, Correlation of Separation Factor Versus Permeability for Polymeric Membranes, J. Membr. Sci. 62 (1991) 165-185.

[7] A. E. Barnabeo, W. S. Creasy and L. M. Robeson, Gas permeability characteristics of nitrile-containing block and random copolymers, J. Polym. Sci. Pol. Chem. 13 (1975) 1979-1986.

[8] K. Steel, Carbon Membranes for Challenging Gas Separations, Ph. D. Dissertation, The University of Texas at Austin, 2000.

[9] A. Singh-Ghosal and W. J. Koros, Air separation properties of flat sheet homogeneous pyrolytic carbon membranes, J. Membr. Sci. 174 (2000) 177-188.

[10] D. Q. Vu, Formation and Characterization of Asymmetric Carbon Molecular Sieve and Mixed Matrix Membranes for Natural Gas Purification, Ph.D. Dissertation, The University of Texas at Austin, 2001.

[11] D. Q. Vu, W. J. Koros and S. J. Miller, High pressure CO2/CH4 separation using carbon molecular sieve hollow fiber membranes, Ind. Eng. Chem. Res. 41 (2002) 367-380.

[12] K. Okamoto, S. Kawamura, M. Yoshino, H. Kita, Y. Hirayama, N. Tanihara and Y. Kusuki, Olefin/paraffin separation through carbonized membranes derived from an asymmetric polyimide hollow fiber membrane, Ind. Eng. Chem. Res. 38 (1999) 4424-4432.

[13] M. Ogawa and Y. Nakano, Separation of CO2/CH4 mixture through carbonized membrane prepared by gel modification, J. Membr. Sci. 173 (2000) 123-132.

[14] Y. Kusuki, H. Shimazaki, N. Tanihara, S. Nakanishi and T. Yoshinaga, Gas permeation properties and characterization of asymmetric carbon membranes prepared by pyrolyzing asymmetric polyimide hollow fiber membrane, J. Membr. Sci. 134 (1997) 245-253.

[15] M. S. Kane, J. F. Goellner, H. C. Foley, R. DiFrancesco, S. J. L. Billinge and L. F. Allard, Symmetry breaking in nanostructure development of carbogenic molecular sieves: Effects of morphological pattern formation on oxygen and nitrogen transport, Chem. Mat. 8 (1996) 2159-2171.

[16] J. Hayashi, H. Mizuta, M. Yamamoto, K. Kusakabe and S. Morooka, Pore size control of carbonized BPDA-pp'ODA polyimide membrane by chemical vapor deposition of carbon, J. Membr. Sci. 124 (1997) 243-251.

[17] J. Hayashi, M. Yamamoto, K. Kusakabe and S. Morooka, Simultaneous Improvement of Permeance and Permselectivity of 3,3',4,4'-Biphenyltetracarboxylic Dianhydride-4,4'-Oxydianiline Polyimide Membrane by Carbonization, Ind. Eng. Chem. Res. 34 (1995) 4364-4370.

[18] C. M. Zimmerman, Advanced Gas Separation Membrane Materials: Hyper Rigid Polymers and Molecular Sieve-Polymer Mixed Matrices, Ph.D. Dissertation, The University of Texas at Austin, 1998.

[19] K. Tanaka, A. Taguchi, J. Q. Hao, H. Kita and K. Okamoto, Permeation and separation properties of polyimide membranes to olefins and paraffins, J. Membr. Sci. 121 (1996) 197-207.

[20] S. A. Jenekhe and P. O. Johnson, Complexation-Mediated Solubilization and Processing of Rigid- Chain and Ladder Polymers in Aprotic Organic-Solvents, Macromolecules 23 (1990) 4419-4429.

[21] H. T. Davis, L. R. Valencourt and C. E. Johnson, Transport processes in composite media, J. Am. Ceram. Soc. 58 (1975) 446-452.

[22] H. T. Davis, The effective medium theory of diffusion in composite media, J. Am. Ceram. Soc. 60 (1977) 499-501.

[23] X. Hong, Y. C. Jean, H. J. Yang, S. S. Jordan and W. J. Koros, Free-volume hole properties of gas-exposed polycarbonate studied by positron annihilation lifetime spectroscopy, Macromolecules 29 (1996) 7859-7864.

[24] Y. Ito, H. F. M. Mohamed, K. Tanaka, K. Okamoto and K. Lee, Sorption of CO2 in polymers observed by positron annihilation technique, J. Radioanal. Nucl. Chem.-Artic. 211 (1996) 211-218.

[25] J. P. Yuan, H. Cao, E. W. Hellmuth and Y. C. Jean, Subnanometer hole properties of CO2-exposed polysulfone studied by positron annihilation lifetime spectroscopy, J. Polym. Sci. Pt. B-Polym. Phys. 36 (1998) 3049-3056.

[26] B. Wang, Z. F. Wang, M. Zhang, W. H. Liu and S. J. Wang, Effect of temperature on the free volume in glassy poly(ethylene terephthalate), Macromolecules 35 (2002) 3993-3996.

CHAPTER 6: PRESSURE AND TEMPERATURE DEPENDENT EFFECTS

6.1 PRESSURE DEPENDENT PERMEABILITY

6.1.1 Pressure Dependent Permeability of Poly(pyrrolone-imides)

The conventional permeation pressure dependence of glassy polymeric membranes with condensable penetrants is discussed in Chapter 2. At low pressures a decreasing permeability is often observed due to saturation of Langmuir unrelaxed free volume sites. At elevated pressures an upturn in the permeation isotherm is often observed due to plasticization.

Previous studies on polypyrrolone materials have found these materials to be permeation plasticization resistant to CO_2. Walker found no upturn in the CO_2 permeation isotherm up to 900 psia for the rigid chain polypyrrolones, 6FDA-6FTA and 6FDA-TADPO [1]. In contrast, various polyimides exhibit upturns in the CO_2 permeability isotherm at feed pressures ranging from 100 – 300 psia [2, 3]. Based on this information it might be expected that the polypyrrolones studied in the work here would maintain plasticization resistance to hydrocarbon penetrants, and that increasing amounts of polyimide in the copolymer would decrease the resistance; however, *this is not what is observed*.

Figure 6.1 shows a pure gas C_3H_6 permeation isotherm for the polypyrrolone 6FDA-TAB at 35^{o}C. Initially, the permeability decreases as

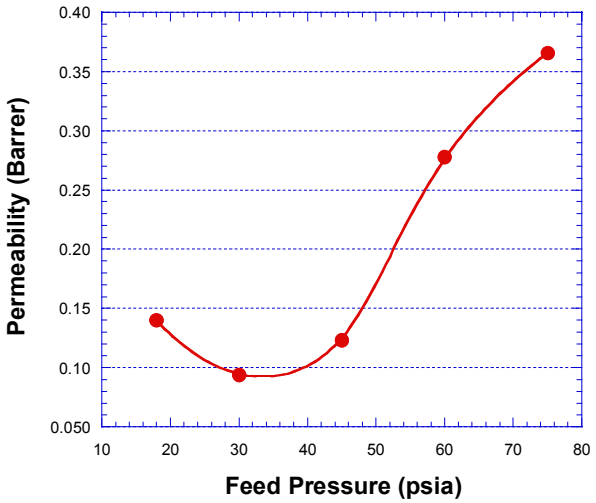

Figure 6.1. C_3H_6 permeability isotherm for 6FDA-TAB at 35°C. The interval between each data point was ~ 2 days.

expected, and reaches a minimum between 2 - 3 atm. Surprisingly, the permeability exhibits a relatively sharp upturn at this low pressure, and increases approximately 300 % up to 75 psia. It should also be noted that apparent permeation plasticization can be a function of both pressure and time for rigid glasses due to non-Fickian responses of the sample. These complex effects add additional time dependence beyond the time-lag estimated using diffusion coefficients determined from steady-state permeation and equimolar sorption results (see Appendix B). The time variable has not specifically been isolated in this case (at a constant pressure); however, it is important to indicate the time interval between each data point, which was approximately 2 days.

The stark contrast in the plasticization resistance between the C_3H_6 data reported here for 6FDA-TAB, polypyrrolone, and the CO_2 data reported by Walker for other polypyrrolones is of further interest. Zimmerman has performed CO_2 permeation for the polypyrrolone, 6FDA-TAB, however only up to 150 psia, which would not be expected to show permeation plasticization. In order to further investigate this issue a CO_2 permeation isotherm was performed up to more elevated pressures. It can be seen in Figure 6.2 that there is no upturn in the CO_2 permeability until ~ 430 psia. This is at a CO_2 concentration of ~ 95 cc (STP) / cc polymer, which is much larger than the concentration of C_3H_6 at the plasticization pressure, ~ 32 cc(STP) / cc polymer. It is likely, in this case, that the diffusion coefficient of the larger C_3H_6 molecule (compared to CO_2) is more strongly affected by free volume changes in the matrix due to penetrant induced swelling. This is very consistent with many past observations of increased diffusion coefficients for larger molecules upon swelling or plasticization.

A C_3H_6 isotherm for the copolymer 6FDA-TAB/DAM(75/25) is shown in Figure 6.3. In this case the upturn in permeability occurs between 3 – 4 atm. The time interval between each data point was two days up until 84 psia. At this point the pressure was held constant for 4 additional days, and one data point was taken each day. After these measurements the pressure was lowered to 48 psia, and the data point was obtained after 2 – 3 days. Clearly, the time dependence of the

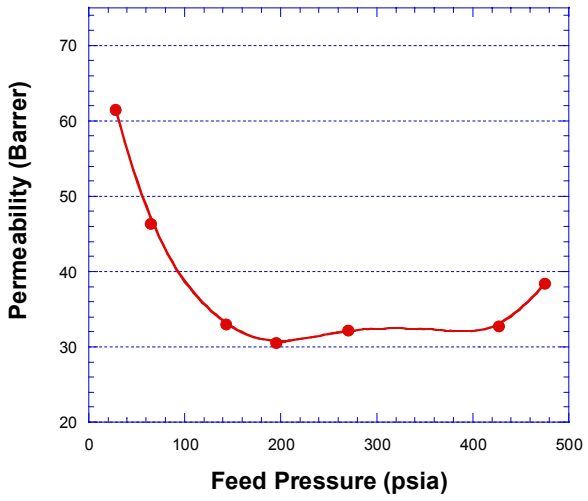

Figure 6.2. CO_2 permeability isotherm for 6FDA-TAB at 35°C. The interval between each data point was ~ 1 day.

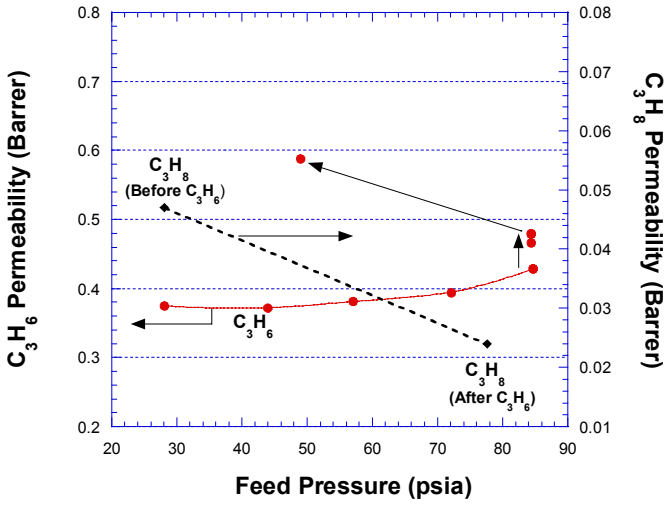

Figure 6.3. ●C_3H_6 permeability isotherm for 6FDA-TAB/DAM(75/25) at 35°C. The interval between each data point was ~ 2 days up to 84 psia. ♦ C_3H_8 data points, the first taken before C_3H_6 data, the second taken *after* C_3H_6 data.

permeability at elevated pressures is very significant. The slope of the permeation upswing could certainly be affected by the time interval of the data collection. The hysteresis in permeability upon lowing the pressure is a phenomenon that has been observed previously [4]. This is indicative of a semi-permanent state, which also provides support for the notion that swelling or dilation of polymer chains has a much larger effect on diffusion compared to penetrant induced flexibility of polymer chains. Interestingly, a high pressure C_3H_8 data point taken after the C_3H_6 conditioning exhibits a decrease in permeability. The data point was taken after one day (> 24 hours) of applied vacuum, and then after 5 days of applied C_3H_8 feed pressure. Although the material is in a semi-permanent swollen state (relative to the initial state), it is believed the C_3H_8 permeability does not increase at elevated pressures because of the large size of the molecule, which is not an intuitive result based on past observations, but is consistent with the hypothesis offered in Section 5.5 regarding penetrant induced dilation of materials that show low flux and low selectivity at 2 atm and 35^{o}C. Essentially, a change in the material structure does not have a large effect on the diffusion coefficient of C_3H_8 similar to what is observed in the structure property arguments discussed in Chapter 5 (see Figure 5.20). Since it is impossible to precisely characterize the behavior of C_3H_8 transport during C_3H_6 conditioning with pure gas tests, this issue is explored further with mixed gas testing.

Figure 6.4 shows the C_3H_6 permeation isotherm for 6FDA-TAB/DAM(50/50). An upturn is observed at ~ 4 atm feed pressure, and in this case the interval between data points is smaller (~ 1 day). From these observed C_3H_6 isotherms there is no clear trend in terms of plasticization resistance as a function of TAB/DAM ratio. All copolymers show an upturn between 2 – 4 atm, which is consistent with many polyimides in the literature, as discussed in Chapter 4. It is evident that the pure polypyrrolone, 6FDA-TAB, does not provide increased plasticization resistance to C_3H_6 in these systems.

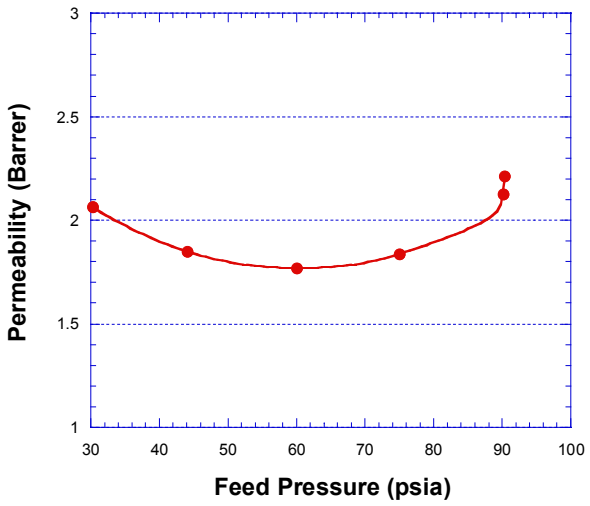

Figure 6.4. C_3H_6 permeability isotherm for 6FDA-TAB/DAM(50/50) at 35°C. The interval between each data point was ~ 1 day up to 90 psia.

6.1.2 Mixed Gas Permeability of Poly(pyrrolone-imides)

Based on the structure-property results given in Chapter 5, it is clear that the materials 6FDA-TAB, and 6FDA-TAB/DAM(75/25) do not behave "normally" for the C_3H_6/C_3H_8 separation (compared to the behavior seen for other gas pairs) because they exhibit low C_3H_6 permeability and low C_3H_6/C_3H_8 selectivity at 2 atm and 35°C; however, these materials have very favorable transport properties for the O_2/N_2 separation and CO_2/CH_4 separation. The examples using both the parallel and EMT models suggest that in these cases of low permeability and low selectivity, it is possible that the materials possess selective entities, but these entities are simply not being utilized or adequately accessed by the penetrants. In the case of the structure-property relationships it was shown that a shift in the distribution of molecular sieving entities, with decreasing TAB/DAM ratio, could lead to a decrease in diffusivity selectivity for certain gas separations (O_2/N_2 and CO_2/CH_4), but an *increase* in selectivity for C_3H_6/C_3H_8 components that "began" at the unusual low flux, low selectivity condition. It follows that there may be other methods to engineer a shift in the distribution of molecular sieving materials, which may lead to improved separation properties of the membrane.

Referring to Figure 5.20 a shift in the free volume distribution to a larger average chain spacing could result in a significant increase in the diffusivity of C_3H_6, with only a moderate increase in the diffusivity of C_3H_8. This, coupled

with the pure gas C_3H_6 permeation isotherms, (which clearly show the tendency of the poly(pyrrolone-imides) to swell or dilate upon exposure to even moderate C_3H_6 feed pressures) leads to the hypothesis that the materials 6FDA-TAB and 6FDA-TAB/DAM(75/25) may show improvements in C_3H_6/C_3H_8 selectivity at elevated pressures, whereas 6FDA-TAB/DAM(50/50) and 6FDA-DAM would likely behave in a classical fashion showing a decrease in C_3H_6/C_3H_8 selectivity at elevated pressures. Mixed gas experiments at elevated pressures and 35^oC were conducted in order to test this hypothesis.

Figure 6.5 shows C_3H_6/C_3H_8 mixed gas results on a log / log plot of permeability and selectivity for the polymers 6FDA-TAB, 6FDA-TAB/DAM(75/25), and 6FDA-TAB/DAM(50/50). The total pressure of the experiment is indicated next to each data point. The C_3H_6/C_3H_8 upper bound defined in Chapter 4 at 2 atm and 50^oC is shown for reference. In this case the upperbound is represented with a dotted line because this boundary is expected to lower (for conventional polymers) under conditions of elevated pressure, as materials begin to show effects of plasticization. It can be seen that with an increase in feed pressure the materials 6FDA-TAB and 6FDA-TAB/DAM(75/25) exhibit a significant *increase in both permeability and selectivity*. On the other hand, as expected, the polymer 6FDA-TAB/DAM(50/50) exhibits an increase in permeability and a decrease in selectivity. It should also be noted that Tanaka *et al.* have reported a decrease in mixed gas selectivity for the polymer 6FDA-DAM

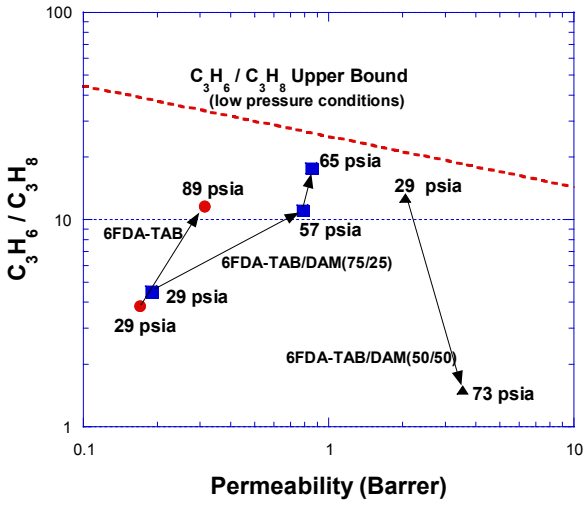

Figure 6.5. Mixed gas C_3H_6/C_3H_8 (50 / 50 feed) at 35°C and variable total pressure for copolymers 6FDA-TAB/DAM.

at 50°C at elevated pressures [5]. More extensive data for this material at 75°C will be discussed in a later section as a case study for the comparison of pure gas and mixed gas C_3H_6/C_3H_8 transport results. The preceding results are noteworthy because they indicate that undesirable materials (under certain conditions) may in fact be the most desirable materials under more industrially relevant feed stream conditions. This also marks an interesting, and previously unreported situation in which using an intrinsic material response, normally thought to be undesirable (polymer swelling), as an advantageous condition to improve transport properties. This approach is much different than the strategy of starting with a high performing material (at low pressure and ambient temperature) and making

material alterations in an effort to suppress the swelling response at elevated feed pressures [6].

6.1.3 Pressure Dependent Permeability of 6FDA-DAM

Tanaka *et al.* have performed pressure dependent C_3H_6/C_3H_8 permeation studies of the pure polyimide, 6FDA-DAM at 50°C [5]. The pure gas results indicate an upturn in the permeability at just over 4 atm. The mixed gas results show a 30 – 40% decline in C_3H_6/C_3H_8 selectivity up to 6 atm total feed pressure, which is surprising because the mixed gas dual mode model would predict at most a 10 % decrease in selectivity in this case. The reason for the decrease in selectivity is due to an increase in C_3H_8 permeability, which is not predicted by the dual mode mixed gas model. Tanaka *et al.* also state that the reason for the decline in selectivity is not presently clear, but offer plasticization as a possibility. Furthermore, Staudt-Bickel and Koros report pressure dependent C_3H_6/C_3H_8 permeation studies of 6FDA-6FpDA at 35°C [7]. In this case the mixed gas selectivity exhibits a 25 – 50% decline from 1 – 4 atm total feed pressure with a 50/50 feed mixture of C_3H_6/C_3H_8. These large declines in mixed gas selectivity are not well understood, but are certainly important from an industrial and academic perspective. Increased understanding of this issue may lead to improved materials design for the C_3H_6/C_3H_8 separation.

Since plasticization is one possibility for the declines in mixed gas selectivity, experiments were conducted in an effort to eliminate or depress this variable. Permeation measurements with the polyimide, 6FDA-DAM were performed at 75°C, because plasticization effects are reduced at higher temperatures where there is significantly less sorption. Pure and mixed gas permeation isotherms are shown in Figure 6.6. The pure gas isotherms show a decrease in permeability up to 90 psia, which indicates minimal plasticization in the pure gas experiments. The dual mode and partial immobilization model was fit to the pure gas permeation isotherms coupled with the pure gas sorption isotherms, and the parameters are given in Table 6.1. These parameters coupled with the dual mode mixed gas model can be used to predict where the mixed gas data should reside based on competition for Langmuir sites. For the C_3H_6 case the model predicts the direction of the trend, but it is not able to quantitatively predict the mixed gas permeation results. For the C_3H_8 case the model predicts a decline in mixed gas permeability, and the experiments show an increase in permeability in the mixed gas case. The bulk flux model [8] was also employed because this model would predict an increase in the C_3H_8 flux compared to the dual mode model. This is the trend observed, but only by a minimal amount. The C_3H_6 permeability is unaffected by the bulk flux prediction. The reason the bulk flux model does not change appreciably in this case is because the sorption at the elevated temperature is relatively low, and henceforth, the average concentration

a)

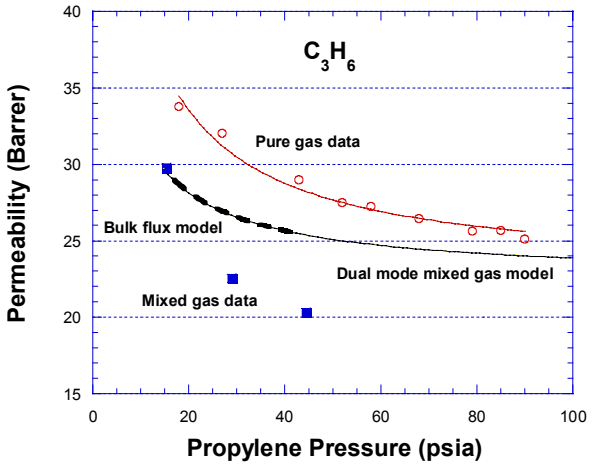

b)

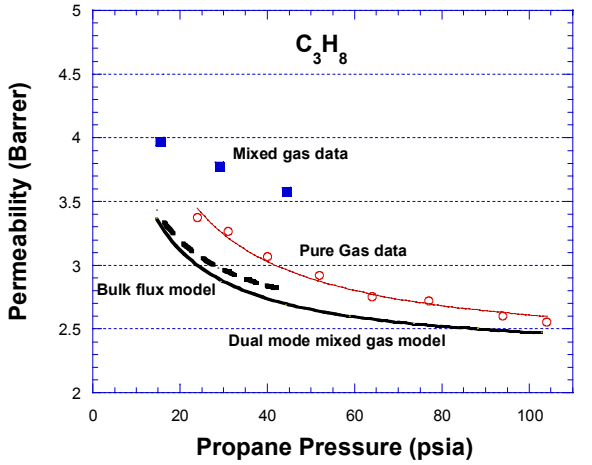

Figure 6.6. Pressure dependent pure and mixed gas permeability for 6FDA-DAM polyimide at 75°C. a) C_3H_6 b) C_3H_8.

in Equation 2.8 is small, resulting in a low fraction of the bulk flux contribution.

Figure 6.7 shows the pure and mixed gas C_3H_6/C_3H_8 selectivity for 6FDA-DAM at 75°C. The mixed gas selectivity falls to ~ 40 % of the pure gas selectivity at a total pressure of 90 psia. The dual mode model and bulk flux model are not able to predict the decline in mixed gas selectivity, and the fact that these models do not deviate appreciably from the pure gas data is expected because the sorption at 75°C is relatively low. While these models are not able to predict the decline in mixed gas selectivity, this analysis does make it possible to rule out the following possible causes: competitive sorption for Langmuir sites, and bulk flux effects. While plasticization effects have been minimized, it is not possible to completely rule out the fact that C_3H_6 may plasticize the polymer, such that its own diffusion coefficient is not affected, however, the diffusion coefficient of the larger C_3H_8 molecule is increased. Interestingly, Steel has observed similar large declines in mixed gas selectivity with carbon molecular sieve membranes, which are not expected to swell or plasticize [9]. However, in the case of the carbon membranes, the C_3H_8 permeability is not elevated in the mixed gas experiment, so this is not completely analogous to the results with the polymeric materials. Another possibility for the elevated C_3H_8 diffusion coefficient is coupling of the diffusion coefficients. This issue is explored for other systems in the literature with regard to the Maxwell-Stefan theory for mass transport [10, 11].

Table 6.1. Dual mode parameters for 6FDA-DAM at 75°C.

	C_3H_6	C_3H_8
k_d	0.150	0.125
C'_H	17.5	10.7
b	0.205	0.266
D_D	7.86×10^{-8}	9.56×10^{-9}
D_H	7.90×10^{-9}	1.53×10^{-9}

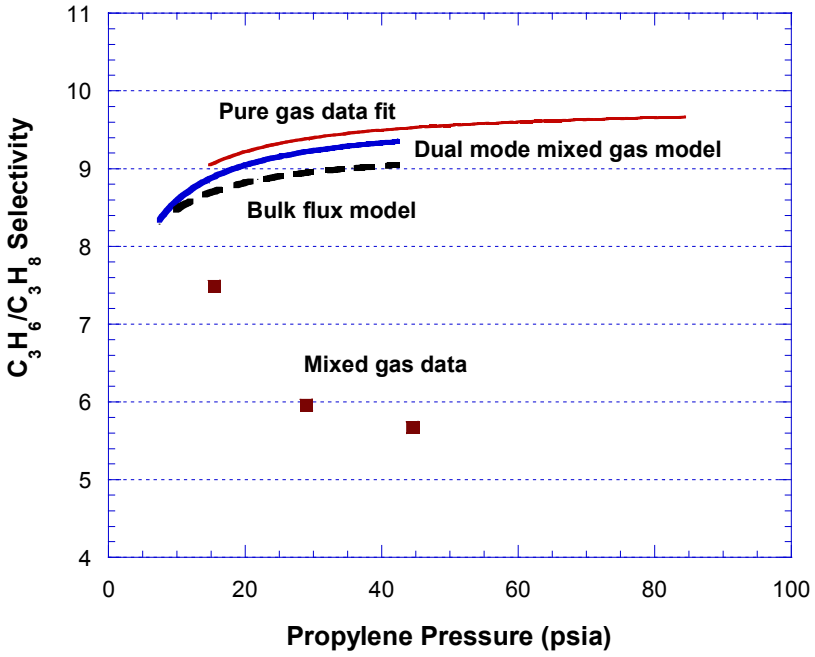

Figure 6.7. C_3H_6/C_3H_8 selectivity for 6FDA-DAM at 75°C. Comparison of the dual mode mixed gas model and the bulk flux model to experimental mixed gas data.

6.2 TEMPERATURE DEPENDENT TRANSPORT

6.2.1 Temperature Dependent Results for 6FDA-DAM

As discussed in Chapter 2, and briefly in Chapter 4, permeation and diffusion coefficients of gas penetrants in polymers typically follow an Arrhenius relationship. The classic result with increasing temperature is an increase in diffusion coefficient, and henceforth, an increase in permeability coefficient, since the increase in diffusivity generally outweighs the decrease in solubility.

Temperature measurements for both permeation and sorption were typically made over the range of 35°C to 75°C, and in some cases up to 90°C. Measurements over the variable temperature range are reported at 2 atm total feed pressure.

Pure gas permeation, sorption, and diffusion results for 6FDA-DAM at 2 atm and variable temperature are shown in Table 6.2. The expected trend is observed as the permeability for each component increases with temperature, and the selectivity decreases. The solubility coefficient for both C_3H_6 and C_3H_8 decreases approximately 50% from 35°C to 75°C. Conversely, the diffusion coefficient of both C_3H_6 and C_3H_8 increases roughly two-fold from 35°C to 75°C. The activation energies for permeation and diffusion are listed in Table 6.3, obtained from the Arrhenius plots, shown in Figure 6.8. The activation energies for permeation are slightly lower than those reported by Tanaka et al [5], however, the activation energies for diffusion are in excellent agreement. Sorption isotherms are shown at variable temperature in Figure 6.9, and dual

mode parameters are provided in Table 6.4. As expected, the Henry's law coefficient, k_D, and the affinity constant, b, decrease with increasing temperature.

Table 6.2. Pure gas C_3H_6/C_3H_8 permeation measurements for 6FDA-DAM at 2 atm and variable temperature.

Temperature (^oC)	P_{C3H6} [a]	P_{C3H8} [a]	S_{C3H6} [b]	S_{C3H8} [b]	D_{C3H6} [c]	D_{C3H8} [c]
35	28.7	2.67	1.153	0.915	$1.29x10^{-8}$	$1.51x10^{-9}$
55	29.9	2.80	0.836	0.754	$1.85x10^{-8}$	$1.92x10^{-9}$
75	32.0	3.27	0.667	0.452	$2.48x10^{-8}$	$3.74x10^{-9}$

[a] = Barrer = $10^{-10}\ \frac{cc(STP)cm}{cm^2\ s\ \ cmHg}$ [b] = $\frac{cc(STP)}{cc\ polymer - psia}$ [c] = cm^2 / s

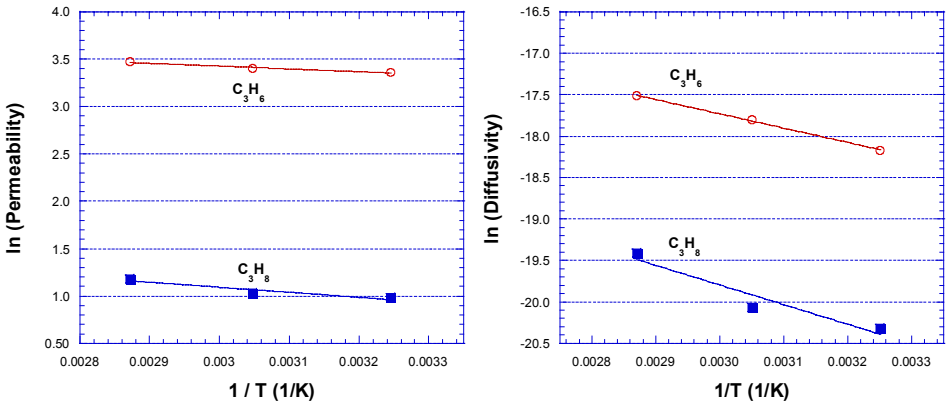

Figure 6.8. Arrhenius Permeation and Diffusivity plots for 6FDA-DAM at 2 atm.

Table 6.3. C_3H_6 and C_3H_8 activation energies and pre-exponential factors for both permeation and diffusion for 6FDA-DAM.

	E_{AP} (kJ/mol)	P_o (Barrer)	E_{AD} (kJ/mol)	D_o (cm^2/sec)
C_3H_6	2.48	73.1	14.6	$3.93x10^{-6}$
C_3H_8	4.48	15.0	20.1	$3.67x10^{-6}$

Table 6.4. List of dual mode parameters in 6FDA-DAM as a function of temperature.

	35°C		55°C		75°C	
	C_3H_6	C_3H_8	C_3H_6	C_3H_8	C_3H_6	C_3H_8
k_d	0.336±0.023	0.184 ±0.012	0.249±0.033	0.140±0.008	0.150±0.012	0.125±0.011
C'_H	25.1±1.3	23.7±0.8	18.8±1.7	20.9±0.6	17.5±0.8	10.7±0.7
b	0.572±0.179	0.296±0.030	0.341±0.103	0.203±0.015	0.205±0.027	0.266±0.051

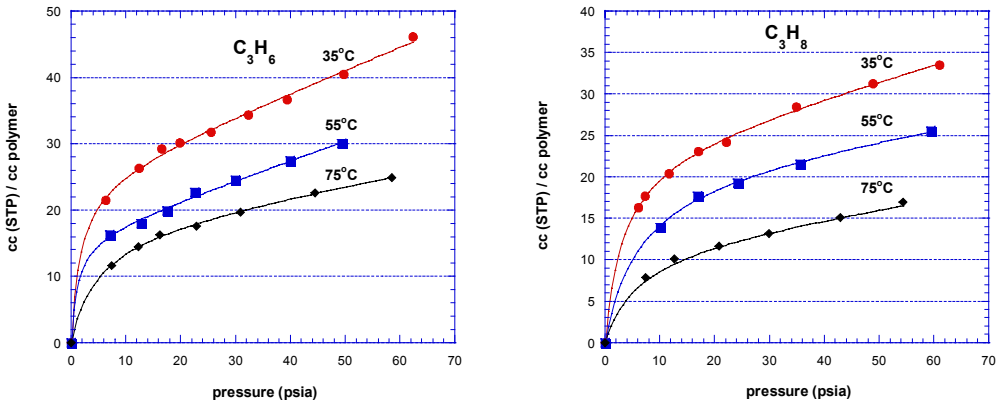

Figure 6.9. C_3H_6/C_3H_8 sorption isotherms in 6FDA-DAM at variable temperatures.

6.2.2 Temperature Dependent Results for 6FDA-TAB/DAM(50/50)

Pure gas C_3H_6/C_3H_8 results for 6FDA-TAB/DAM(5050) were performed at 2 atm total feed pressure and variable temperature. As expected, with an increase in temperature an increase in permeability is observed coupled with a decrease in selectivity, following the classical Arrhenius behavior as shown in Figure 6.10. Sorption isotherms at variable temperature are shown for C_3H_6 and C_3H_8 in Figures 6.11 and 6.12. As expected, the overall sorption capacity of the polymer decreases with temperature. Arrhenius parameters for both permeation and diffusion are provided in Table 6.5. As expected the activation energy for permeation is greater for C_3H_8 compared to C_3H_6, since activation energy scales with penetrant diameter. Due to the negative heat of sorption the activation energy of diffusion is greater than that of permeation, and again the activation energy for diffusion of C_3H_8 is greater than C_3H_6. This results in a declining selectivity with increasing temperature.

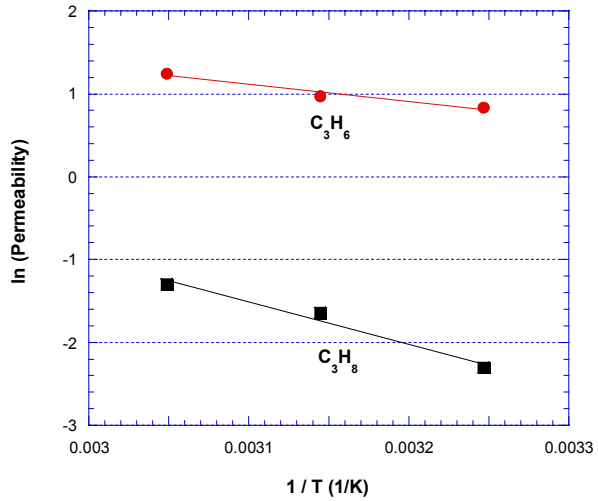

Figure 6.10. C_3H_6/C_3H_8 Arrhenius plots for 6FDA-TAB/DAM(50/50)

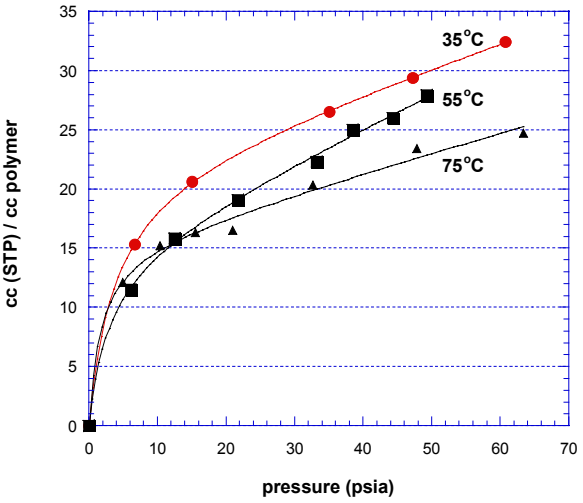

Figure 6.11. C_3H_6 sorption isotherms for the copolymer 6FDA-TAB/DAM(50/50).

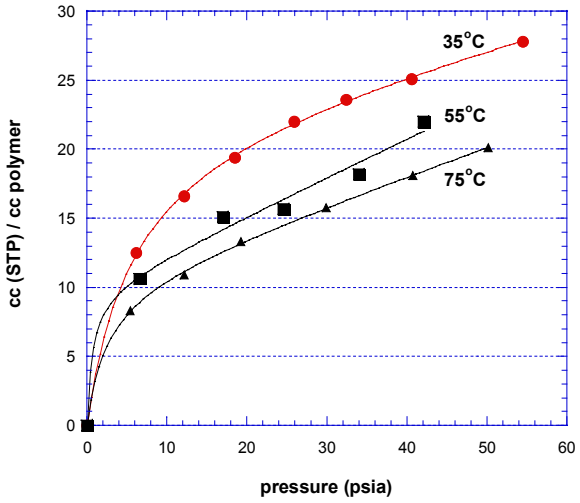

Figure 6.12. C_3H_8 sorption isotherms for the copolymer 6FDA-TAB/DAM(50/50).

Table 6.5. C_3H_6 and C_3H_8 activation energies and pre-exponential factors for both permeation and diffusion for 6FDA-TAB/DAM(50/50).

	E_{AP} (KJ/mol)	P_o (Barrer)	E_{AD} (KJ/mol)	D_o (cm^2/sec)
C_3H_6	17.4	1984	23.3	$1.27x10^{-5}$
C_3H_8	42.3	1.56×10^6	50.7	$2.8x10^{-2}$

6.2.3 Temperature Dependence of 6FDA-TAB/DAM(75/25)

The temperature dependence of 6FDA-TAB/DAM(75/25) for C_3H_6 and C_3H_8 is much different from the expected trend. Results are shown in Table 6.6. The C_3H_6 permeability and diffusivity increase with increasing temperature as expected, however the C_3H_6/C_3H_8 permselectivity and diffusivity selectivity

extend through a surprising maximum with increasing temperature. This trend is also observed with mixed gas results as shown in Figure 6.13, however the mixed gas selectivities are somewhat lower than the pure gas, which is consistent with previously observed trends. The improvement in both permeability and selectivity at elevated temperatures is very attractive from a commercial standpoint. Similar to the results with increasing pressure, this material possessing very unattractive separation properties at 35°C shows much more promising results at the higher temperature. This trend can be examined in further detail in terms of the diffusion coefficients, and the deviation from the Arrhenius relationship.

Figure 6.14 shows an Arrhenius analysis for C_3H_6 and C_3H_8. The C_3H_6 curve follows the expected trend, and the activation energy and pre-exponential factor are reported in Table 6.7. The C_3H_8 curve shows a clear break from the Arrhenius trend, and this break is the reason for the selectivity maximum with temperature. There is essentially no trend in the C_3H_8 diffusion coefficient from 35°C to 55°C, and this is a familiar result. The activation energy and pre-exponential factor were obtained with a fit to only the data points taken at 55°C and 75°C. Using only these points, the C_3H_8 activation energy is larger than C_3H_6 as expected. Specific reasons for this trend will be discussed in section 6.3.

Figure 6.15 shows a mixed gas isotherm for 6FDA-TAB/DAM(75/25) at 75°C up to 113 psia total pressure. This was done in order to investigate if a

selectivity maximum would occur as a function of pressure at this higher temperature. The observed results demonstrate a decreasing C_3H_6 permeability with increasing pressure showing typical dual mode behavior. There is no observed upswing in the C_3H_6 curve, and only a slight increase for C_3H_8, indicating minimal if any permeation plasticization, which is consistent with the depressed concentration of the penetrants at the elevated temperature, and consistent with the results for 6FDA-DAM. The mixed gas selectivity shows only a moderate decreasing trend with increasing pressure, and this is expected in the absence of significant swelling or plasticization.

Table 6.6. C_3H_6/C_3H_8 pure gas permeation results for 6FDA-TAB/DAM(75/25) at 2 atm.

Temperature (°C)	P_{C3H6}	P_{C3H6}/P_{C3H8}	D_{C3H6}	D_{C3H6}/D_{C3H8}
35	0.38	8.0	$2.48\text{x}10^{-10}$	7.7
55	0.55	20.4	$5.49\text{x}10^{-10}$	25.6
75	0.60	14.6	$7.21\text{x}10^{-10}$	10.1

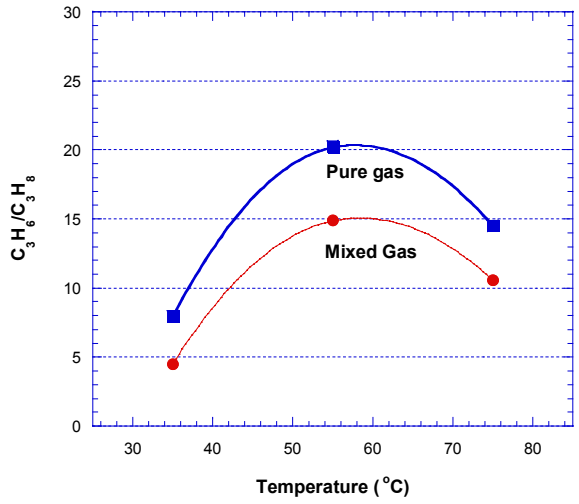

Figure 6.13. Temperature dependent C_3H_6/C_3H_8 selectivity for 6FDA-TAB/DAM(75/25).

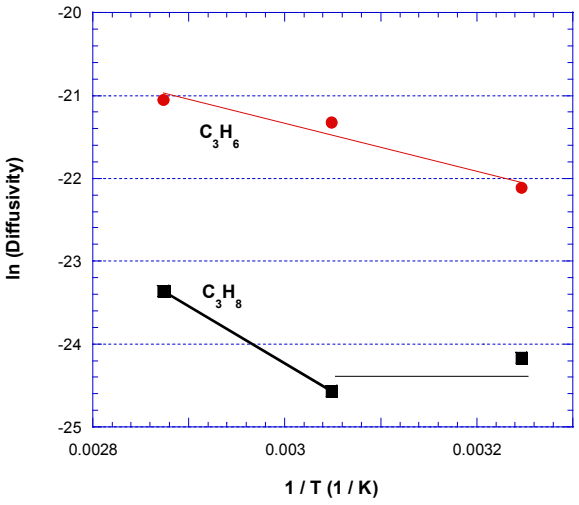

Figure 6.14. Arrhenius analysis of C_3H_6/C_3H_8 diffusion coefficients for 6FDA-TAB/DAM(75/25).

Table 6.7. C_3H_6 and C_3H_8 activation energies and pre-exponential factors for both permeation and diffusion for 6FDA-TAB/DAM(75/25).

	E_{AD} (kJ/mol)	D_o (cm^2/sec)
C_3H_6	23.9	$3.09x10^{-6}$
C_3H_8	57.3	$2.91x10^{-2}$

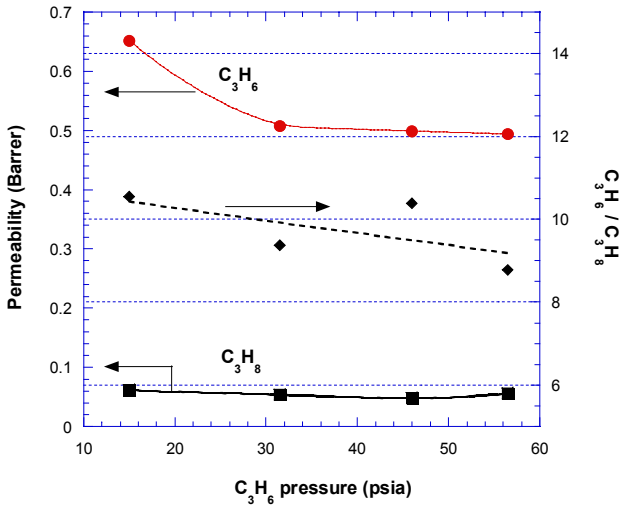

Figure 6.15 C_3H_6/C_3H_8 mixed gas isotherm (50/50 feed) at 75°C for 6FDA-TAB/DAM(75/25).

6.2.4 Temperature Dependence of 6FDA-TAB

Similar to 6FDA-TAB/DAM(75/25), 6FDA-TAB shows low C_3H_6 permeability and low C_3H_6/C_3H_8 selectivity at 35°C, and similarly it was hypothesized in Chapter 5 that this material may show a selectivity maximum

with respect to increasing temperature. Figure 6.16 shows an Arrhenius analysis for C_3H_6/C_3H_8 permeation results. The C_3H_8 curve exhibits a deviation from the Arrhenius trend similar to what is observed with 6FDA-TAB/DAM(75/25), and this results in a maximum selectivity at 55°C. Again, in order to help explain this trend modeling results will be provided in the next section.

Figure 6.17 shows a mixed gas isotherm at 75°C up to 70 psia total pressure. Similar to the 6FDA-TAB/DAM(75/25) copolymer a decreasing permeability is observed for both C_3H_6 and C_3H_8, which is expected due to dual mode effects. Permeation plasticization is again minimized because of lower sorption at the increased temperature, and therefore there is no significant increase in C_3H_6/C_3H_8 selectivity with pressure. Moderate changes in the selectivity over the pressure range considered are observed due to dual mode effects.

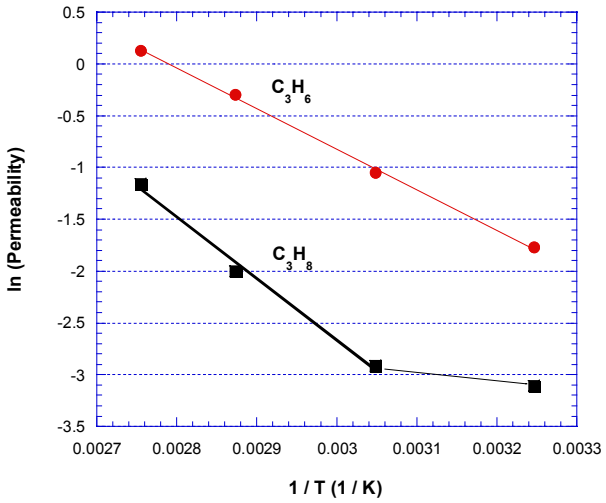

Figure 6.16. C_3H_6/C_3H_8 mixed gas Arrhenius permeation analysis for 6FDA-TAB.

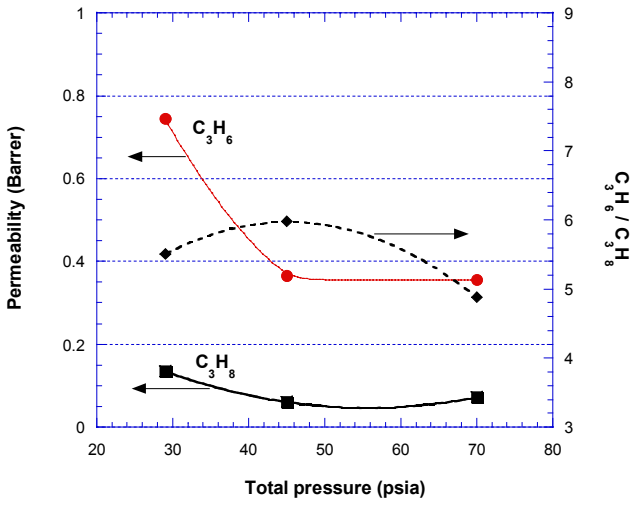

Figure 6.17. C_3H_6/C_3H_8 mixed gas isotherm for 6FDA-TAB at 75°C.

6.3 EXPLANATION FOR THE DEVIATION FROM ARRHENIUS TRENDS

This unusual trend of increasing selectivity with increasing temperature has also been observed in many cases with carbon molecular sieve materials. Kusuki *et al.* observe a maximum in the selectivity with increasing temperature for CO_2 / CH_4 separation [12]. The CH_4 data shows a break from the Arrhenius trend, or a flattening of the Arrhenius curve, similar to the data shown here for the poly(pyrrolone-imides). Fuertes and Centeno observe a maximum in selectivity for a variety of separations, (CO_2/CH_4, CO_2/N_2, He/N_2, O_2/N_2) for different membrane materials formed from carbonization of BPDA-pPDA polyimide [13]. Sedigh *et al.* observe a maximum in selectivity with temperature for the separations CO_2/CH_4, CO/CH_4, and Ar/CH_4 for a carbon membrane prepared from poly(furyl alcohol) [14]. The best illustration of this trend in carbon membranes has been demonstrated by Ogawa and Nakano for the CO_2/CH_4 separation [15]. Three membranes (A, B, and C) have been prepared through gel modification, and characterized with CO_2/CH_4 (15:85) mixed gas feed. The membranes A, B, and C exhibit a selectivity maximum with constant temperature and feed pressure. Membrane C shows both low CO_2 flux, and low CO_2/CH_4 selectivity, similar to the materials outlined in Chapter 5. However, this is the only material that demonstrates an increase in CO_2/CH_4 selectivity with increasing temperature. The reason for this increase is that the CH_4 permeance is *unchanging* with temperature, essentially showing no activation energy for

permeation on an Arrhenius plot, and this is also similar to the trends observed for the poly(pyrrolone-imides) presented here.

These deviations from Arrhenius behavior in the carbon literature have gone largely unexplained. Strano and Foley have recently demonstrated that deviations from Arrhenius behavior may occur through two parallel pathways of transport [16]. One pathway involves activated molecular sieving diffusion through nanopores, and the other incorporates Knudsen diffusion through defect pores. Other researchers have also done similar analyses, which explain deviations from Arrhenius behavior in molecular sieving media due to additional modes of transport (other than molecular sieving) such as Knudsen diffusion and surface diffusion [17, 18]. The following analysis is different in that it will demonstrate the ability to deviate from the Arrhenius relationship incorporating only activated molecular sieving diffusion in the development.

The parallel model for gas diffusion was used in Chapter 5 to explain the selectivity maximum phenomena observed over different material structures:

$$P_{Eff} = \sum_{1}^{n} P_i \bullet \phi_i \qquad (6.1)$$

It can further be assumed that each pore, or each selective entity behaves in an Arrhenius fashion. It is important to note that while experimental observations show deviations from the Arrhenius relationship for bulk materials, it will be shown that these observations can be explained assuming no deviation from the

Arrhenius relationship for individual selective entities. This yields the effective permeability as a function of temperature:

$$P_{Eff} = \sum_{1}^{n} \phi_i \bullet P_{o\,i} \exp\left[\frac{-E_{APi}}{RT}\right] \qquad (6.2)$$

Similarly, this could be extended to the diffusivity using analogous assumptions to those in Chapter 5, but this form can be used to demonstrate the important concepts.

The initial example of 3 hypothetical pores given in Chapter 5 can be extended here. Activation energies and pre-exponential factors for permeation are chosen to closely match the permeabilities given in Table 5.7 at 35°C. Since multiple values could be chosen, the selection of Arrhenius parameters is somewhat arbitrary, and only intended to demonstrate potential existing trends. These values are provided in Table 6.8 for penetrants A and B.

Table 6.8 Arrhenius parameters assigned to hypothetical pores.

	Penetrant A		**Penetrant B**	
	E_a (kJ/mol)	P_o (Barrer)	E_a (kJ/mol)	P_o (Barrer)
pore1	0.01	41	6.0	80
pore2	9.0	150	19.7	200
pore3	22.3	2500	38.2	2500

Figure 6.18 shows permeation curves as a function of temperature for Membrane C (defined in Chapter 5) for penetrants A and B. These plots

demonstrate how deviations from the Arrhenius relationship may occur, and in some cases may result in the observation of a selectivity maximum with temperature. For penetrant A, there is a cross at about 280 K, causing a "switch" in the pore dominating transport, illustrating one reason why bulk materials may deviate from the Arrhenius relationship over extended temperature ranges. In the lower plot (penetrant B) the "switch" occurs at ~ 440 K, and this difference leads to the observation of a selectivity maximum with temperature. Figure 6.19 shows selectivity as a function of temperature for membranes A, B, and C. For membranes A and B the selectivity shows an exponentially decreasing trend with temperature as expected, because no "switch" occurs for these materials. Membrane C demonstrates the unusual selectivity maximum with increasing temperature. Furthermore, this demonstrates, that while membrane B possesses the best separation factor at low temperatures (300 K), membrane C possesses the highest selectivity at elevated temperatures (> 380 K).

This hypothetical discussion is intended to demonstrate one reason why experimental deviations may occur from the Arrhenius relationship in molecular sieving materials. In actual materials many different entities or pore sizes would be likely to exist, which would further complicate the situation. Additional pores could result in more situations of "pore switching" and / or more gradual changes in the Arrhenius curve for the effective permeability.

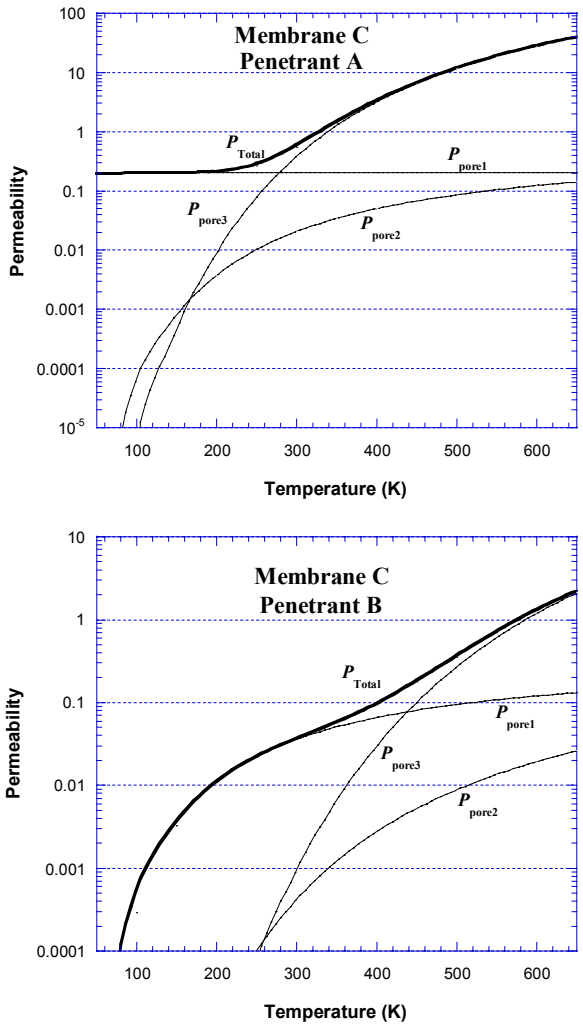

Figure 6.18. Permeability as a function of temperature for Membrane C with 2 penetrants A and B, demonstrating the contribution of all 3 pores.

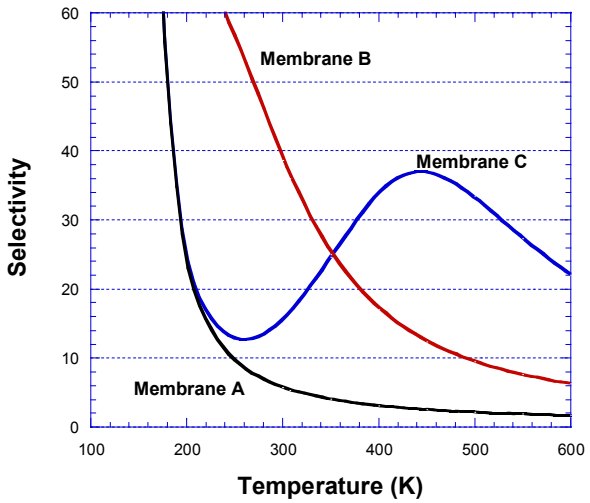

Figure 6.19. Selectivity as a function of temperature for Membranes A, B, and C.

6.4 REFERENCES

[1] D. R. B. Walker, Synthesis and Characterization of Polypyrrolones For Gas Separation Membranes, Ph.D. Dissertation, The University of Texas at Austin, 1993.

[2] A. Bos, I. G. M. Punt, M. Wessling and H. Strathmann, CO_2-induced plasticization phenomena in glassy polymers, J. Membr. Sci. 155 (1999) 67-78.

[3] C. Staudt-Bickel and W. J. Koros, Improvement of CO_2/CH_4 separation characteristics of polyimides by chemical crosslinking, J. Membr. Sci. 155 (1999) 145-154.

[4] S. M. Jordan and W. J. Koros, Characterization of CO_2-Induced Conditioning of Substituted Polycarbonates Using Various Exchange Penetrants, J. Membr. Sci. 51 (1990) 233-247.

[5] K. Tanaka, A. Taguchi, J. Q. Hao, H. Kita and K. Okamoto, Permeation and separation properties of polyimide membranes to olefins and paraffins, J. Membr. Sci. 121 (1996) 197-207.

[6] J. D. Wind, Improving Polyimide Membrane Resistance to CO_2 Plasticization in Natural Gas Separations, Ph D. Dissertation, The University of Texas at Austin, 2002.

[7] C. Staudt-Bickel and W. J. Koros, Olefin/paraffin gas separations with 6FDA-based polyimide membranes, J. Membr. Sci. 170 (2000) 205-214.

[8] H. D. Kamaruddin and W. J. Koros, Some observations about the application of Fick's first law for membrane separation of multicomponent mixtures, J. Membr. Sci. 135 (1997) 147.

[9] K. Steel, Carbon Membranes for Challenging Gas Separations, Ph. D. Dissertation, The University of Texas at Austin, 2000.

[10] L. J. P. Vandenbroeke and R. Krishna, Experimental-Verification of the Maxwell-Stefan Theory for Micropore Diffusion, Chem. Eng. Sci. 50 (1995) 2507-2522.

[11] R. Krishna and J. A. Wesselingh, Review article number 50 - The Maxwell-Stefan approach to mass transfer, Chem. Eng. Sci. 52 (1997) 861-911.

[12] Y. Kusuki, H. Shimazaki, N. Tanihara, S. Nakanishi and T. Yoshinaga, Gas permeation properties and characterization of asymmetric carbon membranes prepared by pyrolyzing asymmetric polyimide hollow fiber membrane, J. Membr. Sci. 134 (1997) 245-253.

[13] A. B. Fuertes and T. A. Centeno, Preparation of supported asymmetric carbon molecular sieve membranes, J. Membr. Sci. 144 (1998) 105-111.

[14] M. G. Sedigh, W. J. Onstot, L. F. Xu, W. L. Peng, T. T. Tsotsis and M. Sahimi, Experiments and simulation of transport and separation of gas mixtures in carbon molecular sieve membranes, J. Phys. Chem. A 102 (1998) 8580-8589.

[15] M. Ogawa and Y. Nakano, Separation of CO_2/CH_4 mixture through carbonized membrane prepared by gel modification, J. Membr. Sci. 173 (2000) 123-132.

[16] M. S. Strano and H. C. Foley, Temperature- and pressure-dependent transient analysis of single component permeation through nanoporous carbon membranes, Carbon 40 (2002) 1029-1041.

[17] A. J. Burggraaf, Single gas permeation of thin zeolite (MFI) membranes: theory and analysis of experimental observations, J. Membr. Sci. 162 (1999) 295-295.

[18] J. Gilron and A. Soffer, Knudsen diffusion in microporous carbon membranes with molecular sieving character, In press (2002)

CHAPTER 7: CONCLUSIONS AND RECOMMENDATIONS

7.1 CONCLUSIONS FOR OBJECTIVE ONE

1) Define the C_3H_6/C_3H_8 upper bound curve.

An experimental upper bound curve for the C_3H_6/C_3H_8 separation using polymer membranes has been presented and defined at 50°C with pure gas measurements. It would be expected that a C_3H_6/C_3H_8 "mixed gas" upper bound curve would lie slightly below the pure gas case defined here, based on the decline in C_3H_6/C_3H_8 mixed gas selectivity compared to pure gas C_3H_6/C_3H_8 measurements reported in the literature [1, 2]. However, it is difficult to adequately define a C_3H_6/C_3H_8 "mixed gas" upper bound because the data is limited. Additionally, the reasons for the decline in C_3H_6/C_3H_8 mixed gas selectivity (compared to C_3H_6/C_3H_8 pure gas selectivity) are not well understood, and, consequently, it would be difficult to represent this accurately with a model. Therefore, the analysis was limited to the C_3H_6/C_3H_8 pure gas permeability measurements.

At this point the data reported by Shimazu *et al.* [3] are not included in the development of this upper bound because we believe the data are questionable. Using the same experimental protocol, permeation and sorption results have been obtained that are considerably different from those reported previously [3]. Additionally, it has been shown that other literature data exists [2], which are also

extremely conflicting with the measurements reported previously. Therefore, it appears that more work needs to be done to adequately evaluate and explain this data.

A prediction of the C_3H_6/C_3H_8 upper bound was also presented using an extension of the analysis by Freeman [4], which correlates remarkably well with the experimental upper bound defined here. The theory would predict that there are essentially two methods to "move" or "beat" the currently existing upper bound, and these are discussed in Chapter 4. Based on this discussion it is recommended that future work focus on achieving improvements in the solubility selectivity for olefin / paraffin separations. This can be accomplished through the use of π bonding interactions with the olefin. Some preliminary work with this strategy is discussed in Appendix A.

7.2 CONCLUSIONS AND RECOMMENDATIONS FOR OBJECTIVE TWO

2. Synthesize a family of poly(pyrrolone-imide) copolymers. Investigate the effects of subtle changes of alternating bulky and flat monomer groups on gas transport properties.

A family of poly(pyrrolone-imide) copolymers (6FDA-TAB/DAM) was synthesized in order to investigate how the ratio of TAB/DAM monomers in the polymer chain affects transport properties of various gas molecules. For smaller molecules such as O_2/N_2 and CO_2/CH_4 a familiar trend of decreasing permeability

and increasing selectivity was observed with increasing TAB/DAM ratio. Surprisingly, for C_3H_6/C_3H_8 separation a selectivity maximum was observed over the range of material structures. It was further shown that this is due to unexpected trends in the diffusion coefficient for the largest gas molecule tested, C_3H_8. This trend of a selectivity maximum over a range of material structures has also been observed for carbon molecular sieve materials for a variety of gas separations; however, this trend has gone largely unnoticed within the literature. By making the assumption that the pore size distribution in carbon materials is analogous to the free volume distribution in rigid polymeric materials, it is possible to obtain a physical picture and a mathematical description of the selectivity maximum in both types of molecular sieving materials. A novel assumption was made, which considers using models for composite materials as a means to account for different selective entities as separate elements of a bulk material. Five different composite models were considered for further examination, and both the parallel and effective medium theory models were used for additional study. Both of these latter models were able to demonstrate how the selectivity maximum may occur for larger gas molecules and not smaller ones for the same system of materials under consideration. This lends insight into why certain materials are "undesirable" only in certain cases, and how they may be engineered to obtain improved transport properties under alternate operating conditions.

In order to further study the concept of relating a composite model to the pore size distribution of a carbon material, it is recommended to do extensive

measurements on one particular family of carbon molecular sieve membranes, along with pore size distribution measurements. For instance, if 7 differently sized pores are characterized, it would be necessary to do permeation measurements on 7 different materials of alternating distribution in order to properly fit the models discussed here. This was outside the scope of this work, but would be useful in the future to further support the concept of describing the molecular sieving materials using a composite model.

Since the composite modeling work performed here suggests that the size of the molecule is most important in determining whether or not the selectivity maximum is observed, it would be of value to examine permeation and sorption data of larger molecules over the same range of material structures. This would add further validity to the concepts and trends discussed here with regard to the dependence of the diffusion coefficient on changes in the material structure.

The ultra-rigid aromatic polymers discussed in this work are currently not soluble in typical organic solvents. From a processing standpoint it would be useful to investigate low-temperature treatments for the ring-closure step and / or methods for dissolving the cured polymer. Jenekhe and Johnson have demonstrated that solubilization of heteroaromatic rigid-chain polymers, similar to the ones in this work, can be achieved through the addition of metal halide Lewis acids to certain organic solvents [5]. These Lewis acids form electron-donor acceptor complexes with the polymer chains, reducing intermolecular attractions between chains, decreasing chain stiffness, and thereby aiding in solvation of the polymer. This technique has been applied to a multitude of rigid

chain polymers, and it has been demonstrated that the solutions can be processed to form films and coatings with the same properties as the virgin polymer. Based on this evidence it is believed that if the poly(pyrrolone-imides) discussed in this work were to be scaled up for use in a commercial process (with the goal of forming asymmetric fibers) it would be straightforward (albeit time consuming) to isolate the best Lewis acid / solvent pair that would be able to successfully process these materials.

7.3 CONCLUSIONS AND RECOMMENDATIONS FOR OBJECTIVE THREE

3. Perform pressure and temperature dependent gas transport experiments (both pure and mixed gas) in order to understand the behavior of C_3H_6 / C_3H_8 transport at elevated temperatures and pressures.

Pressure and temperature dependant studies have been examined in Chapter 6. The first interesting conclusion is that while rigid polypyrrolones provide enhanced permeation plasticization resistance for CO_2 in comparison to many polyimides, this does not hold true for C_3H_6. It is observed for polypyrrolones, polyimides, and hybrid materials that C_3H_6 permeation plasticization generally occurs between 2 – 5 atm feed pressure.

It has also been observed for the materials 6FDA-DAM, and 6FDA-TAB/DAM(50/50) that a decline in mixed gas C_3H_6/C_3H_8 separation factor occurs at elevated pressures due to swelling induced plasticization. This is expected

based on many previously observed trends in the literature. Typically, when separating molecules based on size, plasticization results in a larger increase of the diffusion coefficient of the larger molecule, thereby providing a decrease in the overall separation factor.

As hypothesized in Chapter 5, penetrant induced swelling of 6FDA-TAB and 6FDA-TAB/DAM(75/25) at elevated pressures (above 2 atm) results in improvements in both the C_3H_6 permeability and C_3H_6/C_3H_8 selectivity (observed in both pure and mixed gas experiments). This is consistent with the fact that the C_3H_8 diffusion coefficient remains largely unaffected upon changes in material structure (similar to the structure-transport property results). The strategy employed here, which *improves* transport properties of a low performance material with penetrant induced swelling, is much different than the more conventional strategy of beginning with a high performing material and making material alterations to *reduce* swelling effects at elevated pressures. However, more investigations would need to be conducted in order to employ the present strategy for commercial use. Since thin films typically exhibit stronger plasticization responses [6] (and thin skin asymmetric fibers would be used commercially) more work would need to be done to isolate the most promising asymmetric materials, as these may be somewhat different than the dense film results shown here. Additionally, since swelling effects often have a long-term relaxational response, further studies (such as permeation, sorption, and dilation) that isolate long-term responses at constant pressure would be in order.

7.4 CONCLUSIONS FOR OBJECTIVE FOUR

4. Determine complementary physical properties of rigid poly (pyrrolone-imide) copolymers.

The glass transition temperature of the copolymers discussed here was investigated using differential scanning calorimetry (DSC). A Tg was observed for the polyimide, 6FDA-DAM, as expected, and no Tg (below 560^{o}C) was observed for the other copolymers.

The d-spacing of polymers studied here was measured using wide angle x-ray diffraction (WAXD). For some polymers, two d-spacings were observed, indicating somewhat of a bimodal distribution in the chain distances. It was also observed that with increased TAB/DAM ratio, the chain spacing distribution shifted towards lower average segmental distances, as expected. The data correlates with the decrease in diffusion coefficient of all molecules tested with increasing TAB/DAM ratio.

Density measurements of copolymers were performed using a density gradient column. It is observed that there is an increase in the density with increasing TAB/DAM ratio, and this is expected based on the ability of the tetra-amine monomer to pack more efficiently. This also correlates with the observed trends in permeability and diffusion coefficients.

7.5 CONCLUSIONS AND RECOMMENDATIONS FOR OBJECTIVE FIVE

5. Investigate the cause for significant declines (40 %) in mixed gas C_3H_6/C_3H_8 selectivity measurements compared to pure gas measurements.

Since many materials reported in the literature for the C_3H_6/C_3H_8 separation show tremendous drops in mixed gas selectivity measurements (usually close to 40 %) compared to pure gas permeability experiments [1, 2], it is of significant use to explore this phenomena with the expectation that added knowledge could guide future materials research. Possibilities investigated in the work here included plasticization, competitive sorption, and bulk flux effects. Measurements were conducted on the polyimide, 6FDA-DAM, at 75^{o}C in order to minimize the effects of plasticization. This also depresses the overall concentration of penetrants in the polymer. The dual mode mixed gas model was applied as well as the bulk flux model. In both cases it is clear that these models are not able to account for the decline in mixed gas selectivity. The possibility still exists that C_3H_6 plasticizes the polymer, such that its own diffusion coefficient is unaffected, however the diffusion coefficient of C_3H_8 is largely affected. Another possibility is that competitive diffusion or coupling of the diffusion coefficients is a large factor in these declines in selectivity.

Valuable future work in this endeavor would include mixed gas sorption measurements. While these measurements are very difficult to perform, the

results would provide valuable information about the transport characteristics of mixture feed streams. Mixed gas permeation experiments over a range of compositions would also be valuable in order to understand the effect of C_3H_6 on the diffusion coefficient of C_3H_8. Furthermore, it would be of interest to investigate the Maxwell-Stefan theory of mass transport, which incorporates coupling of the diffusion coefficients in multicomponent flow [7, 8].

7.6 REFERENCES

[1] K. Tanaka, A. Taguchi, J. Q. Hao, H. Kita and K. Okamoto, Permeation and separation properties of polyimide membranes to olefins and paraffins, J. Membr. Sci. 121 (1996) 197-207.

[2] C. Staudt-Bickel and W. J. Koros, Olefin/paraffin gas separations with 6FDA-based polyimide membranes, J. Membr. Sci. 170 (2000) 205-214.

[3] A. Shimazu, T. Miyazaki, M. Maeda and K. Ikeda, Relationships between the chemical structures and the solubility, diffusivity, and permselectivity of propylene and propane in 6FDA-based polyimides, J. Polym. Sci. Pt. B-Polym. Phys. 38 (2000) 2525-2536.

[4] B. D. Freeman, Basis of permeability/selectivity tradeoff relations in polymeric gas separation membranes, Macromolecules 32 (1999) 375-380.

[5] S. A. Jenekhe and P. O. Johnson, Complexation-Mediated Solubilization and Processing of Rigid- Chain and Ladder Polymers in Aprotic Organic-Solvents, Macromolecules 23 (1990) 4419-4429.

[6] M. Wessling, M. L. Lopez and H. Strathmann, Accelerated plasticization of thin-film composite membranes used in gas separation, Sep. Purif. Technol. 24 (2001) 223-233.

[7] R. Krishna and J. A. Wesselingh, Review article number 50 - The Maxwell-Stefan approach to mass transfer, Chem. Eng. Sci. 52 (1997) 861-911.

[8] L. J. P. Vandenbroeke and R. Krishna, Experimental-Verification of the Maxwell-Stefan Theory for Micropore Diffusion, Chem. Eng. Sci. 50 (1995) 2507-2522.

Appendix A: Transport Results of Dithiolene/Polyimide Blends

INTRODUCTION

According to Freeman's analysis outlined previously in Chapter 4 [1], the "upper bound" for conventional polymers used for gas separations can be shown to follow equation A.1:

$$\alpha_{A/B} = \frac{\beta_{A/B}}{P_A^{\lambda_{A/B}}} \qquad (A.1)$$

The parameter, $\lambda_{A/B}$ can be shown to be proportional to the square of the size difference of the two gas molecules, $(d_A/d_B)^2$. Consequently, this parameter cannot be manipulated through materials engineering. Therefore, according to the theory, in order to "move" the upper bound limit, the strategy must be to increase the β parameter, which can be shown to be proportional to the value, $S_A\ (S_A/S_B)^{\lambda}$, as well as a parameter f, which relates to the interchain spacing. Previous work in our group has attempted to increase the diffusivity selectivity through an increase in the chain rigidity by using polypyrrolone materials [2]. However, another approach to "elevating" the upper bound is to improve the solubility of the "fast gas" (C_3H_6 in this case), thereby increasing the solubility selectivity, and increasing β. The solubility of an olefin in a polymeric material is a parameter that can be engineered through the use of π-bonding interactions.

Many previous researchers have examined the viability of fixed site facilitated membranes for the separation of olefins from paraffins, and the reader is referred to only a few articles here [3-5], although numerous others exist in the literature, which have also been discussed in Chapter 4. Typically I-B metals, such as silver, are dissolved in polymer membranes in a salt form. Examples of silver salts conventionally used include $AgBF_4$ and $AgNO_3$. Once dissolved in the polymer, the salt dissociates, and the silver cation is able to form a complex with an olefin due to the interaction of the π-orbital of the olefin with the σ and $\pi-$orbital of the metal.

These fixed site facilitated membranes have shown varying levels of success in terms of separation efficiency. Extraordinarily high pure gas selectivities have been reported for C_3H_6/C_3H_8 (> 4000) as well as C_2H_4/C_2H_6 (> 5000) at 80 wt % $AgBF_4$ in PEO. However, the mixed gas selectivity in this system is only reported for C_2H_4/C_2H_6, and it is much lower (120) at the same $AgBF_4$ concentration under 100 psig total feed pressure [6]. Nevertheless, a mixed gas selectivity this high for C_2H_4/C_2H_6 is still exceptional compared to the selectivity of conventional polymers, which normally possess C_2H_4/C_2H_6 selectivities in the range of 3 – 5.

These fixed site facilitated membranes still have a major practical problem, however, due to the poor chemical stability of the metal ion – olefin complex. This metal-olefin complex is easily poisoned by small amounts of

hydrogen gas, carbon monoxide, acetylene, or hydrogen sulfide in the feed stream. Silver ions also have the potential to react with acetylene to form an explosive silver acetylide salt.

A search has been ongoing to find a material which can form a π-bond complex with olefins, while still maintaining stability in the presence of the aforementioned impurity gases. An additional constraint is that the material should be able to dissolve in state-of-the-art polyimide membranes. The overall strategy is to maintain the high diffusivity selectivity (D_A / D_B) already available with polyimides, and enhance this diffusivity selectivity by a factor of the improved solubility selectivity (S_A / S_B). For a conventional polyimide with a C_3H_6/C_3H_8 selectivity of 15, a small increase in the solubility selectivity from 1.0 to 2.0 would double the overall C_3H_6/C_3H_8 selectivity to a value of 30, as well as doubling the C_3H_6 flux.

A recent publication reports that dithiolene materials of the form $M[S_2C_2R_2]_2^n$ (shown in Figure A.1) can react selectively and reversibly with light olefins, and that the reaction is not poisoned by any of the aforementioned gases[7]. Furthermore, dithiolene materials dissolve readily in conventional organic solvents, such as toluene and dimethylacetamide.

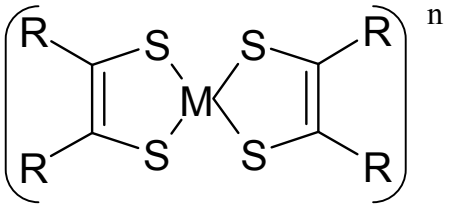

Figure A.1. General structure of dithiolene complex where M is a metal cation (e.g. Ni, Pd, Pt), R is a substituent group (e.g. CN, CF_3, C_6H_5, CH_3, etc.), and n is the valence charge (e.g. 0, -1, -2).

EXPERIMENTAL

We were able to obtain research samples of 9 dithiolene materials from Dr. Joel Miller at the University of Utah, Salt Lake City. The nine materials are shown in Table A.1.

In an effort to try and evaluate all 9 dithiolene complexes, experiments were conducted that consisted of bubbling low pressure (atmospheric) C_3H_6 through a solution of the dithiolene complex in question. The results of these experiments are shown in Table A.2. Some of the complexes were not soluble in toluene, but were soluble in dimethylacetamide. The goal of the experiment was to try and detect a color change over time, which would signal a chemical complexation with propylene. The only dithiolene material that underwent a significant change was complex #2, $Ni[S_2C_2(CF_3)_2]_2$, and this occurred in under 30 minutes. All other dithiolenes showed no color change under C_3H_6 bubbling, with the exception of dithiolene #5. This complex underwent a slight color change from yellow to light orange. The assumption from this would be that the

olefin binding is very weak, as it appears the energy (reflected in the color) is not changed appreciably.

Table A.1. Chemical Formula of dithiolene materials tested.

#	**Chemical Formula**
1	$Ni[S_2C_2(CH_3)_2]_2$
2	$Ni[S_2C_2(CF_3)_2]_2$
3	$Ni[S_2C_2(C_6H_4OCH_3)_2]_2$
4	$[C_6H_4S_4]\{Ni[S_2C_2(CF_3)_2]\}^-$
5	$[N(n\text{-}C_4H_9)_4]\{Ni[S_2C_2(CN)_2]_2\}^-$
6	$[N(n\text{-}C_4H_9)_4]\{Ni[S_2(C_6H_3CH_3)]_2\}^-$
7	$[N(n\text{-}C_4H_9)_4]\{Pt[S_2(C_6H_3CH_3)]_2\}^-$
8	$[N(n\text{-}C_4H_9)_4]\{Fe[S_2(C_6H_3CH_3)]_2\}^-$
9	$[N(C_2H_5)_4]\{Co[S_2(C_2(CN)_2]_2\}^-$

Table A.2. Results of C_3H_6 bubbling experiments for the 9 dithiolene samples examined.

Dithiolene Complex	Solvent	Color	Time of C_3H_6 bubbling	Color change
#1	Toluene	deep purple	3 hrs	No change
#2	Toluene	dark with purple tint	30 minutes	yellowish - green
#3	Toluene	dark forest green	3 hrs	No change
#4	Toluene	light yellow	3 hrs	No change
#5	DMAc	yellow	3 hrs	light orange (very slight change)
#6	Toluene	green with blue tint	3 hrs	No change
#7	Toluene	light blue	3 hrs	No change
#8	DMAc	light red	3 hrs	No change
#9	DMAc	yellow	3 hrs	No change

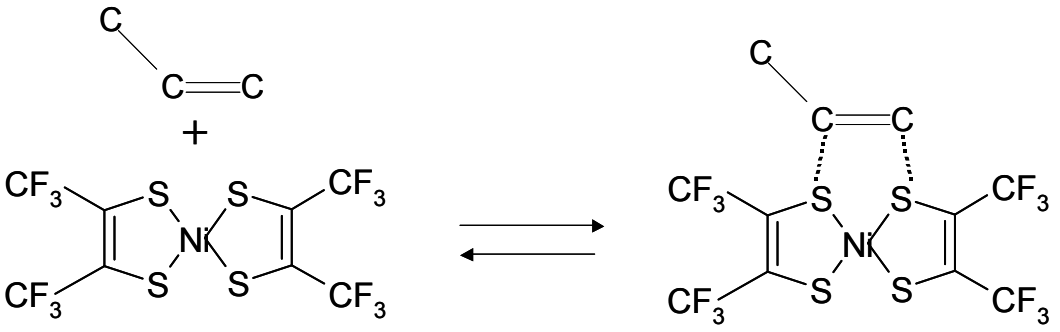

Figure A.2. Proposed C_3H_6 complexation with $Ni[S_2C_2(CF_3)_2]_2$

The observation that $Ni[S_2C_2(CF_3)_2]_2$ undergoes complexation with C_3H_6 is actually quite consistent with previous experiments in the literature. Olson,

Mayweg, and Schrauzer have conducted polarographic half-wave potential measurements on a number of materials of the form $[MS_4C_4R_4]^n$ [8]. Essentially, this measures the half-wave potential of the reaction:

$$MS_4C_4R_4 + e \rightarrow MS_4C_4R_4^-$$

Measurements were conducted on materials containing metals, **M**, of Ni, Pd, or Pt, and **R** groups of CN, CF_3, C_6H_5, CH_3, C_2H_5, and H. The metal which displayed the largest half-wave potential was nickel. The **R** group which showed the highest half-wave potential was CN with CF_3 following a close second. This suggests that the two best dithiolene materials to act as π electron acceptors would be $Ni[S_2C_2(CF_3)_2]_2$ and $Ni[S_2C_2(CN)_2]_2$. The measurements also show that the complexes that are negatively charged (n = -1) have negative half-wave potentials. The interpretation from this is that energy needs to be added in order for the anion to accept an electron. This is consistent with the results in Table A.2. Here, none of the anionic dithiolene materials (numbers 4 – 9) form an olefin complex. $Ni[S_2C_2(CF_3)_2]_2$ does form an olefin complex, which would be expected from the half-wave measurements. It would also be expected that $Ni[S_2C_2(CN)_2]_2$ would form a slightly stronger complex, however probably not to the extent that there would be added value in synthesizing this material.

Clearly, complex #2, $Ni[S_2C_2(CF_3)_2]_2$, is the most promising of those tested to begin work with polymer membranes in the hopes of increasing C_3H_6/C_3H_8 solubility selectivity. For the polymer material, we initially chose a

commercially available, state-of-the-art polyimide. A Matrimid®/dithiolene (10 % by wt) dense film was cast using dicloromethane as the solvent. The resulting film was dark green (compared to the bright yellow color of pure Matrimid®), however, it was not homogeneously dispersed. The dithiolene appeared to be leaching out along the edges, and it was concluded that the polymer and dithiolene materials were not sufficiently miscible in this case.

The decision was then made to cast a film using 6FDA-6FpDA polyimide as the polymer matrix due to the presence of CF_3 groups in both the polymer and the dithiolene complex, $Ni[S_2C_2(CF_3)_2]_2$, which should aid in miscibility. Films were cast on Teflon plates using conventional film casting techniques with dicloromethane as the casting solvent. The films were then dried at 120°C for at least 8 hours under vacuum. Homogenous films were formed that were also transparent dark green (shown in Figure A.3), compared to the pure 6FDA-6FpDA film, which is clear. After successfully achieving a polyimide / dithiolene homogenous blend, we began C_3H_6/C_3H_8 pure gas permeation and sorption experiments using the material 6FDA-6FpDA / $Ni[S_2C_2(CF_3)_2]_2$ (11 wt %).

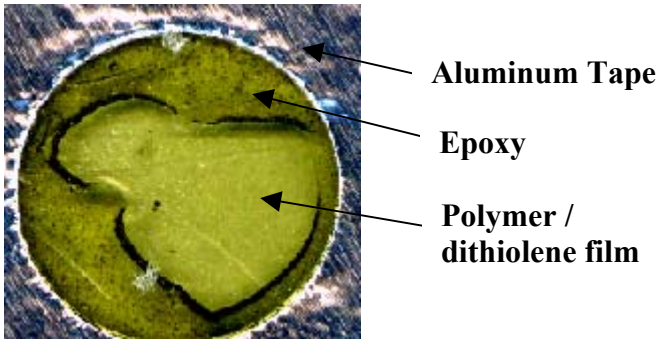

Figure A.3. Scanned image of 6FDA-6FpDA / $Ni[S_2C_2(CF_3)_2]_2$ (11 wt %) illustrating a homogenous dark green color in comparison to the clear, pure polyimide.

TRANSPORT RESULTS

C_3H_6/C_3H_8 Solubility Results

Initially pure gas C_3H_6/C_3H_8 sorption experiments were conducted for both the pure polymer, 6FDA-6FpDA, and the 6FDA-6FpDA / $Ni[S_2C_2(CF_3)_2]_2$ (11 wt %) blend, both processed using the same protocol. The results are shown in Figure A.3 on a plot of gas concentration versus equilibrium feed pressure. These results were fit to the dual mode model describing gas sorption in both a Langmuir environment and a Henry's law environment:

$$S = \frac{c}{p} = k_D + \frac{C'_H b}{1 + b p} \qquad \text{(B.2)}$$

where k_D is the Henry's law constant, C'_H is the Langmuir capacity constant, and b is the Langmuir affinity constant. The sorption isotherms are shown in Figure A.4. The results of the fitted parameters are shown in Table A.3.

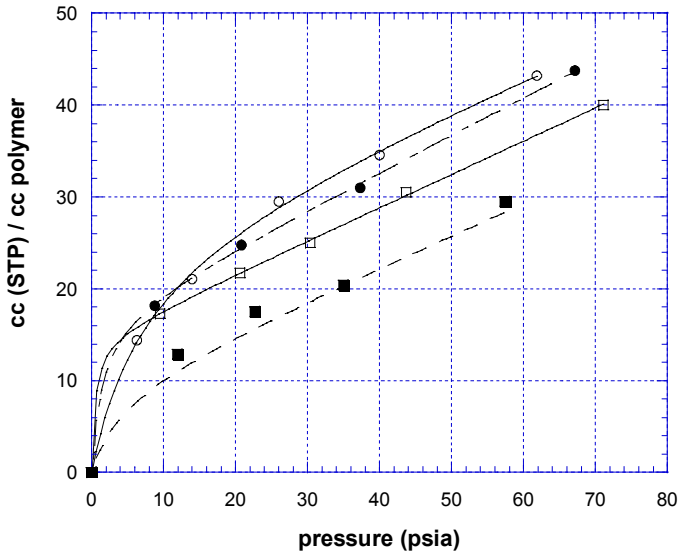

Figure A.4. Penetrant sorption in polymer films at 35 °C. ● C_3H_6 in 6FDA-6FpDA / $Ni[S_2C_2(CF_3)_2]_2$; ○ C_3H_6 in 6FDA-6FpDA ; □ C_3H_8 in 6FDA-6FpDA; ■ C_3H_8 in 6FDA-6FpDA / $Ni[S_2C_2(CF_3)_2]_2$.

It is clear from the data in Table A.3 that there is a significant increase in b, the affinity constant, for C_3H_6 in the dithiolene containing material, as expected. Furthermore, there is also a fortuitous increase in the Henry's law constant, k_D, for C_3H_6 within the material 6FDA-6FpDA / $Ni[S_2C_2(CF_3)_2]_2$, compared to the pure polyimide. There is no statistically significant trend for the Henry's law constant of C_3H_8 between each material, as expected, and it was not possible to determine any trends in the affinity constant, b, for C_3H_8 due to a large error in the fit for the pure polymer, 6FDA-6FpDA. Additional low pressure data points would be needed in order to improve this fit.

It would be expected that the C'_H parameter would increase for C_3H_6 in the dithiolene-containing blend, and that C'_H for C_3H_8 would remain relatively constant. Surprisingly, this is not what is observed. In both cases (C_3H_6 and

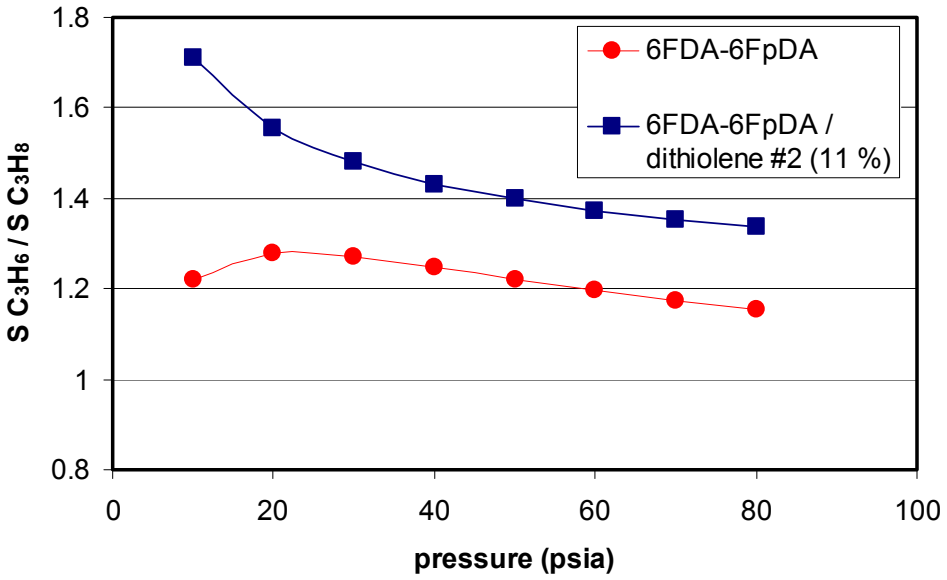

Figure A.5. Comparison of C_3H_6/C_3H_8 solubility selectivity for 6FDA-6FpDA polyimide with dithiolene additive.

C_3H_8) the C'_H parameter is depressed. This suggests that the dithiolene works to decrease the available defect free volume within the matrix. One possibility is that the dithiolene acts somewhat as a plasticizer, depressing the Tg of the matrix. Previous studies have shown correlations between the matrix Tg, and the C'_H parameter [9].

Using the dual mode data, it is possible to plot the pure gas C_3H_6/C_3H_8 solubility selectivity as a function of feed pressure for each of the materials studied (Figure A.5). Clearly, the solubility selectivity is improved at all pressures over the range studied. The increase in the C_3H_6 affinity constant, b, provides a large increase in the overall solubility selectivity at low pressures. The increase in the C_3H_6 Henry's law constant maintains an increase in the solubility selectivity at higher pressures.

Table A.3. Dual mode parameters for C_3H_6/C_3H_8 in 6FDA-6FpDA and 6FDA-6FpDA / $Ni[S_2C_2(CF_3)_2]_2$.

Membrane Material	**Gas**	$\mathbf{k_D}$ cc (STP) / cc polymer - psia	$\mathbf{C'_H}$ cc (STP) / cc polymer	**b** $psia^{-1}$
6FDA-6FpDA	C_3H_6	0.32	26.4	0.14
6FDA-6FpDA / $Ni[S_2C_2(CF_3)_2]_2$	C_3H_6	0.40	17.2	0.70
6FDA-6FpDA	C_3H_8	0.36	14.6	-
6FDA-6FpDA / $Ni[S_2C_2(CF_3)_2]_2$	C_3H_8	0.34	9.9	0.37

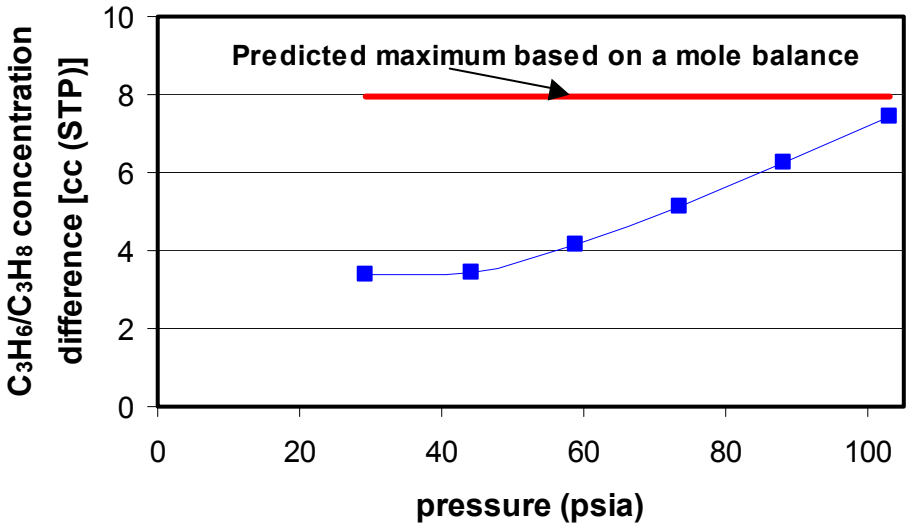

Figure A.6. Difference in C_3H_6/C_3H_8 concentration due to dithiolene additive. The upper flat line represents the calculated value assuming all added dithiolene forms a complex.

Figure A.6 illustrates the difference in C_3H_6/C_3H_8 concentration due to the dithiolene additive. The concentration difference increases with increased pressure, which indicates that the olefin is able to "access" more dithiolene molecules as the concentration increases in the polymer. The upper limit represents the calculated maximum enhancement based on a mole balance assuming all dithiolene molecules form a complex. As expected the experimental measurements approach this value as the pressure is increased.

C_3H_6/C_3H_8 Permeation Results

Pure gas permeation results were conducted for the material 6FDA-6FpDA / $Ni[S_2C_2(CF_3)_2]_2$ (11 wt %) at 2 atm feed pressure, and these results are compared to the pure 6FDA-6FpDA polyimide (Table A.4). Surprisingly, the C_3H_6 permeability is *depressed* by approximately a factor of 3 in the dithiolene containing polyimide. The C_3H_8 permeation coefficient is largely unaffected resulting in a significantly lower pure gas C_3H_6/C_3H_8 selectivity (4.9 compared to 16.0). At the outset, this result seems rather discouraging, but alternatively it can be viewed as quite good that there is a strong effect (even if it happens to be a negative one in this case). Before attempting to explain these results it is useful to examine mixed gas C_3H_6/C_3H_8 permeation results, shown in Figure A.7. At low feed pressures, the C_3H_6 permeability is roughly the same as the pure gas measurement; however, the C_3H_8 permeability is significantly lower, resulting in a much larger selectivity (~ 11).

The depression in the pure gas C_3H_6 permeability, (yet not the pure gas C_3H_8 permeability) yields the conclusion that the Henry's law diffusion coefficient of C_3H_6 is lower in the dithiolene/polyimide membrane, and this is not surprising considering the attractive interaction between the dithiolene and the olefin. The consistent mixed gas C_3H_6 permeation coefficient supports this assertion. However, in the mixed gas experiment the C_3H_8 permeability coefficient is depressed resulting in an improved C_3H_6/C_3H_8 selectivity. This

would result from competitive sorption, which can be predicted from the dual mode model, and this explains the low pressure results shown in Figure A.7. Presumably the upturn in permeability isotherm, and the downturn in selectivity, are a result of conventional plasticization, which would cause a decline in the diffusivity selectivity.

Table A.4. C_3H_6/C_3H_8 pure gas permeability for materials 6FDA-6FpDA and 6FDA-6FpDA / $Ni[S_2C_2(CF_3)_2]_2$ (11 wt %) at 35°C.

Material	**C_3H_6 Permeability** (Barrer)	**C_3H_6 / C_3H_8**
6FDA-6FpDA	0.89	16.0
6FDA-6FpDA / $Ni[S_2C_2(CF_3)_2]_2$	0.25	4.9

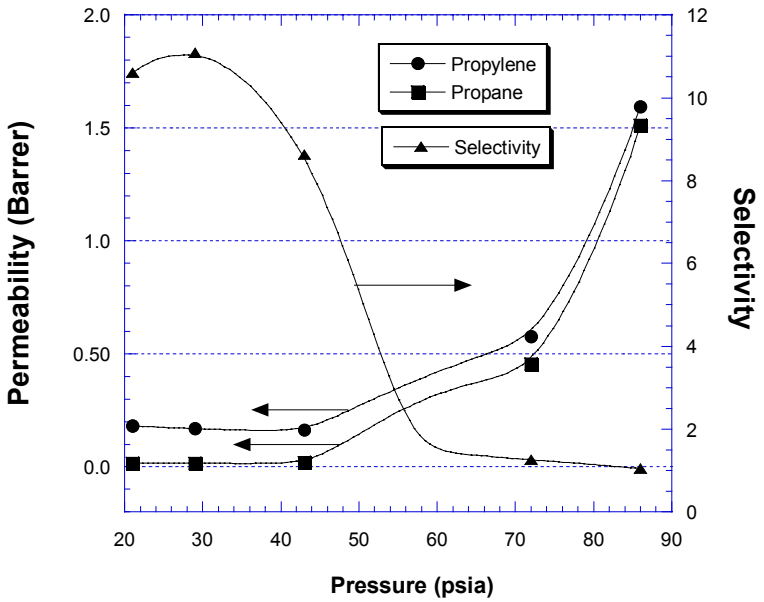

Figure A.7. Mixed gas C_3H_6/C_3H_8 (50 / 50 Feed) permeation results at 35°C for the material 6FDA-6FpDA / $Ni[S_2C_2(CF_3)_2]_2$ (11 wt %).

RECOMMENDATIONS

There are many directions that this work could proceed in the future. A few suggestions will be provided in this section. In terms of the transport properties it would be of interest to investigate larger dithiolene loadings, to understand the effect on both sorption and diffusion. Examining the effect of non-reacting dithiolenes on permeation and sorption would also be of interest to understand how the polymer is affected by the addition of the molecule, and to decouple the effects an active dithiolene shows on C_3H_6 permeation and sorption. It would also be of use to investigate alternate feed compositions in the mixed gas

permeation experiments. This would help to test the hypothesis that competitive sorption leads to an improvement in the mixed gas results (compared to the pure gas). Furthermore, it would be of interest to investigate the kinetics of the olefin / dithiolene complexation, as well as the kinetics of the reverse reaction. This could be done by *in situ* monitoring of C_3H_6 bubbling experiments with a UV spectrometer.

REFERENCES

[1] B. D. Freeman, Basis of Permeability/Selectivity Tradeoff Relation in Polymeric Gas Separation Membranes, Macromolecules 32 (1999) 375-380.

[2] C. M. Zimmerman, Advanced Gas Separation Membrane Materials: Hyper Rigid Polymers and Molecular Sieve-Polymer Mixed Matrices, Ph.D. Dissertation, The University of Texas at Austin, 1998.

[3] I. Pinnau and L. G. Toy, Solid polymer electrolyte composite membranes for olefin/paraffin separation, J. Membr. Sci. 184 (2001) 39-48.

[4] Y. S. Park, J. Won and Y. S. Kang, Facilitated transport of olefin through solid PAAm and PAAm-graft composite membranes with silver ions, J. Membr. Sci. 183 (2001) 163-170.

[5] S. Bai, S. Sridhar and A. A. Khan, Metal-ion mediated separation of propylene from propane using PPO membranes, J. Membr. Sci. 147 (1998) 131-139.

[6] I. Pinnau and L. G. Toy, Solid polymer electrolyte composite membranes for olefin/paraffin separation, J. Membr. Sci. 184 (2001) 39-48.

[7] K. Wang and E. I. Stiefel, Toward Separation and Purification of Olefins Using Dithiolene Complexes: An Electrochemical Approach, Science 291 (2001) 106.

[8] D. C. Olson, V. P. Mayweg and G. N. Schrauzer, Polarographic Study of Coordination Compounds with Delocalized Ground States. Substituent Effects in Bis- and Trisdithiodiketone Complexes of Transition Metals, J. Am. Chem. Soc. 88 (1966) 4876-4882.

[9] W. J. Koros and D. R. Paul, CO_2 Sorption in Poly(Ethylene-Terephthalate) above and Below Glass-Transition, J. Polym. Sci. Pt. B-Polym. Phys. 16 (1978) 1947-1963.

Appendix B: Experimental Permeation and Dilation

PERMEATION

Leak rate measurements were made by applying vacuum on both the upstream and downstream for at least 12 hours (after the epoxy has cured). Valves were then closed and the dP/dt rate was measured for at least 8 hours, and this was typically done before and after a permeation experiment. For permeation measurements reported here the leak rate was typically less than 10% of the slowest gas flux, and in rare cases up to 20% of the slowest gas flux. In all of the cases exceeding 10% of the flux, mixed gas experiments were also conducted to verify the validity of the pure gas C_3H_6/C_3H_8 measurements. Since the mixed gas experiment measures the selectivity through an entirely different technique (the use of a GC), this is a very suitable method of validating the pure gas measurements, although some deviations are still expected, based on the arguments in Chapter 6.

It is also important to consider the time lag for achieving steady-state conditions in the permeation experiments. The time lag is defined as:

$$\theta = \frac{\ell^2}{6D} \qquad \text{(B.1)}$$

where ℓ is the thickness of the membrane, and D is the average diffusion coefficient of the penetrant in the material. The smallest diffusion coefficient reported in the work here is C_3H_8 in 6FDA-TAB, which is 2.7×10^{-11} cm^2/sec. For these measurements a film thickness of no greater than 25 μm was used. This equates to a time lag of 11 hours. Before taking a measurement a time period of

~4θ was given to achieve adequate steady-state (in some cases up to 2 days). Steady-state conditions were validated by repeating measurements several times at constant pressure in a non-plasticized condition, which in many cases for the C_3H_6/C_3H_8 permeation measurements may be at a feed pressure as low as 2 atm.

THERMAL EXPANSION COEFFICIENT MEASUREMENTS

The expansion of the polymeric materials with temperature is of interest because the increase in permeability with temperature shows similar results to the penetrant induced swelling increases in permeability (with increasing pressure), and measurement of the thermal expansion coefficient may lend insight into these similarities. As discussed in Chapter 3 these measurements were made using dynamic ellipsometry. Figure B.1 demonstrates an example of the data obtained in terms of the thickness change with temperature for the polymer 6FDA-DAM.

The thermal expansion coefficient can be calculated from the thickness vs. temperature curve using the average thickness as the normalizing value. Table B.1 lists the average thermal expansion coefficients for all copolymers. The average thermal expansion coefficient can be used to determine the average dilation of the material, and this value is given over a 20^{o}C range in Table B.1.

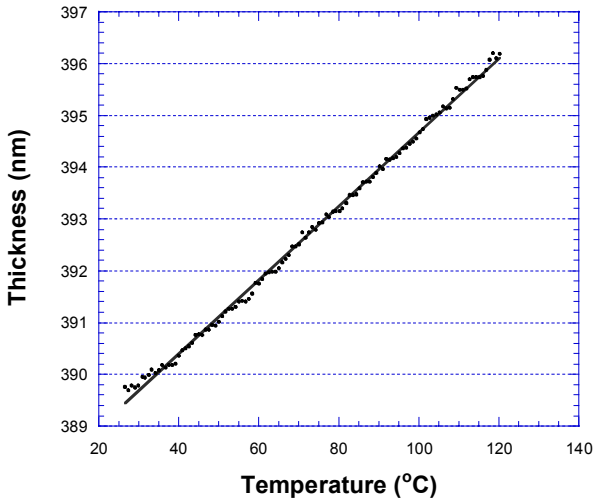

Figure B.1. Change in thickness with temperature for 6FDA-DAM measured using dynamic ellipsometry.

The range of 20°C is chosen because this is the typical interval between permeation measurements. Over the range of material structures the dilation that occurs in this temperature range is 0.32 – 0.77 %. This indicates that only minimal swelling is necessary to have significant effects on the permeability of the hydrocarbon molecules examined here.

Table B.1. Thermal expansion coefficients of copolymers studied in this work.

Polymer	**α (K^{-1})**	**Percent Dilation (range of 20°C)**
6FDA-TAB	2.82×10^{-4}	0.56 %
6FDA-TAB/DAM(75/25)	3.83×10^{-4}	0.77 %
6FDA-TAB/DAM(50/50)	1.62×10^{-4}	0.32 %
6FDA-DAM	1.82×10^{-4}	0.36 %

Appendix C: FORTRAN Program for Solving the Effective Medium Theory

```
program poresv5

c       This program solves the effective medium approximation for 3 different
c       pore values given the permeability or diffusivity of the fast and slow gas
        through
c       each pore.  The inputs are the 6 permeability #'s for the fast and slow
        gases
c       for each pore size.  Right now it is only possible to use 3 different pore
c        sizes.
c       New to version 4 - this program uses Newton's method for converging
        based on only the series model as an initial guess. c

c       use MSIMSLMS
        implicit none
        integer    max
        parameter  (max=10)



c       Declaration of variables internal to the program
        real       zero,p1fast,p2fast,p3fast,p1slow,p2slow,p3slow
        real       volfrac1,volfrac2,volfrac3,selec,der
        real       pmfg2
        real       pmsg2
        real       zguess2
        integer     n,a

c     define variables

c     a= a counter number to increase the volume fraction
c     der = the derivative of the effective medium equation
c     n = a counter number for the iterations to solve the equation

c

c       Beginning of program

        zero=0.00001
```

```
c       Load input parameter file.
        print *,'Loading data...'
        open(unit=29,file="inputpores.dat",status="old")
        open(unit=39,file="outputpores2.dat",status="old")
        read(29,*)  P1fast
        read(29,*)  P2fast
        read(29,*)       p3fast
        read(29,*)  p1slow
        read(29,*)  p2slow
        read(29,*)  p3slow

        volfrac3=0
     volfrac2=0
     a=0
c      Begin calculating the selectivity matrix, start with pore 3 at a constant value


       do while (volfrac3.le.1)

            do while (volfrac2.le.(1.05-a*0.1))

               volfrac1=1-volfrac3-volfrac2

c      Check volume fraction calculation
            if ((volfrac1.lt.(-0.001)).or.(volfrac1.gt.(1.001)))then
                print *, 'error:  volfractions are out of bounds'
                 stop
               end if

c      Guess a value for the medium effective permeability of the fast gas
c
c       The guess is based on the series model


            pmfg2=1/((volfrac1/p1fast)+(volfrac2/p2fast)+
     +          (volfrac3/p3fast))


            zguess2=volfrac1*((pmfg2-p1fast)/(p1fast+2*pmfg2))+
     +                 volfrac2*((pmfg2-p2fast)/(p2fast+2*pmfg2))+
        +                   volfrac3*((pmfg2-p3fast)/(p3fast+2*pmfg2))
```

```
            n=0

          do while ((ABS(zguess2).gt.zero).and.(n.le.25))

c          Calculate the derivative at pmfg2
             der=(3*volfrac1*p1fast)/(p1fast+2*pmfg2)**2+
     +            (3*volfrac2*p2fast)/(p2fast+2*pmfg2)**2+
     +            (3*volfrac3*p3fast)/(p3fast+2*pmfg2)**2

c          Calculate new guess of pmfg2

             pmfg2= pmfg2-zguess2/der

c          calculate new zguess 2

             zguess2=volfrac1*((pmfg2-p1fast)/(p1fast+2*pmfg2))+
     +                volfrac2*((pmfg2-p2fast)/(p2fast+2*pmfg2))+
     +                   volfrac3*((pmfg2-p3fast)/(p3fast+2*pmfg2))

               n=n+1

              if (n.eq.15) then

                print *, 'error: not converging'

              end if

           end do

           print *,'converged on fast gas, switching loops'


c        Determine the effective permeability of the slow gas

c       Guess a  values for the medium effective permeability of the slow gas
c         The guess is based upon the series model


             pmsg2=1/((volfrac1/p1slow)+(volfrac2/p2slow)+
     +            (volfrac3/p3slow))
```

```
            zguess2=volfrac1*((pmsg2-p1slow)/(p1slow+2*pmsg2))+
     +                 volfrac2*((pmsg2-p2slow)/(p2slow+2*pmsg2))+
          +                 volfrac3*((pmsg2-p3slow)/(p3slow+2*pmsg2))


            n=0

            do while ((ABS(zguess2).gt.zero).and.(n.le.25))

c           Calculate the derivative at pmfg2
              der=(3*volfrac1*p1slow)/(p1slow+2*pmsg2)**2+
     +           (3*volfrac2*p2slow)/(p2slow+2*pmsg2)**2+
     +           (3*volfrac3*p3slow)/(p3slow+2*pmsg2)**2

c           Calculate new guess of pmfg2

            pmsg2= pmsg2-zguess2/der

c           calculate new zguess 2

            zguess2=volfrac1*((pmsg2-p1slow)/(p1slow+2*pmsg2))+
     +                 volfrac2*((pmsg2-p2slow)/(p2slow+2*pmsg2))+
          +                 volfrac3*((pmsg2-p3slow)/(p3slow+2*pmsg2))

              n=n+1

            if (n.ge.24) then

               print *, 'error: not converging'

            end if

          end do

          print *,'fast gas perm=',pmfg2
          print *,'slow gas perm=',pmsg2
               selec=pmfg2/pmsg2
              print *,'selectivity=',selec

         write (39,*) volfrac1,volfrac2,volfrac3,selec
         print *, volfrac1,volfrac2,selec
```

```
            volfrac2=volfrac2+0.1

        end do

        volfrac2=0
        a=a+1

        volfrac3=volfrac3+0.1

        end do



        print *,'calculation completed.'

    stop
        end
```

Appendix D: Additional Data and Information on Masking Techniques

Additional Data

Files for Figures and data can be found on the CD, which should accompany this text. From Kaliedagraph QPC files the raw data can be determined by selecting 'Plot', and then 'Extract Data' from the menu bar.

Additional Masking Technique for Rigid Membrane Materials:

Many portions of this technique were developed by Cathy Zimmerman and Zen Mogri, and it is a technique usually used for brittle materials (e.g. polypyrrolones or carbon membranes). First a cell must be used, which only has an o-ring on the downstream side. The upstream is open (no o-ring). Then, the film is masked in the conventional method with 2 annular pieces of aluminum tape. The masked film is then cut such that the outer diameter of the mask is significantly larger than the inner diameter, and the outer diameter is approximately half the diameter of the cell (this can vary a lot depending on area of the film). One new piece of aluminum tape mask is created such that the inner diameter is slightly larger than the area of the film, and the outer diameter is slightly smaller than that of the cell (o-ring). A piece of filter paper is placed between the masked film and the cell. The new piece of aluminum tape is then placed over the masked film taping (sealing) the film to the bottom cell. Usually

it is most effective to start on the inside ring of the tape and press outwards in an effort to make a perfect seal. The bottom half of this cell (having a masked film which is sealed) can then be connected to the downstream of a permeation system leaving the membrane open to the air. Vacuum is pulled on the membrane, and the downstream pressure is observed. Inevitably the pressure will not reach the normal vacuum pressure of the system meaning there are leaks and epoxy should be applied to the membrane. Five minute epoxy is used around the outside area of the film covering the film tape interface, and the interface of the two pieces of aluminum tape. This is done while constantly observing the downstream pressure. At this point, sealing the membrane becomes an exercise in trouble shooting.

Trouble Shooting the Membrane Seal:

If the downstream pressure goes down to (approximately) the normal vacuum pressure: the membrane is sealed. But, it is always valuable to do an order of magnitude check. After the pressure has leveled out (~an hour) air is allowed to permeate through the membrane. The increase in downstream pressure is recorded over some time period (maybe a minute). In this case the time lag for permeation should not be an issue, because air has been permeating through the membrane the entire time. Using the membrane thickness, approximate area, driving force (14.7 psia) temperature, etc, an order of magnitude permeability for

air can be calculated. If the O_2/N_2 permeability of the material is known, the total air permeability should be somewhere in between. If the calculated result is an order of magnitude or more larger a leak probably exists. Regardless the permeability will likely be slightly higher due to molecules (mostly moisture) desorbing off of the walls of the downstream volume, but this is not a problem since it is only an order of magnitude calculation. If the O_2/N_2 permeabilities are not known, it would probably be wise to be skeptical about an air permeabilty of 1000 Barrer or higher.

If the downstream pressure does not go down to normal vacuum pressure: a leak probably exists. Again, it is wise to do an order of magnitude check. With experience this takes seconds by simply closing the dowstream valve. If the pressure rise is too great over time it will likely be immediately obvious. If a leak exists, it probably resides in one (or more) of four places. 1) Epoxy/ membrane / tape interface , 2) aluminum tape and cell, 3) the VCR fitting in the bottom of the cell, or 4) break or defect in the membrane.

First,it is wise to try pushing down around the aluminum tape mask in an effort to eliminate any leaks between the mask and the cell. It is important to always observe the downstream pressure. Next, it is best to check for leaks in the film or film epoxy interface. A flashlight can be used to try and detect breaks in the film. Additionally a piece of latex (cut a piece from a glove) can be placed over the film. The latex is pulled across the film and carefully pressed down

gently. If the latex is sucked down, and the downstream pressure begins to lower there is a defect/break in the flm or a leak at the film epoxy interface. If the latter is true it is usually possible to see the break in the latex as it will be pulled harder at that point (then the latex is removed and epoxy is applied at that point). If a point of stress cannot be seen in the laytex, there may be a defect in the film. It is also possible to where a latex glove and cover different areas of the film with one's finger in order to determine where the leak is. If the latex does not pull down, and there is no leak in the seal, there may be a leak in the cell. This can be checked (although this should be a last resort) by removing the film and covering the cell with a piece of aluminum tape and pulling vacuum again. Finding a leak at the mask or epoxy interface is often challenging, and also comes with experience.

Bibliography

[1] Facts and figures, Chemical and Engineering News. 77 (1999) 32-39.

[2] S. Bai, S. Sridhar and A. A. Khan, Metal-ion mediated separation of propylene from propane using PPO membranes, J. Membr. Sci. 147 (1998) 131-139.

[3] S. Bai, S. Sridhar and A. A. Khan, Recovery of propylene from refinery off-gas using metal incorporated ethylcellulose membranes, J. Membr. Sci. 174 (2000) 67-79.

[4] R. W. Baker, Future directions of membrane gas separation technology, Ind. Eng. Chem. Res. 41 (2002) 1393-1411.

[5] A. E. Barnabeo, W. S. Creasy and L. M. Robeson, Gas permeability characteristics of nitrile-containing block and random copolymers, J. Polym. Sci. Pol. Chem. 13 (1975) 1979-1986.

[6] R. Barrer, Nature of the diffusion process in rubber, Nature 140 (1937) 106.

[7] V. L. Bell and R. A. Jewell, Synthesis and properties of polyimidazopyrrolones, J. Polym. Sci., Polym. Chem. Ed. 5 (1967) 3043-60.

[8] A. A. Berlin, B. I. Liogon'kii and G. M. Shamraev, Thermostable polymers from dianhydrides of aromatic tetracarboxylic acids and tetra-amines, Russian Chemical Reviews 40 (1971) 284-300.

[9] A. Bos, I. G. M. Punt, M. Wessling and H. Strathmann, CO_2-induced plasticization phenomena in glassy polymers, 155 (1999) 67-78.

[10] A. J. Burggraaf, Single gas permeation of thin zeolite (mfi) membranes: Theory and analysis of experimental observations, J. Membr. Sci. 162 (1999) 295-295.

[11] D. F. Cadogan and C. J. Howick, in: Kirk-Othmer encyclopedia of chemical technology, John Wiley and Sons, Inc, 1996.

[12] L. M. Costello and W. J. Koros, Temperature dependence of gas sorption and transport properties in polymers: Measurement and applications, Ind. Eng. Chem. Res. 31 (1996) 2708-2714.

[13] J. Crank and G. S. Park, Diffusion in polymers, Academic Press, London, 1968.

[14] H. T. Davis, The effective medium theory of diffusion in composite media, J. Am. Ceram. Soc. 60 (1977) 499-501.

[15] H. T. Davis, L. R. Valencourt and C. E. Johnson, Transport processes in composite media, J. Am. Ceram. Soc. 58 (1975) 446-452.

[16] J. C. Davis, R. J. Valus, R. Eshraghi and A. E. Velikoff, Facilitated transport membrane hybrid systems for olefin purification, Sep. Sci. Technol. 28 (1993) 463-476.

[17] F. Dawans and C. S. Marvel, Polymers from ortho aromatic tetraamines and aromatic dianhydrides, J. Polymer Sci, Part A 3 (1965) 3549-3571.

[18] P. Eisele and R. Killpack, in: Ullman's encyclopedia of industrial chemistry, 1993, pp. 211-222.

[19] R. B. Eldridge, Olefin paraffin separation technology - a review, Ind. Eng. Chem. Res. 32 (1993) 2208-2212.

[20] B. D. Freeman, Basis of permeability/selectivity tradeoff relation in polymeric gas separation membranes, Macromolecules 32 (1999) 375-380.

[21] B. D. Freeman, Basis of permeability/selectivity tradeoff relations in polymeric gas separation membranes, Macromolecules 32 (1999) 375-380.

[22] A. B. Fuertes and T. A. Centeno, Preparation of supported asymmetric carbon molecular sieve membranes, J. Membr. Sci. 144 (1998) 105-111.

[23] J. Gilron and A. Soffer, Knudsen diffusion in microporous carbon membranes with molecular sieving character, In press (2002).

[24] J. Hayashi, H. Mizuta, M. Yamamoto, K. Kusakabe and S. Morooka, Pore size control of carbonized bpda-pp'oda polyimide membrane by chemical vapor deposition of carbon, J. Membr. Sci. 124 (1997) 243-251.

[25] J. Hayashi, M. Yamamoto, K. Kusakabe and S. Morooka, Simultaneous improvement of permeance and permselectivity of 3,3',4,4'-biphenyltetracarboxylic dianhydride-4,4'-oxydianiline polyimide membrane by carbonization, Ind. Eng. Chem. Res. 34 (1995) 4364-4370.

[26] E. J. Henley and M. L. D. Santos, Permeation of vapors through polymers at low temperature and elevated pressures, 13 (1967) 1117-1119.

[27] A. L. Hines and R. N. Maddox, Mass transfer fundamentals and applications, Prentice Hall PTR, Englewood Cliffs, 1985.

[28] J. H. Hirchfelder, C. F. Curtiss and R. B. Bird, Molecular theory of gases and liquids, Wiley, New York, 1964.

[29] W. S. Ho and D. C. Dalrymple, Facilitated transport of olefins in Ag+-containing polymer membranes, J. Membr. Sci. 91 (1994) 13-25.

[30] S. U. Hong, J. H. Jin, J. Won and Y. S. Kang, Polymer-salt complexes containing silver ions and their application to facilitated olefin transport membranes, Adv. Mater. 12 (2000) 968.

[31] X. Hong, Y. C. Jean, H. J. Yang, S. S. Jordan and W. J. Koros, Free-volume hole properties of gas-exposed polycarbonate studied by positron annihilation lifetime spectroscopy, Macromolecules 29 (1996) 7859-7864.

[32] G. H. Hsiue and J. S. Yang, Novel methods in separation of olefin/paraffin mixtures by functional polymeric membranes, J. Membr. Sci. 82 (1993) 117-128.

[33] O. M. Ilinich and K. I. Zamaraev, Separation of ethylene and ethane over polyphenyleneoxides membranes - transient increase of selectivity, J. Membr. Sci. 82 (1993) 149-155.

[34] O. M. Ilinitch, private communication, 2002.

[35] O. M. Ilinitch, A. A. Lapkin and K. I. Zamaraev, Propylene in polyphenylene oxides membranes - unusual permeability vs pressure behavior, J. Membr. Sci. 98 (1995) 287-290.

[36] O. M. Ilinitch, G. L. Semin, M. V. Chertova and K. I. Zamaraev, Novel polymeric membranes for separation of hydrocarbons, J. Membr. Sci. 66 (1992) 1-8.

[37] A. Ito and S. T. Hwang, Permeation of propane and propylene through cellulosic polymer membranes, J. Appl. Polym. Sci. 38 (1989) 483-490.

[38] Y. Ito, H. F. M. Mohamed, K. Tanaka, K. Okamoto and K. Lee, Sorption of CO_2 in polymers observed by positron annihilation technique, J. Radioanal. Nucl. Chem.-Artic. 211 (1996) 211-218.

[39] S. A. Jenekhe and P. O. Johnson, Complexation-mediated solubilization and processing of rigid- chain and ladder polymers in aprotic organic-solvents, Macromolecules 23 (1990) 4419-4429.

[40] S. M. Jordan and W. J. Koros, Characterization of CO_2-induced conditioning of substituted polycarbonates using various exchange penetrants, J. Membr. Sci. 51 (1990) 233-247.

[41] H. D. Kamaruddin and W. J. Koros, Some observations about the application of fick's first law for membrane separation of multicomponent mixtures, J. Membr. Sci. 135 (1997) 147-159.

[42] M. S. Kane, J. F. Goellner, H. C. Foley, R. DiFrancesco, S. J. L. Billinge and L. F. Allard, Symmetry breaking in nanostructure development of carbogenic molecular sieves: Effects of morphological pattern formation on oxygen and nitrogen transport, Chem. Mat. 8 (1996) 2159-2171.

[43] Y. H. Kim, J. H. Ryu, J. Y. Bae, Y. S. Kang and H. S. Kim, Reactive polymer membranes containing cuprous complexes in olefin/paraffin separation, Chem. Commun. (2000) 195-196.

[44] G. H. Koops, private communication, 2002.

[45] W. J. Koros, A. H. Chan and D. R. Paul, Sorption and transport of various gases in polycarbonate, J. Membr. Sci 2 (1977) 165-190.

[46] W. J. Koros and D. R. Paul, CO_2 sorption in poly(ethylene-terephthalate) above and below glass-transition, J. Polym. Sci. Pt. B-Polym. Phys. 16 (1978) 1947-1963.

[47] W. J. Koros and D. R. Paul, Design considerations for measurement of gas sorption in polymers by pressure decay, J. Polym. Sci., Polym. Phys. Ed. 14 (1976) 1903.

[48] R. Krishna and J. A. Wesselingh, Review article number 50 - The Maxwell-Stefan approach to mass transfer, Chem. Eng. Sci. 52 (1997) 861-911.

[49] J. J. Krol, M. Boerrigter and G. H. Koops, Polyimide hollow fiber gas separation membranes: Preparation and the suppression of plasticization in propane/propylene environments, J. Membr. Sci. 184 (2001) 275-286.

[50] Y. Kusuki, H. Shimazaki, N. Tanihara, S. Nakanishi and T. Yoshinaga, Gas permeation properties and characterization of asymmetric carbon membranes prepared by pyrolyzing asymmetric polyimide hollow fiber membrane, J. Membr. Sci. 134 (1997) 245-253.

[51] K. R. Lee and S. T. Hwang, Separation of propylene and propane by polyimide hollow-fiber membrane module, J. Membr. Sci. 73 (1992) 37-45.

[52] J. W. B. M.R. Schoenberg, C.G. Papadopoulos, in: Kirk-othmer encyclopedia, 1995, pp. 228-246.

[53] K. C. Obrien, W. J. Koros, T. A. Barbari and E. S. Sanders, A new technique for the measurement of multicomponent gas- transport through polymeric films, J. Membr. Sci. 29 (1986) 229-238.

[54] M. Ogawa and Y. Nakano, Separation of CO_2/CH_4 mixture through carbonized membrane prepared by gel modification, J. Membr. Sci. 173 (2000) 123-132.

[55] K. Okamoto, private communication, 2001.

[56] K. Okamoto, S. Kawamura, M. Yoshino, H. Kita, Y. Hirayama, N. Tanihara and Y. Kusuki, Olefin/paraffin separation through carbonized membranes derived from an asymmetric polyimide hollow fiber membrane, Ind. Eng. Chem. Res. 38 (1999) 4424-4432.

[57] K. Okamoto, K. Noborio, J. Hao, K. Tanaka and H. Kita, Permeation and separation properties of polyimide membranes to 1,3-butadiene and n-butane, J. Membr. Sci. 134 (1997) 171-179.

[58] D. C. Olson, V. P. Mayweg and G. N. Schrauzer, Polarographic study of coordination compounds with delocalized ground states. Substituent effects in bis- and trisdithiodiketone complexes of transition metals, J. Am. Chem. Soc. 88 (1966) 4876-4882.

[59] Y. S. Park, J. Won and Y. S. Kang, Facilitated transport of olefin through solid paam and paam- graft composite membranes with silver ions, J. Membr. Sci. 183 (2001) 163-170.

[60] D. R. Paul and O. M. Ebralima, Hydraulic permeation of liquids through swollen polymeric networks .3. Generalized correlation, J. Appl. Polym. Sci. 19 (1975) 2759-2771.

[61] J. H. Petropoulos, Quantitative analysis of gaseous diffusion in glassy polymers, J. Polymer Sci. Part A-2 8 (1970) 1797-1801.

[62] I. Pinnau and L. G. Toy, Solid polymer electrolyte composite membranes for olefin/paraffin separation, J. Membr. Sci. 184 (2001) 39-48.

[63] P. S. Rallabandi, A. P. Thompson and D. M. Ford, A molecular modeling study of entropic and energetic selectivities in air separation with glassy polymers, Macromolecules 33 (2000) 3142-3152.

[64] L. M. Robeson, Correlation of separation factor versus permeability for polymeric membranes, J. Membr. Sci. 62 (1991) 165-185.

[65] K. J. L. S. Glasstone, H. Eyring, The theory of rate processes, 1st ed, McGraw-Hill Book Co., Inc., New York, 1941.

[66] R. Sadeghbeigi, Fluid catalytic cracking handbook, Gulf Publishing Company, Houston, TX, 2000.

[67] E. S. Sanders, Penetrant-induced plasticization and gas permeation in glassy polymers, J. Membr. Sci. 37 (1988) 63-80.

[68] M. G. Sedigh, W. J. Onstot, L. F. Xu, W. L. Peng, T. T. Tsotsis and M. Sahimi, Experiments and simulation of transport and separation of gas mixtures in carbon molecular sieve membranes, J. Phys. Chem. A 102 (1998) 8580-8589.

[69] D. Sek, E. Schab-Balcerzak, E. Grabiec, A. Volozhin and T. Chamenko, New semiladder polymers: Iii. Synthesis and properties of new poly(etherimidazopyrrolone)s, Polymer. 41 (2000) 49-56.

[70] V. P. Shantarovich, I. B. Kevdina, Y. P. Yampolskii and A. Y. Alentiev, Positron annihilation lifetime study of high and low free volume glassy polymers: Effects of free volume sizes on the permeability and permselectivity, Macromolecules 33 (2000) 7453-7466.

[71] A. Shimazu, Method of selectively separating unsaturated hydrocarbon, 5,749,943, Petroleum Energy Center, Tokyo, Japan, 1998.

[72] A. Shimazu, T. Miyazaki, M. Maeda and K. Ikeda, Relationships between the chemical structures and the solubility, diffusivity, and permselectivity of propylene and propane in 6FDA-based polyimides, J. Polym. Sci. Pt. B-Polym. Phys. 38 (2000) 2525-2536.

[73] A. Shimazu, T. Miyazaki, T. Matsushita, M. Maeda and K. Ikeda, Relationships between chemical structures and solubility, diffusivity, and permselectivity of 1,3-butadiene and n-butane in 6FDA-based polyimides, J. Polym. Sci. Pt. B-Polym. Phys. 37 (1999) 2941-2949.

[74] A. Shimazu, T. Miyazaki, T. Matsushita, M. Maeda and K. Ikeda, Relationships between chemical structures and solubility, diffusivity, and permselectivity of 1,3-butadiene and n-butane in 6FDA-based polyimides, J. Polym. Sci. Pt. B-Polym. Phys. 37 (1999) 2941-2949.

[75] A. Singh and W. J. Koros, Significance of entropic selectivity for advanced gas separation membranes, Ind. Eng. Chem. Res. 35 (1996) 1231-1234.

[76] A. Singh-Ghosal and W. J. Koros, Air separation properties of flat sheet homogeneous pyrolytic carbon membranes, J. Membr. Sci. 174 (2000) 177-188.

[77] A. Singh-Ghosal and W. J. Koros, Air separation properties of flat sheet homogeneous pyrolytic carbon membranes, J. Membr. Sci. 174 (2000) 177-188.

[78] A. Singh-Ghosal and W. J. Koros, Energetic and entropic contributions to mobility selectivity in glassy polymers for gas separation membranes, Ind. Eng. Chem. Res. 38 (1999) 3647-3654.

[79] S. M. Sirard, P. F. Green and K. P. Johnston, Spectroscopic ellipsometry investigation of the swelling of poly(dimethylsiloxane) thin films with high pressure carbon dioxide, J. Phys. Chem. B 105 (2001) 766-772.

[80] S. Sridhar and A. A. Khan, Simulation studies for the separation of propylene and propane by ethylcellulose membrane, J. Membr. Sci. 159 (1999) 209-219.

[81] V. Stannet, in: Diffusion in polymers, Academic Press, New York, 1968.

[82] C. Staudt-Bickel and W. J. Koros, Improvement of CO_2/CH_4 separation characteristics of polyimides by chemical crosslinking, J. Membr. Sci. 155 (1999) 145-154.

[83] C. Staudt-Bickel and W. J. Koros, Olefin/paraffin gas separations with 6FDA-based polyimide membranes, J. Membr. Sci. 170 (2000) 205-214.

[84] K. Steel, Carbon membranes for challenging gas separations, Ph. D. Dissertation, The University of Texas at Austin, 2000.

[85] M. S. Strano and H. C. Foley, Temperature- and pressure-dependent transient analysis of single component permeation through nanoporous carbon membranes, Carbon 40 (2002) 1029-1041.

[86] D. Styrkas, S. J. Doran, V. Gilchrist, J. L. Keddie, J. R. Lu, E. Murphy, R. Sackin, T.-J. Su and A. Tzitzinou, Polymer surfaces and interfaces III, John Wiley and Sons, New York, 1999.

[87] S. Sunderrajan, B. D. Freeman, C. K. Hall and I. Pinnau, Propane and propylene sorption in solid polymer electrolytes based on poly(ethylene oxide) and silver salts, J. Membr. Sci. 182 (2001) 1-12.

[88] K. Tanaka, A. Taguchi, J. Q. Hao, H. Kita and K. Okamoto, Permeation and separation properties of polyimide membranes to olefins and paraffins, J. Membr. Sci. 121 (1996) 197-207.

[89] H. G. Tompkins and W. A. McGahan, Spectroscopic ellipsometry and reflectometry, John Wiley & Sons, Inc, New York, 1999.

[90] L. J. P. Vandenbroeke and R. Krishna, Experimental-verification of the Maxwell-Stefan theory for micropore diffusion, Chem. Eng. Sci. 50 (1995) 2507-2522.

[91] W. R. Vieth and K. J. Sladek, A model for diffusion in a glassy polymer, J. Colloid Sci. 20 (1965) 1014-1033.

[92] D. Q. Vu, Formation and characterization of asymmetric carbon molecular sieve and mixed matrix membranes for natural gas purification, Ph.D. Dissertation, The University of Texas at Austin, 2001.

[93] D. Q. Vu, W. J. Koros and S. J. Miller, High pressure CO_2/CH_4 separation using carbon molecular sieve hollow fiber membranes, Ind. Eng. Chem. Res. 41 (2002) 367-380.

[94] D. R. B. Walker, Synthesis and characterization of polypyrrolones for gas separation membranes, Ph.D. Dissertation, The University of Texas at Austin, 1993.

[95] B. Wang, Z. F. Wang, M. Zhang, W. H. Liu and S. J. Wang, Effect of temperature on the free volume in glassy poly(ethylene terephthalate), Macromolecules 35 (2002) 3993-3996.

[96] K. Wang and E. I. Stiefel, Toward separation and purification of olefins using dithiolene complexes: An electrochemical approach, Science 291 (2001) 106.

[97] M. Wessling, Relaxation phenomena in dense gas separation membranes, The University of Twente, 1992.

[98] M. Wessling, M. L. Lopez and H. Strathmann, Accelerated plasticization of thin-film composite membranes used in gas separation, Sep. Purif. Technol. 24 (2001) 223-233.

[99] J. D. Wind, Improving polyimide membrane resistance to CO_2 plasticization in natural gas separations, Ph D. Dissertation, The University of Texas at Austin, 2002.

[100] Y. P. Yampolskii, A. P. Korikov, V. P. Shantarovich, K. Nagai, B. D. Freeman, T. Masuda, M. Teraguchi and G. Kwak, Gas permeability and free volume of highly branched substituted acetylene polymers, Macromolecules 34 (2001) 1788-1796.

[101] J. P. Yuan, H. Cao, E. W. Hellmuth and Y. C. Jean, Subnanometer hole properties of CO_2-exposed polysulfone studied by positron annihilation lifetime spectroscopy, J. Polym. Sci. Pt. B-Polym. Phys. 36 (1998) 3049-3056.

[102] W. Zhou, X. Gao and F. Lu, Silicon-containing polypyrrolone for gas-separation application, J. Applied Polymer Sci. 51 (1994) 855-861.

[103] C. M. Zimmerman, Advanced gas separation membrane materials: Hyper rigid polymers and molecular sieve-polymer mixed matrices, Ph.D. Dissertation, The University of Texas at Austin, 1998.

[104] C. M. Zimmerman and W. J. Koros, Entropic selectivity analysis of a series of polypyrrolones for gas separation membranes, Macromolecules 32 (1999) 3341-3346.

[105] C. M. Zimmerman and W. J. Koros, Polypyrrolones for membrane gas separations. I. Structural comparison of gas transport and sorption properties, J. Polym. Sci. Part B 37 (1999) 1235-1249.

[106] C. M. Zimmerman and W. J. Koros, Polypyrrolones for membrane gas separations. II. Activation energies and heats of sorption, J. Polym. Sci. Pt. B-Polym. Phys. 37 (1999) 1251-1265.

Vita

Ryan Lance Burns was born in New Port Richey, Florida on June 21, 1976 as the son of Phillip Lance Burns and Marguerite Linda Burns. After graduating from Gulf High School in New Port Richey, Florida in June of 1994 he entered the Georgia Institute of Technology and graduated with a Bachelor of Science degree in Chemical Engineering in June of 1998. In August of 1998 he entered graduate school at the University of Texas at Austin as a Ph D student working under Dr. William J. Koros.

Permanent address: 4015 Speedway Apt #2
Austin, TX 78751

This dissertation was typed by the author.